# SYNTHESIS AND CHARACTERIZATION OF NANO-DIAMOND REINFORCED CHITOSAN FOR TISSUE ENGINEERING

A Thesis Submitted to the College of

Graduate Studies and Research

In Partial Fulfillment of the Requirements

For the Degree of Master of Science

In the Department of Mechanical Engineering

University of Saskatchewan

Saskatoon

By

YU SUN

**PERMISSION TO USE**

In presenting this thesis in partial fulfillment of the requirements for a Postgraduate degree from the University of Saskatchewan, I agree that the Libraries of this University may make it freely available for inspection. I further agree that permission for copying of this thesis in any manner, in whole or in part, for scholarly purposes may be granted by the professor Qiaoqin Yang who supervised my thesis work or, in her absence, by the Head of the Department or the Dean of the College in which my thesis work was done. It is understood that any copying or publication or use of this thesis or parts thereof for financial gain shall not be allowed without my written permission. It is also understood that due recognition shall be given to me and to the University of Saskatchewan in any scholarly use which may be made of any material in my thesis.

Requests for permission to copy or to make other use of material in this thesis in whole or part should be addressed to:

Head of the Department of Mechanical Engineering

University of Saskatchewan

57 Campus Drive

Saskatoon, Saskatchewan S7N 5A9

Canada

**ABSTRACT**

In recent years, tissue engineering has shown great potential in treatment of injured tissues which aims to create artificial structures for cells to regenerate new tissues for replacing the damaged and diseased ones. The selection of scaffold materials is one of the critical factors affecting tissue healing process. Among a wide range of scaffold materials, chitosan (CS) has been demonstrated as an ideal material due to its biocompatibility, nontoxicity, biodegradability, antibacterial activity and favorable strength and stiffness. However, its insufficient mechanical properties limits its feasibility and scope for clinical application, especially for bone scaffolds. The main purpose of the study is to explore the potential of incorporation of nanofillers into CS to enhance the mechanical properties for tissue engineering. In this work, nanodiamond (ND) is applied and studied due to its high surface to volume ratio, rich surface chemistry, high mechanical strength, and excellent biocompatibility.

ND/CS nanocomposites with different diamond concentration from 1wt. % to 5wt. % were synthetized through a solution casting method. The microstructure and mechanical properties of the composites were characterized using scanning electron microscopy (SEM), X-ray diffraction (XRD), Fourier transform infrared spectroscopy (FTIR), Differential scanning calorimetry (DSC), and nanoindentation.

Compared with pristine CS, the addition of ND resulted in a dramatic improvement of mechanical properties, including a 239%, 276%, 321%, 333%, and 343% increase in Young's modulus and 68%, 96%, 114%, 118%, and 127% increase in hardness when ND amount is 1wt. %, 2wt. %, 3wt. %, 4wt. %, and 5wt. %, respectively. The strong interaction between ND surface groups and chitosan matrix is of great importance in changing polymer structure and improving mechanical properties. The cell viability and cytotoxicity of the nanocomposite were also studied using MTT (3-(4, 5-dimethylthiazol-2-yl)-2, 5-diphenyltetrazolium bromide) assay. The results show that the addition of ND has no negative effect on cell viability and the

nanocomposites have no cytotoxicity.

**ACKNOWLEDGMENTS**

I would like to express my most sincere appreciation to my supervisor, mentor, and dissertation advisor extraordinaire, Prof. Qiaoqin Yang. Without her expertise, advice, and encouragement throughout the research period, it would not have been possible for me to accomplish this research and dissertation. I would also like to thank other committee members Dr. Daniel Chen and Dr. Ike Oguocha. Their insight, feedback, and advice was influential and essential through the dissertation writing process.

I also want to thank Dr. David Schreyer, Dr. William Kulyk, and Dr. Safa Kasap for providing me with great valuable knowledge, comments in biomedical and material engineering area. I also appreciate it that Robert (Bob) J. Wilson. Technician Robert (Bob) J. Peace (Mechanical Engineering) and research associate Tuanjie Chang (Anatomy and Cell Biology) and Guosheng Liu (Biology) provided me with essential technical tutorial and assistance in using spectral analysis instruments, mechanical measurement apparatus and biological experimental equipment.

My special thanks are given to my group colleagues, also my friends Yang Lezhi, Zhang Chunzi, and Zhang Linlin, along with Liu Chenglin, Zhu Ning and Hou Huishu who have been working in Daniel Chen's research group of tissue engineering department. Their honesty and camaraderie have been accompanied by my growth. Without their love, encouragement and assistance, I would never have been through my toughest time and achieve my academic goals.

My sincere acknowledgement also goes to the support of scholarship from College of Graduate Studies and Research of the University of Saskatchewan in Mechanical Engineering.

Finally, I would like to express gratitude to my parents and all families who are living far away but never stopped loving or supporting me. What I have achieved today, I owe it to their constant love, high expectation and encouragement for all the time.

**DEDICATION**

I dedicated this work to my grandparents and parents for their love and support.

TABLE OF CONTENTS

**LIST OF TABLES**

**LIST OF FIGURES**

**LIST OF EQUATIONS**

## LIST OF ABBREVIATIONS

| | |
|---|---|
| 2D | Two dimensional |
| 3D | Three dimensional |
| AS-ND | As received nanodiamond |
| CNT | Carbon nanotube |
| CS | Chitosan |
| DIW | Deionized water |
| DMEM | Dulbecco's Modified Eagle Medium |
| EDC | 1-Ethyl-3-(3-dimethylaminopropyl) carbodiimide |
| EDTA | Ethylenediaminetetraacetic acid |
| FBS | Fetal bovine serum |
| F-ND | Functionalized nanodiamond |
| FTIR | Fourier transform infrared spectroscopy |
| HA | Hydroxyapatite |
| MEMS | Microelectromechanical Systems |
| MTT | 3-(4, 5-dimethylthiazol-2-yl)-2, 5-diphenyltetrazolium bromide |
| ND | Nanodiamond |
| PBS | Phosphate buffer solution |
| PA-11 | Polyamide -11 |
| PGA | Polyglycolic acid |
| PLGA | Polyglycolic acid |
| PLLA | Poly (L-lactic acid) |
| PVA | Poly (vinyl alcohol) |
| ROS | Reactive oxygen species |

| | |
|---|---|
| SEM | Scanning electron microscopy |
| SSA | Specific surface area |
| Td | Degradation temperature |
| Tg | Glass transition temperature |
| XRD | X-ray diffraction |

# CHAPTER 1 INTRODUCTION

## 1.1 Overview

Tissue engineering has shown great potential in treatment of injured tissues including bone tissues. Bone injuries as results of high impact sports, motor vehicle accidents, osteoporosis and tumors are one of the most common worldwide health concerns. Malfunction or loss of bone and bone tissue leads to dramatic degradation of people's life quality and may cause severe consequences both socioeconomically and psychologically. This situation is grim especially for people who are aged, suffer from obesity, and lack physical activity. Statistically, bone injuries occur at an annual rate of 2.4 per 100 population [1]. In the United States, there were over 2 million bone injuries in 2005, costing $17 billion. By 2025, annual bone injuries and costs are projected to increase by 50% and $25 billion, respectively [2]. The major therapy used for clinical treatments of bone repair and regeneration, to date, is conventional bone grafting. Annually in the United States, over half a million patients receive bone defect repairs [3]. However, problems still persist due to disease transmission and limited supply. Engineered bone tissue, as an alternative approach to treating bone injuries has shown great potential for bone injury treatment since the defected bones are repaired and regenerated over time using the biological substitutes instead of replacing them [4]. Nevertheless, its clinical application is limited by several challenges, one of which is to design a biodegradable and biocompatible scaffold with sufficient mechanical strength that is comparable to natural bone [5].

## 1.2 Objectives

This research aims to synthesize a functional composite material with desirable properties including biocompatibility, biodegradability and enhanced mechanical strength for tissue scaffolds with enhanced mechanical properties by introducing nanodiamond (ND) fillers to chitosan (CS) matrix. The interaction between CS and ND, the structural, mechanical and

biological properties of the composites are also investigated. The specific objectives were to:

1) Develop appropriate surface functionalization of NDs for improving affinity with matrix,
2) Fabricate of CS/ND composites with low ND agglomeration,
3) Characterize the microstructure of the composites to investigate the effect of ND incorporation, and
4) Evaluate the mechanical improvement, the cell viability, and the cytotoxicity of the composites.

### 1.3 Thesis Organization

This thesis is consist of five chapters. Chapter 1 presents the motivation, objectives and the organization of the thesis. Chapter 2 presents a comprehensive literature review on related areas and issues. Chapter 3 describes the techniques used for synthesis and characterization of the composite materials. Chapter 4 reports the results on structures and properties of the composite materials and has a discussion on the mechanisms involved. Chapter 5 summarizes and concludes the research work, and recommends future works.

# CHAPTER 2 LITERATURE REVIEW

## 2.1 Tissue Engineering

### 2.1.1 Introduction of Tissue Engineering

The term “tissue engineering” is first used by Wolter/Meyer in the literature in 1985 on the research of endothelium like layer on PMMA in the eye [6]. The generalized concept of “tissue engineering” was introduced in medicine by national science foundation of US in 1987 [7]. It was the first time that the authority of this term was established. The definition that was agreed on was: “Tissue Engineering is the application of the principles and methods of engineering and life sciences toward the fundamental understanding of structure-function relationships in normal and pathologic mammalian tissue and the development of biological substitutes to restore, maintain, or improve function” [8]. Tissue engineering is based on medical research combining multidisciplinary approach including cell and tissue culture approaches in late 1960s. In 1970s, W.T. Green conducted a series of experiments in order to generate cartilage in a bone scaffold with chondrocyte culture technique [9]. Even though the result was without any success, this approach of regeneration was recorded and further innovated. A milestone of development of tissue engineering was made by Dr. Joseph Vacanti from Boston Children’s Hospital and Dr. Robert Langer from M.I.T. Their article published in Science in 1993 opened up new possibilities for tissue engineering and brought this technology to the forefront of public discourse [10]. At present, tissue engineering shows its great potential and has been considered as one of the most prospective technologies. Significant research has been conducted by scientists from biology, material, engineering, and biomechanics, along with cell biology technique, molecular biological techniques, animal experiment technique, and biological materials synthesis, which has greatly promoted the development of tissue engineering.

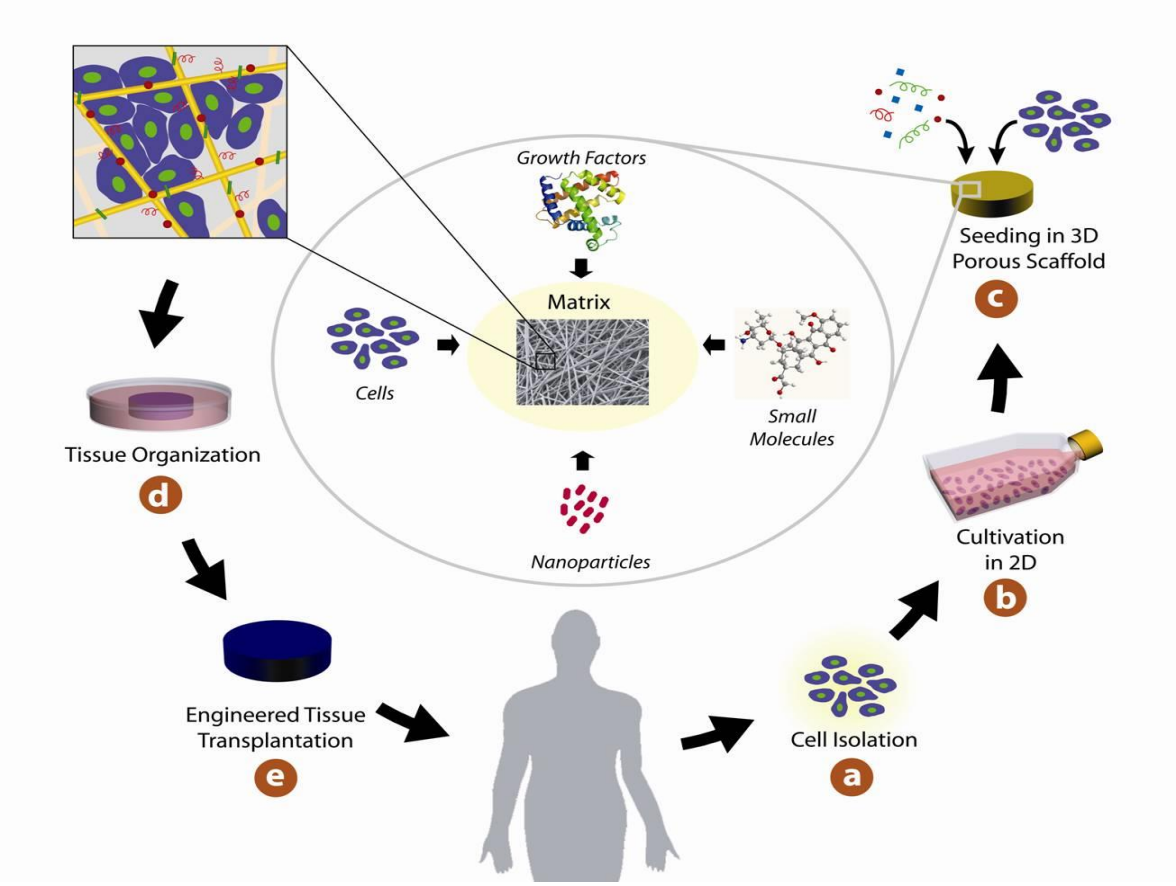


Figure 2.1. General principles of tissue engineering [11].

Tissue engineering aims to create artificial structures to repair and replace damaged and diseased tissues or organs. It involves viable cells, biomolecules, and a structural scaffold (Figure 2.1). At first point, cells are isolated from the individual. Different types of cells are extracted via various methods which usually include centrifugation of cells in fluid tissues such as blood cells while enzymes trypsin or collagenase technique are usually applied for cells in solid tissues. These cells are further cultured under a physiological condition.

The scaffold is a structure to support cell migration, growth, attachment, and differentiation, and to maintain the tissue development and organization in a mature and healthy state. To reach these goals, scaffold are usually fabricated with biodegradable materials, which are capable to dissolve themselves over time within the period of tissue formation, so the second surgery is not required. Besides, a high porosity is also necessary for cell seeding. After the scaffold is

seeded with cells and bathed with right growth factors, cells begin to multiply and fill up the scaffold. Subsequently, once the cells have attached and begin to grow, the scaffold will be implanted into the body. Initially, scaffold will provide a mechanical structure which will break down as the gradual dissolving of itself, the mechanical load will be taken over by the newly formed tissue. Eventually, blood vessels will invade the new tissue and make the new tissue blended with the surroundings.

### 2.1.2 Bone Tissue Engineering

#### 2.1.2.1 Bone Fundamentals

The human skeleton gives the body a shape and provides physical support for the system contained within. It also forms the part of muscular system that enables the people to move. Bones provide protection for organs and also store minerals. They are strong but have a relatively light weight. Composed of periosteum, bone tissue and marrow, bones have rich blood vessels and living cells which help them grow and regenerate.

##### 2.1.2.1.1 Hierarchical Structural Organization of Bone

Five types of bones can be found in human body including long, short, flat, irregular and sesamoid bones. Specifically, long bone has greater dimension in length than width; short bones are cube shaped ones of the wrist and ankle which form within tendons; flat bones are thin, flattened and slightly curved, with a layer of spongy bone in between two parallel layers of compact bones, sternum, and most skull bones are flat bones; irregular bones as implied by their name are the ones with complicated shapes such as vertebrae and hip bones; the last one is sesamoid bone. Embedded in tendons, patella is the only sesamoid bone in human body which is also known as knee bone.

A typical long bone structure contains two typical bone textures: compact bone and spongy

bone, as depicted in Figure 2.2. The compact bone has a dense outer layer and also called cortical bone. It is composed of osteons (150-250 μm in diameter), each of which is centered around one to two blood vessels in the central or Haversian canal (25-50 μm in diameter). The spongy bone contains a network of trabeculae where the red bone marrow is located producing blood cells. At the top end of long bones, epiphysis plates separate the spongy bone location which are basically referred to as growth place while next to it is the proximal epiphysis where the cartilage attaches to tendons or ligaments. The diaphysis is the center of the bone as the shaft, inside which periosteum resides. Periosteum is the outer, fibrous, protective layer covering the entire bone. In the middle of hollow structure diaphysis, there is another type of marrow comprised of adipose tissue and yellow bone marrow. The space that contains yellow marrow is the medullary cavity. Articular cartilage is the pad of hyaline cartilage on the epiphyses where long bones articulate or join. It covers the surface at the end of spongy bone for reducing the friction and absorbing shock.

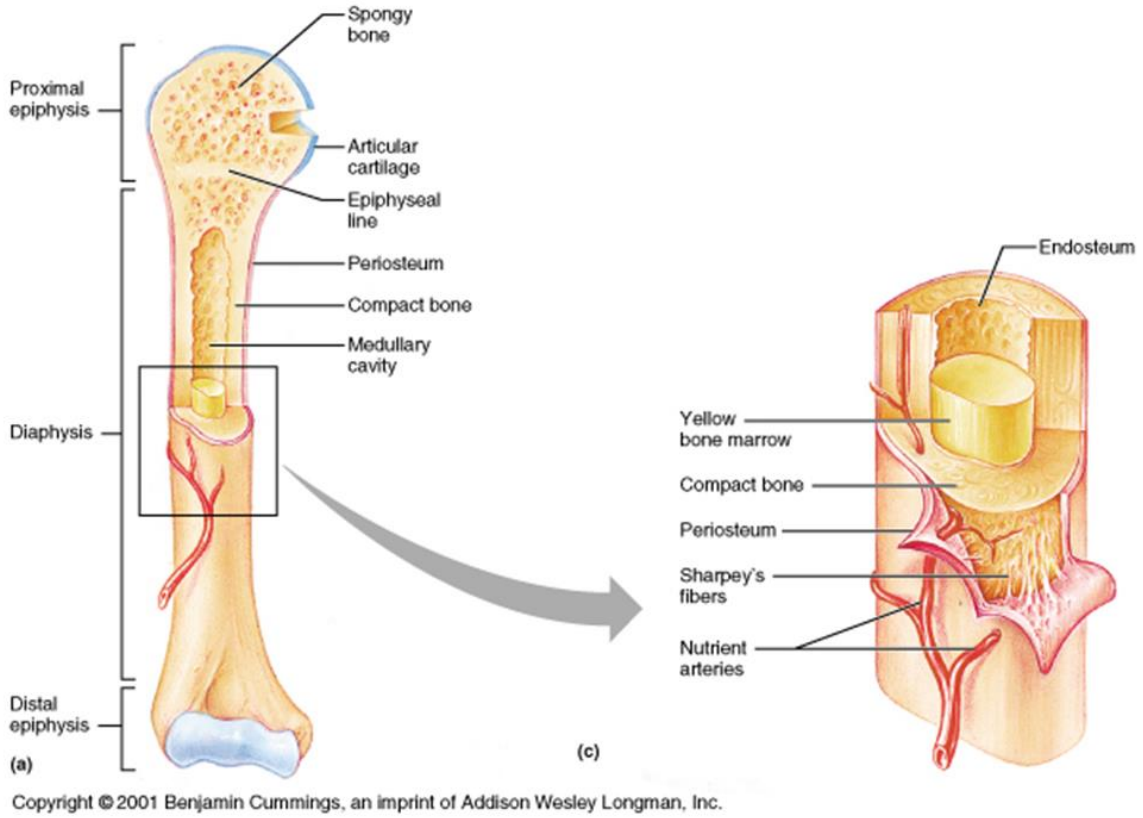


Figure 2.2. Microscopic structure of a typical long bone [12].

Osteon or Haversian system (Figure 2.3) is the unit of compact bone. They are ring-like circles (150-250 μm in diameter). Through the central canal (25-50 μm in diameter) part of osteon, which is also known as Haversian canal, the blood vessels distribute in vertical way. The 10-20 layers of osteon are called lamella, and in between each two layers osteocytes or bone cells are distributed in lacuna.

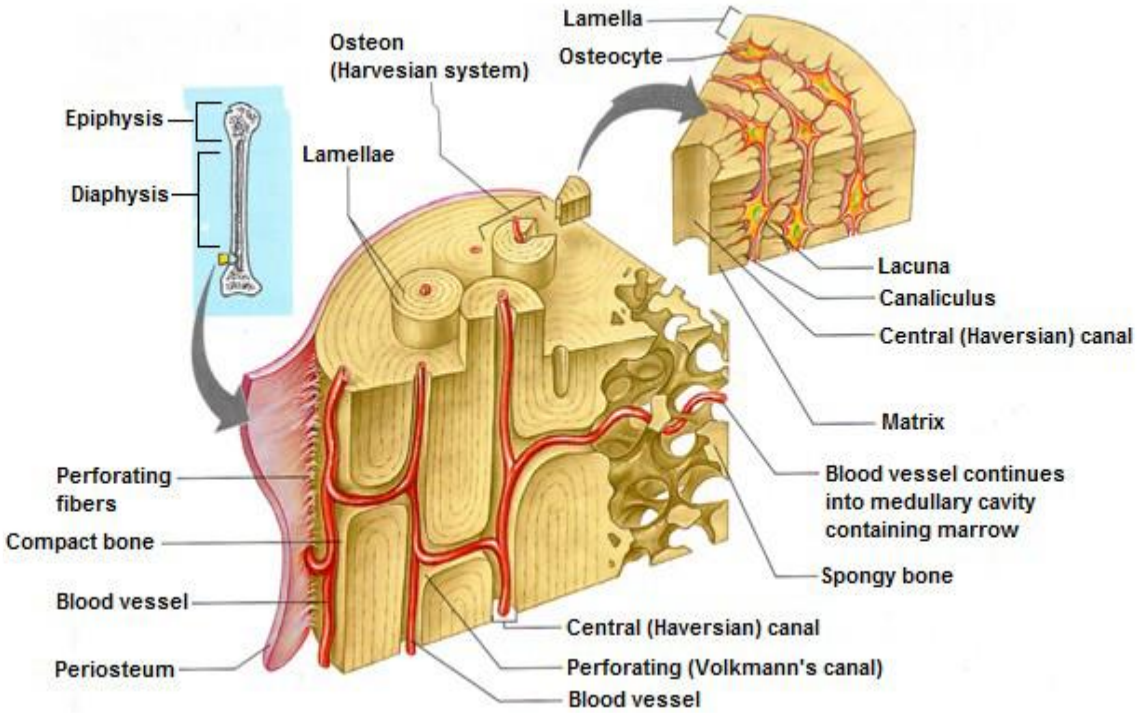


Figure 2.3. Bone structure and Haversian system [13].

Lamella (3-7 μm in thickness) further breaks down to collagen fiber bundle. Collagen fibrils in each bundle are tightly and parallelly bound to each other with a diameter of 30-80 nm. Orientation of bundles differs in different lamella layers.

Plate-like and needle-like organized carbonated hydroxyapatite (HA) crystals are located in interzone of collagen fibrils or collagen fibers (Figure 2.4). The mineralization crystals have a width of around 20 nm, thickness of 1.5-5nm and 40-60 nm in length. These collagen fibrils and mineralization crystals along with vitronectin, laminin and fibronection make up the extracellular matrix.

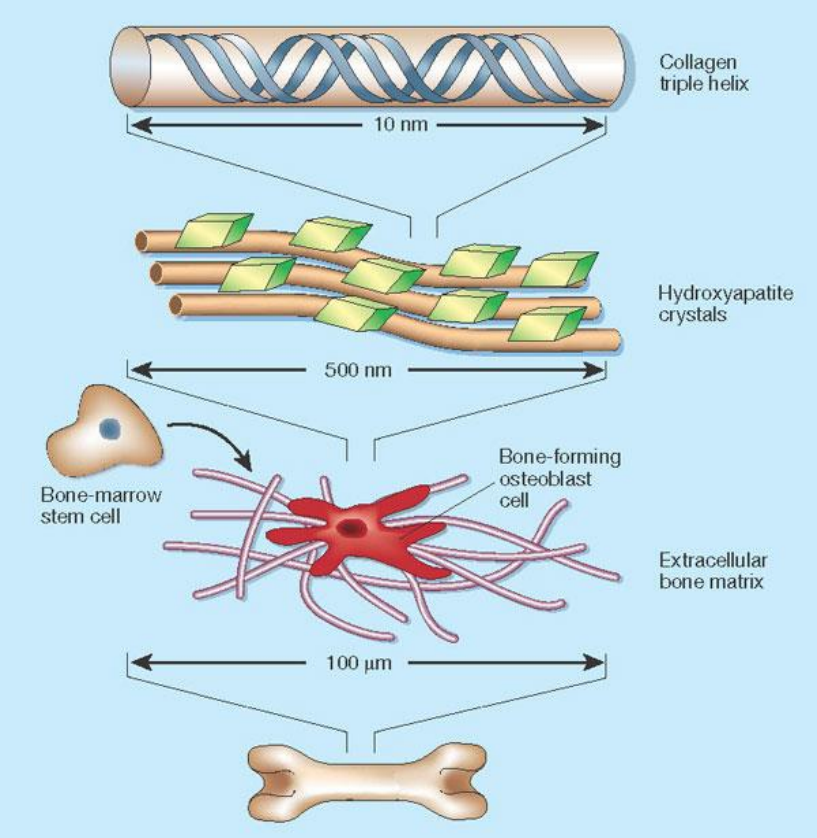


Figure 2.4. Collagen fibrils and mineralization crystals arrangement in bone [14].

#### 2.1.2.1.2 Organization of Bone

Bone tissue is a type of connective tissue with the constitution of various cells and calcified cell matrix (bone matrix). Bone matrix consists of 60%-70% inorganic components and 30%-40% organic components which are organized in a way so that bones possess enough strength to support and protect organs and bodies while maintaining a lightweight.

Inorganic components, also known as bone mineral, are mostly needle-like or plate-like carbonated hydroxyapatite crystals (HA, $Ca_{10}(PO_4)_6(OH)_2$), orienting along the longitudinal direction of collagen fibers bundle. Besides, bone matrix also contains magnesium, sodium, potassium ions as well as some microelements such as zinc, manganese, molybdenum and fluorine. Bone tissue preserves 99% of calcium in human body. This warehouse of calcium serves multiple functions such as adjusting calcium equilibrium and keeping stability of inorganic environment in the body. The organic part is mainly composed of collagen and

amorphous matrix. Most of collagen is Type I while there are also a few Type V. Collagen accounts for 90% of the organic part. Amorphous matrix is mostly gelatin, consisting of protein polysaccharide such as chondroitin sulfate and keratan sulfate. The framework of amorphous matrix allows stem cells to occupy the vacancy and serve an adhesion function for collagenous fiber. Besides, noncollagenous glycoproteins of amorphous matrix offer binding sites between calcium ion and hydroxyapatite which will improve the affinity and play a vital role in bone development and regeneration. Extracellular matrix provides mechanical strength as well as a key effect on cells adhesion, proliferation and differentiation. Therefore, it is of great importance to have an in-depth understanding of how extracellular matrix works. The research in this regard, ranging from the early research of HA applied material, inorganic/organic composite material to nano scale scaffold material, reflects a progressive development of material from macroscopic to microcosmic scales and an increasing adaptation in anatomic and functional aspects.

Osteogenic cell is located in periosteum which covers the outside of bone. Stem cell has a potential to differentiate into osteoblasts and osteoclasts.

The osteoblasts are responsible for the formation of new bone. Osteoblasts are fusiform or triquetrous small cells which originate from the differentiation of osteogenic cell or the periosteum and the marrow. The progress of development, differentiation and gene expression of this functional cell can be divided into three steps: reproduction period, mature period and calcification period. The osteoblast builds up collagen fibers to form a framework first on which calcium phosphate can be deposited and hardened. There are two main functions of osteoblast: compounding and secreting organic ingredients osteoid of extracellular matrix. In this process, the osteoblasts will be remained and trapped inside gradually, become osteocyte and begin to participate in bone resorption and metabolism.

The osteoclasts are lager cells in Howship's lacuna which are responsible for the breakdown

of bones. Osteoclasts have rich phosphatase and tartrate-resistant acid phosphatase. These enzymes released will breakdown the bone tissue for the osteoclasts to resorb. In a few weeks' time, the bone will be absorbed and finally become calcium and phosphorus ions. The interaction of osteoclasts with osteoblasts is very important in bone remodeling.

#### 2.1.2.1.3 Development of Bone

Development of bone originates from mesenchymal during embryonic period. The mesenchyme is a connective tissue in germinal layer, consisting of multipotent precursor mesenchymal stem cells and amorphous matrix. In accordance with the ways of transformation from a preexisting mesenchymal tissue to bone tissue, there are two developmental modes of bone formation, which are intramembranous ossification and endochondral ossification.

Intramembranous ossification primarily takes place in the bones of skull, jaw and collar. During the process, mesenchymal cells proliferate and condense along with the invasion of blood vessels. Then they form connective forms which is a membrane like layer. Subsequently, some mesenchymal stem cells differentiate into osteoblasts. Osteoblasts secrete collagen proteoglycan matrix that result in the binding of calcium salts. With the calcification of osteoid, more osteoblasts are separated from calcification region and become bone cells. As calcification proceeds, bony spicules radiate out and form the primordial bone tissue known as the ossification center. Bony spicules interlace reticulately becoming primordial trabecular bone. As the space is further occupied entirely, irregular concentric circle plate is formed on surface which constitutes part of the original Haversian system.

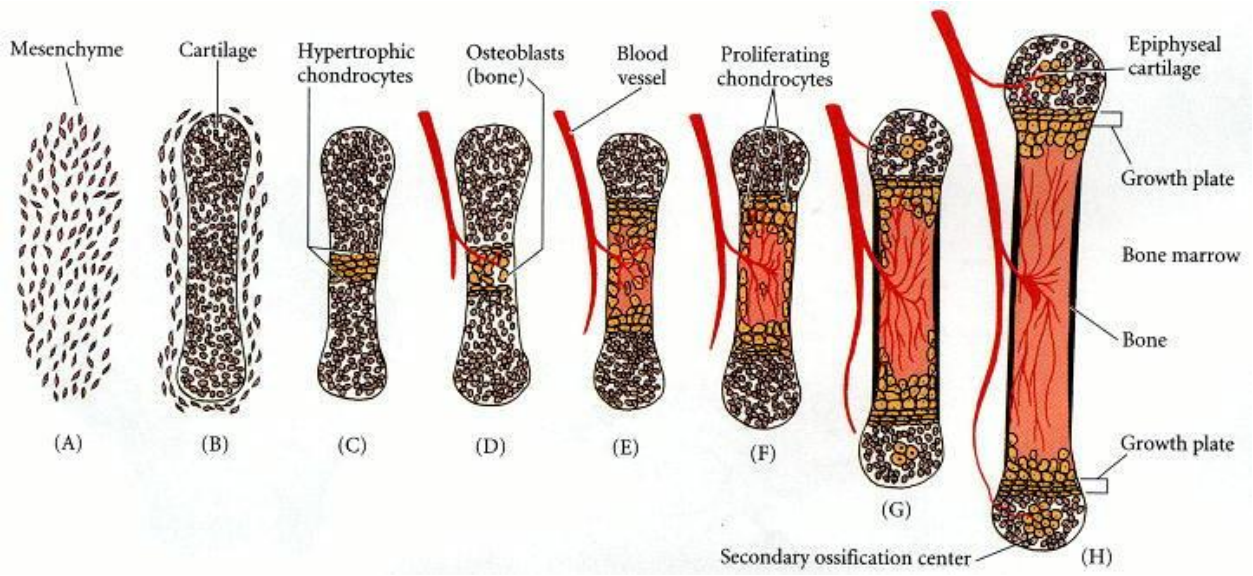


Figure 2.5. Schematic diagram of endochondral ossification [15].

In endochondral ossification as shown in Figure 2.5, cartilage is initially generated as the "model" of the bone to be replaced. Chondrocytes at the center enlarge and begin to die first which is known as the primary ossification center while the place where the next round of death occurs within epiphyses is called secondary ossification centers. As the matrix starts to calcify, blood vessels and nerves begin to invade. In the meantime, the periosteum formed around the bone starts to produce osteoblasts. Osteoblasts then get trapped by hard extracellular matrix as osteocytes forms spongy bone. Concurrently, the periosteum continues to produce osteoblasts until there is no space for them to enter the spongy bone. Then they start building up around the periphery of the spongy bone and eventually form compact bone along the outside of spongy bone.

#### 2.1.2.2 Bone Injuries and Conventional Therapies

Bone injuries are medical conditions including a variety of bone failure such as bone fracture, bone missing, and bone disease. Bone injuries can be caused by trauma injury, osteoporosis, bone cancer, and osteogenesis imperfecta. Bone, when injured, has the ability to

gradually regenerate and heal the damaged part at a very slow rate. However, this process requires fracture to be small rather than large. Severe fracture needs bone replacement or other major treatment. For nonunion fractures, lumbar spine fusion, joint arthrodesis, or revision arthroplasty, bone grafts are surgical procedures that are currently utilized in a wide array of clinical settings to fix these issues because they are histocompatible and non-immunogenic, and they possess all necessary properties required of a bone graft material such as bone morphogenetic proteins (BMPs) along with other essential osteoinduction, osteoconduction components and porous structure. However, reported by a number of studies, the considerable shortcomings and limitations of the current clinical treatments for bone repair and regeneration including autologous and allogeneic transplantations using autografts and allografts still exist.

In autografts (grafted tissue is from patient's own tissue), reported by Goulet [16], harvesting bone from the patient's iliac crest may result in high morbidity up to a probability of over 30% including bleeding, infection, chronic pain and inflammation at the harvest site. Harvesting cartilage tissue may cause difficulty in restoring proper joint architecture and altered load bearing capacity. In addition, any bone tissue harvesting requires a second surgery which is also an increase of risk. Allografts is an alternate technique (grafted tissue is taken from another person) due to the high morbidity and limited supply of autografts which is considered as the second common technique used clinically. It involves three types which are undermineralized, freeze-dried bone allograft (FDBA) and demineralized bone matrix (DBM). Even though allograft is also osteoconductive, no donor site morbidity, and available in different shapes and sizes, compared with autografts, the risks of immunoreactions (immunogenic rejection) and transmission of infections are more often associated with allografts. Moreover, because the donor grafts are devitalized via irradiation or freeze-drying, osteoinductive properties are reduced to make it more difficult to direct bone tissue repair [17]. Thus growth factors and osteogenic cells have to be incorporated in allografts procedures.

Besides, allografts market is also experiencing an obvious insufficient supply and unmet demand with limited obtainable quantities [18]. Other commonly used bone repair techniques involve intramedullary nailing; plating; dynamic external fixation, electric stimulation, and mosaicplasty which uses several small grafts to fill a single defect [19]. In spite of the disadvantages of each technique, these mentioned techniques have been shown to improve repair of bone. However, none of the current treatment are capable of repairing bone defects and regenerating tissue that demonstrates chemical and physical properties similar to native bone tissue. The primary challenge is still to find or fabricate a material provided with high native bone-like characteristics such as high load bearing, osteoinductive, low patient morbidity, structure flexibility, sufficient supply and reasonable costs.

The number of patients who have bone damage caused by trauma, congenital malformation, inflammation and tumor has been increasing in recent years. In the United State alone, over half a million patients receive bone defect repairs, with a cost of over billions of dollars [20]. The current clinically available solutions for these problems rely on bone graft which is defined as a medical treatment to replace damaged bone with the bones from patient, other people or bone banks. However, as discussed above, in addition to the expensive procedure and limited supply, some complications may also occur, such as bone nonunion and blood loss, incidence of postoperative infection and risk of disease transmission. Engineered bone tissue is a potential candidate with plenty of supply and features to avoid disease transmission for the bone injury treatment, and has aroused interest in scientific communities for decades.

Bone tissue engineering involving various combinations of materials and biologics thus offers an alternative strategy for repairing and restoring the function of bone. The principle of that is to cultivate osteoblast in vitro and implant them with scaffolds into the damaged part. Biodegradable part of scaffold goes through degradation process and finally are absorbed or discharged by circulatory system while inorganic components dissolve and the particles are

re-arranged with calcium to become bioactive bone tissue [21, 22].

Compared with auto graft and allograft, synthetic scaffolds implantation is more effective and has better performance. Less seed cells are needed, which could be further cultured in vitro; less immunogenicity are needed to be fabricated into accurate three-dimensional shape according to specific circumstance. In the past decade, a great number of synthetic scaffolds have been designed and investigated which drives forward bone engineering dramatically.

The strategy in bone tissue is based on the seeding and in vitro culture of primary osteoblast cells on a three-dimensional scaffolds. These structures would be finally implanted into a bone defect. The cells would generate the extracellular matrix of new bone tissue, where the scaffold would provide a 3D environment for the cells to adhere, proliferate, and differentiate.

On the basis of tissue engineering, bone tissue engineering includes seed cells, bioactive factor and scaffold. Seed cells are typically set as osteoblast or stem cells, due to a strong ability of proliferation and potential of multi-directional differentiation. They can be expediently separated, extracted, cultured and purified, thus, are one of the most advantageous and ideal seed cells for bone engineering. Bioactive factor from autocrine and paracrine is polypeptide include bone morphogenetic protein (BMP), transforming growth factor (TGF-b), insulin-like growth factor (IGF), Fibroblast Growth Factor (bFGF).

Scaffold is the key to bone tissue engineering which acts as the carrier for osteoblasts and BMSC to adhere, structure supporter for proliferation and differentiation, guiding the regeneration of tissue and vessels. Therefore, an ideal scaffold should have the following characteristics: preferable biocompatibility to maintain eumorphism of seed cells; appropriate biodegradation with no inflammation immune response occurs during the process; an adjustable rate of degradation that is comparable to tissue regeneration; feasibility to fabricated in three-dimensional interconnected porous structure for cells adhesion, proliferation, and deposition of bone matrix. Besides, scaffold should also be able to provide an adequate initial

mechanical support for cells, as for bone tissue scaffold, similar mechanical properties to natural bone are desirable; last but not least, scaffold should provide surfaces that can be modified and combined with bioactive components to assist bone regeneration.

## 2.2 Scaffold Materials

The selection of biomaterials for tissue engineering plays a key role in achieving desired scaffolds. Of all types of materials, natural and synthetic biodegradable materials are the first choice. Degradable materials in human body can be easily absorbed or removed with metastasis, thus a secondary surgery is no longer required. Certain materials such as polystyrene, poly-l-lactic acid (PLLA), polyglycolic acid (PGA) and poly-dl-lactic-co-glycolic acid (PLGA) [23], as well as collagen [24], alginate [25] and chitosan [26] have been widely investigated and designed for different functional features and properties for the feasibility of clinical applications. However, in many applications, particularly for bone scaffolds, the strength and stiffness of aforementioned polymers are not sufficient.

### 2.2.1 Conventional Bone Tissue Engineering Scaffold Materials

Conventional materials for bone scaffold are commonly porous, composite materials comprised of ceramics, synthetic polymers, natural polymers, or other biomaterials [27].

Ceramic scaffolds typically have high mechanical stiffness, but low elasticity. From the aspect of bone, they have excellent biocompatibility due to their chemical and structural similarity to the mineral phase of bones. Numerous research of 1960s showed that the osteoconduction and ion-exchange properties of ceramics can promote their interactions with osteogenic cells, which is important for bone differentiation. In the late 1970s, ceramics have been used for coating implant surface to enhance integration with the host bone. In 1985, Furlong and Osborn first applied ceramic coating to femoral components, and this technique

was also used in dental and orthopedic surgery to fill bone defects subsequently [28]. Nevertheless, their drawbacks are obvious. Brittleness, difficulty of shaping for implantation and difficulty in controlling degradation rate limit further application.

Polylactic acid (PLA), poly-l-lactic acid (PLLA), polyglycolic acid (PGA) and poly-dl-lactic-co-glycolic acid (PLGA) are aliphatic polyesters synthetic polymers, and have been widely used in the field of tissue engineering as the most common artificial extracellular matrix. Many techniques such as gas foaming, phase separation, suoercritical fluid processing and 3D printing for specific shape and microstructure facilitate the fabrication of scaffold materials. The degradation products of polylactic acid and polyglycolic acid are lactic acid and glycolic acid which participate in the reaction of tricarboxylic acid cycle (Kerb's cycle) can be excreted from the body. But drawbacks still exist such as poor hydrophilia, insufficient mechanical properties, lack of cellular recognition site, and risk of rejection due to reduced bioactivity. It is difficult to control degradation rate of individual polymer, an over rapid rate can decrease regional pH, and result in cell and tissue aseptic inflammation.

Natural materials have also been proved as suitable materials for scaffold constructions because of their biocompatibility. These materials are collagen, the main composition of bone tissue and extracellular matrix, proteoglycans, alginate, chitosan, and etc. Typically, natural polymers are more biologically active, and exhibit excellent cell adhesion. However, problems still remain due to high fabricating cost, sophisticated technological process, and immunogenicity present. Especially for bone tissue engineering, their poor strength does not match physical demand of the healthy surrounding bone and may not provide stable structure for cell growth as bone scaffolds. Ideally, the scaffold should be provided with enough mechanical strength for surgical handling during implantation and support the load that bone would sustain until the natural bone can regenerate at the surgery site. The mechanical properties of bone vary widely with density. Cancellous bone, as an example, has 50-500 Mpa

modulus which can serve as design goals for bone regeneration.

### 2.2.2 Polymer Nanocomposite Materials for Bone Tissue Engineering

It is noticed that even though ceramics, synthetic and natural materials have been well developed and modified for bone tissue engineering, there are still difficulties for a single material to meet all requirements for mechanical, biological and functional properties. This necessitates considerable research in developing composite scaffolds comprising a number of phases as novel materials for bone tissue engineering. Composite materials are aiming to imitate the composite of natural bone and obtain combined effect to eliminate the disadvantages of individual material, of which, polymer based nanocomposite materials are very promising. To date, much effort has been made on developing and designing such composites with fillers in nanometer scale. For example, alkaline fillers are used to neutralize the acidic degradation products of polylactic acid. Inorganic HA incorporated collagen is designed to provide compressive strength and generate bioactivity [29]. Of recent promising hybrid materials, the nanocomposite system with nanoscale ceramic fillers and polymer matrix has shown great performance improvement because the nanosized inorganic component is likely more bioactive than a micro-sized one. Fillers in nanoscale, when interacted with polymer matrix, result in a larger surface area following a function shown in Figure 2.6. When the nanofillers interact with the polymer matrix, a new interphase forms. If this interphase is strong, the load and heat will be transferred from polymer matrix to the nanofillers. Smaller size of the fillers will result in larger specific surface area (SSA), which means that the contact and interacting area between polymer matrix and fillers is larger. The interphase plays crucial role in determining the properties of the composites. Appropriate selection of matrix and fillers along with certain treatment can significantly increase the quality of the interphase and thus lead to great improvement in mechanical and thermal properties. Besides, due to high surface

area to volume ratio, highly porous scaffolds with exceptional mechanical properties can be fabricated with a wide variety of topographical features that encourage cell adhesion and proliferation.

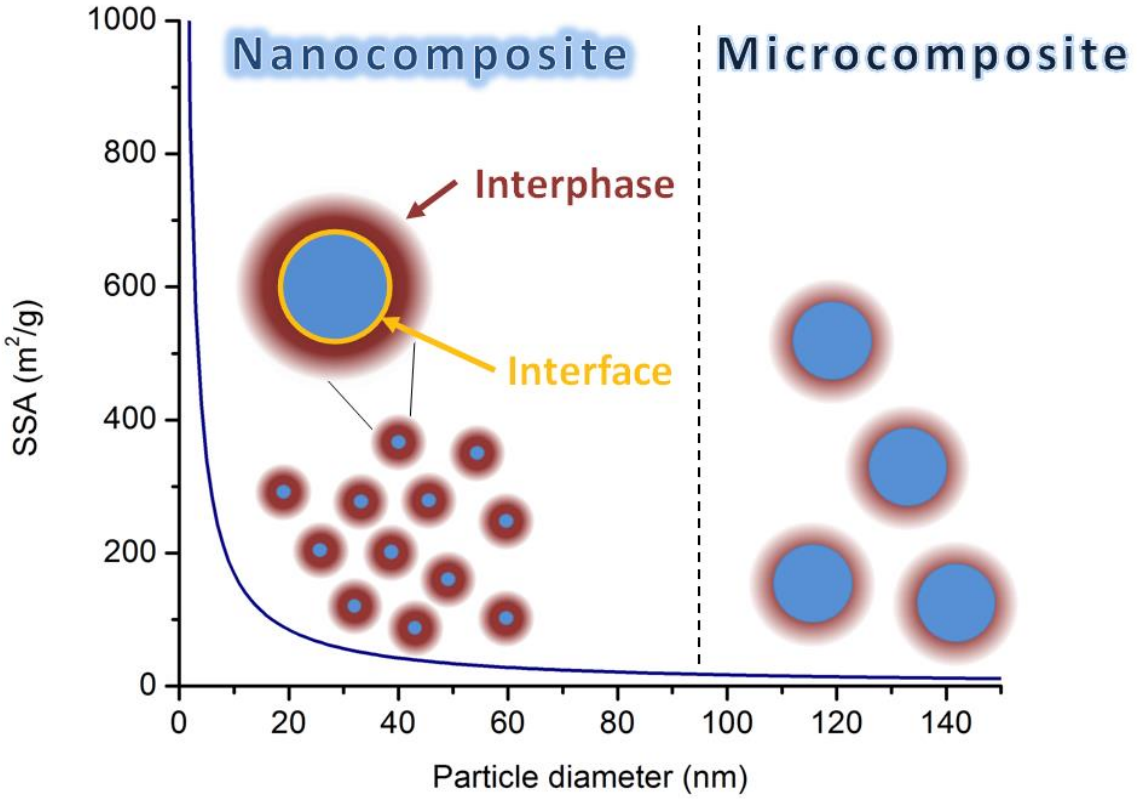


Figure 2.6. Specific surface area (SSA) as a function of particle diameter. Nanocomposite is defined as the composites containing particles smaller than 100 nm [30].

Although composite materials combining two or more phases with enhanced functions and features extend the options of scaffold for bone tissue engineering significantly and gives a direction of future research on optional scaffold materials for bone tissue engineering, obstacles and challenges still exist: one challenge is to achieve a strong interphase between polymer matrix and fillers. As discussed previously, the interphase is the key part that dominates the eventual properties of the composites. Fillers without any potential chemical radicals or chemical groups may not interact with polymer matrix. Instead of improving mechanical properties, fillers in this type are regarded as defects where crack growth may

increase and lead to mechanical instability. Another major challenge is to obtain a uniform dispersion without massive agglomeration. Owing to the high surface energy, fillers in nano scale tend to agglomerate to reduce surface area. Other factors including surface charge, structure and matrix viscosity also have effects on agglomeration of nanofillers when incorporated into polymer matrix. One common method to reduce this Van der Waals attraction was using ultrasonication [31, 32].

### 2.2.3 CS/ND Scaffold for Bone Tissue Engineering

**CS polymer matrix**

CS is a linear polysaccharide (Figure.2.7), obtained from the deacetylation of chitin which is the primary structural polymer of the exoskeleton of crustaceans, cuticles of insects, and cell wall of fungi [33, 34].With an estimated annual production of 13.7 thousand metric tons for 2010 and a world market of 1.3 billion US dollars per year, which is expected to be 4.22 billion in 2020 [35], CS has been for a wide array of applications in food processing, for example, to decrease germination and outgrowth of Clostridium perfringens spore during the process of chilling ground beef and turkey, and prevents oxidation in food products [36], as well as wastewater treatment, agriculture. Besides, in supplement realm, CS as an “excellent fat trapper due to its remarkable property of binding with lipids and fats is also recommended as an ad-in. As more innovatory applications have been approved in recent years by FDA for commercializing of patents, CS is more extensively used especially in biomedical areas. CS was first discovered by Rouget in 1895 [37] and later named by Hoppe seyler in 1894[38]. It is composed of glucosamine and N-acetyl glucosamine with β(1-4) link. The molecular weight of CS may ranges from 300 to more than 1000 kDa [39]. Degree of deacetylation (DD) is a key feature of CS affecting its crystallinity, biodegradation, cell attachments and proliferation [33]. It has been reported that high DD CS may trigger inflammation [40]. Amount of free amino and

N-acetyl groups determines solubility of CS. In acidic environment, CS can be dissolved completely in acid solution which makes it feasible to be produced in shapes of any required structures: microspheres, membranes, sponges, fibers, and 3D porous etc. for scaffold fabrication [39]. From the point of biological properties, cationic nature of CS allows electrostatic interactions with anionic glycosaminoglycans (GAGs) and proteoglycans. CS solution under a pH less than 6.5 carries a high value of positive charge which interact with the negative surface of living tissues such as proteins, nucleic acids to obtain electrical neutrality [41].

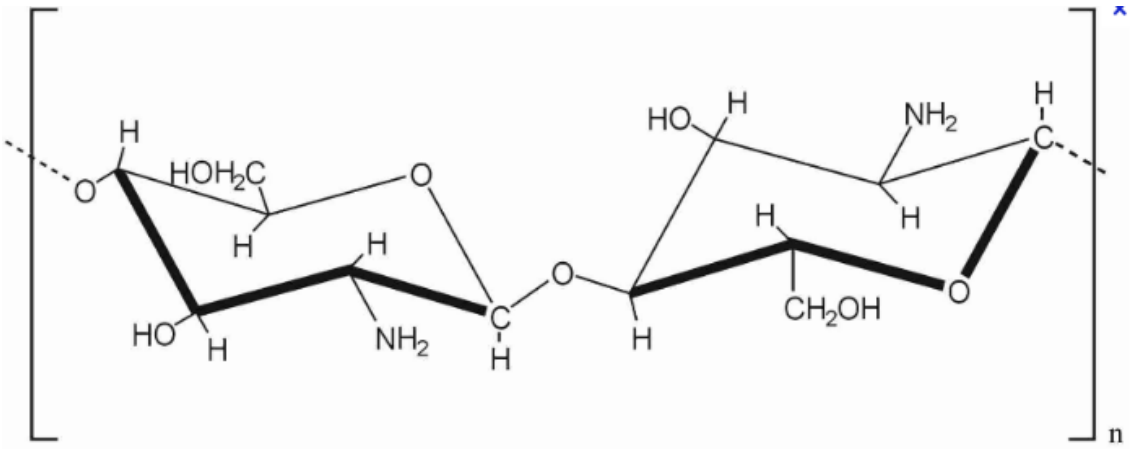


Figure 2.7. Chemical Structure of CS, composed of distributed β-(1-4)-linked D-glucosamine (deacetylated unit) and N-acetyl-D-glucosamine (acetylated unit) [41].

As a promising scaffold material for bone tissue engineering, CS has demonstrated essential features including biodegradability and biocompatibility [42-44]. Previous research indicated CS could be a potent wound-healing accelerator [39], cytokines producer [45], and can inhibit infection [46]. Abundance of free amino groups also allows various chemical modification for specific purposes. Due to a number of key advantages, CS shows great research value in fabricating scaffolds and is definitely a favorable choice as the matrix of composite scaffolds.

Therefore, numerous CS matrix scaffolds have been proposed and developed in recent years including glutaraldehyde cross-linked CS/collagen [47], PLLA–CS–HA composite scaffolds

[48], CS-alginate hybrid scaffolds [49] and Carbon nanotubes (CNT) modified CS [50]. However, with efforts made in the last several decades, CS have not been used in clinical practice. Rather than proposed improvements, drawbacks and side effects appear and become its limitations. For example, glutaraldehyde, as a biofunctional crosslinking reagent, can bridge amino groups between two adjacent polypeptide chains. It has been reported that glutaraldehyde is used as crosslinking agent because of its water solubility, high cross linking efficiency and low cost [51]. However, several studies in late $20^{th}$ century indicated that glutaraldehyde has a high acute inhalation toxicity and impairs the biocompatibility of biomaterials including CS [52]. CNTs were once considered as promising filler materials for polymer enhancement, but their applications have been inhibited by the poor dispersion, weak bonding with polymer chains, and cytotoxicity [53-55]. HA with content less than 10wt. % did not change the mechanical properties significantly as previous reported [56], while a higher proportion causes difficulties in degradation rate control [57, 58]. Some research also indicated that without a proper treatment, it may cause phase segregation and non-homogeneity in the structure and poor adhesion between components and HA might lead to a decrease in the compressive strength and other mechanical properties [59].

**Nanofillers for polymer matrix**

Nano fillers are incorporated into polymer matrices at rates from 1% to 10% (in mass) [60], and can be categorized according to either dimension (Table 2.1) or their organic status. Graphene is an example of 2D filler whereas CNT is defined as 1D filler. Particles like nano silica ($SiO_2$), titanium dioxide ($TiO_2$), and calcium carbonate ($CaCO_3$) are inorganic 0D fillers. Correspondingly, coir nanofiller and cellulosic nanofiller derived naturally and defined as organic fillers are also applied to polymer matrix.

A perfect candidate filler in polymer matrix for biomedical applications require numerous

factors: high strength and stiffness, resistance to corrosion in natural hazardous environment, nontoxicity, biocompatibility and low costs.

Table 2.1. Classification of nano fillers [61].

| **One-dimensional nano fillers** | **Dimensional measurement (Thickness)** | **Two-dimensional nano fillers** | **Dimensional measurement (Diameter)** | **Three-dimensional nano fillers** | **Dimensional measurement (All dimension)** |
|---|---|---|---|---|---|
| Plates < 100nm | | Nano tubes < 100nm | | Nanometric < 100nm | |
| Laminas < 100nm | | Nano fibers < 100nm | | Silica beads | |
| Shells < 100nm | | | | | |

a) Carbon Nanotubes (CNTs)

CNTs were discovered in early 1990s [62] and attracted great attention since then. CNTs are allotropes of carbon with a cylindrical nanostructure that can be categorized into three types: Single-wall CNTs (SWCNTs), Double-wall CNTs (DWCNTs) and Multi-wall CNTs (MWCNTs). These nanotubes present unique properties such as high stiffness, high heat conductivity (up to $3000 W.m^{-1}.K^{-1}$), and high Young's modulus (up to 1TPa for SWCNTs, 270 - 950GPa for MWCNTs) [63]. With all these properties, CNTs have been extensively used as nanocomposite fillers to enhance polymer properties for drug delivery, biosensors, and diagnostics etc. [64-66]. However, reports have claimed that CNTs could be poor in dispersion and weak in interacting with polymer matrix [67]. Besides, considerable experimental data related to CNT toxicity has been released such as oxidative stress, inflammatory responses, malignant transformation, DNA damage and mutation [68]

b) Nano-Silica

Nano-silica as another nanofiller has been investigated to enhance polymers, and proved to have the ability to improve in vitro biological features of scaffolds [69]. However, numerous reports are claiming that the addition of nano-silica results in decrease in the nanocomposite

tensile strength. This implies that the nanoparticles in the composites might agglomerate and cannot provide load-bearing capacity due to their weak bonding with the polymer matrix [70] [71].

c) HA

HA has been extensively used to fabricate implant owing to its similarity with mineral constituents found in hard tissue (i.e. teeth and bones) [72, 73]. Owing to its high level of biocompatibility, it is a common material for fabricating dense and porous bioceramics [74]. Nonetheless, sintered HA bioceramics cannot be applied as heavy load-bearing bones due to its low mechanical properties [75]. Thus, it's applications are limited to bioactive constituency in composites, coatings on metal implants and granular fillers for direct incorporation into human tissues [72-74].

d) NDs

NDs were first produced by detonation in the USSR in 1960s, but they remained essentially unknown to the rest of the world until the end of 1980s [76]. At the beginning in late 1990s, a number of important breakthroughs led to a wider interest in these particles [77]. With outstanding properties of super hardness, high Young's modulus, superior thermal conductivity and biocompatibility, ND is considered as a very promising material for various applications in the fields of chemistry, optical spectroscopy, physical and mechanical engineering, biological and biomedical engineering, and so on [78].

NDs produced by detonation is composed of nano-scale particles in a diameter of around 5 nm. A ND particle consists of an inert diamond core terminated with rich surface functional groups (Figure 2.8). The chemical reactivity on surface allows a variety of wet and gas chemistry techniques to be employed to tailor the properties of NDs for specific purposes, such as biomolecules attachment for drug delivery [79], microelectromechanical (MEMS) devices [80] and cardiovascular devices [81]. The primary core of detonation ND is $sp^3$ hybridized

carbon, by sharing carbon-based composition with many biological components, ND is stable and presents a biocompatible interface with no generation of reactive oxygen species (ROS) include oxygen ions and peroxides which are chemically reactive molecules containing oxygen [82]. It has also been claimed that ND can be internalized at a variety of concentrations by individual cells and expelled through body circulatory system [83]. Due to these features, ND has been studied for biomedical applications as a composite additive, a drug delivery carrier, a multiple radical donor, implants and coating materials [84]. Therefore, this work purposely chooses ND as a filler in CS matrix because of its non-cytotoxicity and modification potential compared with most other filler materials.

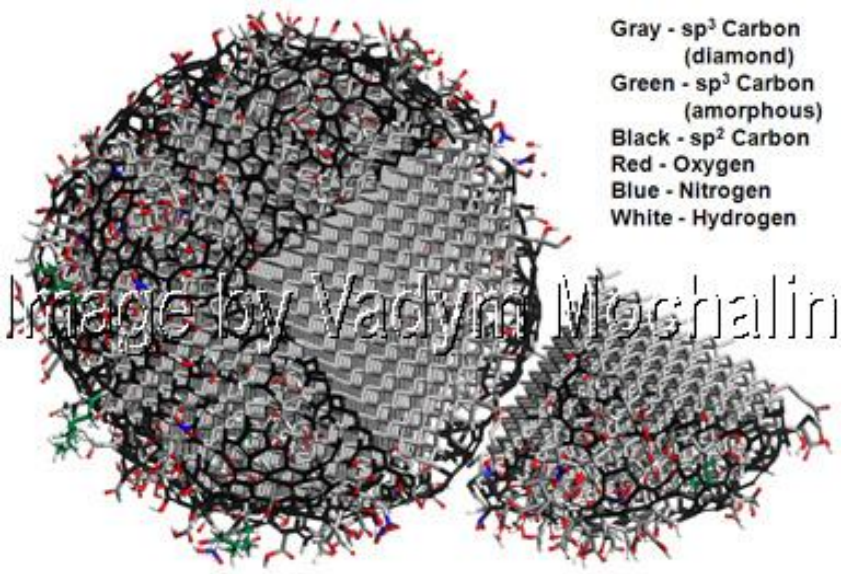


Figure 2.8. Model of a single ND particle (diameter = 5 nm) [85].

To fully benefit from the uniqueness of ND, functionalization is the key to utilizing ND for certain applications. Both wet and gas chemical treatment can be applied to modify its surface [85]. Hydroxide radical and carboxyl groups are most preferred for polymer matrix reinforcement due to the fact that OH- and COOH- terminated ND is directly involved in the reaction or interaction with polymer chains forming a covalent or non-covalent bonded

network with polymer matrix.

**Polymer/ND nanocomposite**

Due to the limitation of other nanofillers and the unique properties of ND, polymer matrix composites with detonation NDs as a filler have been recently investigated and those novel composite materials have shown incomparable advantages [39, 86]. Research efforts made on polymer/ND composites has been reported in literatures, including poly (vinyl alcohol) (PVA)/ND fabricated by solution casting[87], poly (l-lactic acid) (PLLA)/ND [88], and polyamide-11 (PA-11)/ND [89]. Those researches have extended the prospect of developing polymer/ND composites.

Most of the research focused on the mechanical properties of polymer/ND composites and illustrated an improvement in mechanical properties with low concentration of NDs (Table 2.2) which are comparable to human cortical bone with Young's modulus of 5-27 Gpa [90] and hardness of 0.62-0.74 Gpa [91] . The results indicate that appropriate functionalization of NDs is required for different polymer matrix. However up to now, no attempts have been made to produce CS/ND composites and evaluate its mechanical properties and biocompatibility, which is the focus of this thesis project.

Table 2.2. Mechanical improvement in various polymer/ND composite films compared to neat polymers.

| **Polymer matrix** | **ND content (wt. %)** | **Young's modulus (Gpa)** | **Improvement (%)** | **Hardness (Gpa)** | **Improvement (%)** |
|---|---|---|---|---|---|
| PLLA [88] | 5 | 5.9±0.3 | 129 | 0.26±0.01 | 420 |
| Epoxy [92] | 25 | 3.4±0.5 | 350 | 0.2 | 300 |
| PVA [87] | 10 | 9.2 ± 0.4 | 248 | / | / |
| PA-11 [87] | 10 | 3.5±0.1 | 75 | 0.09 | 60 |

## 2.3 Processing Techniques

There are many techniques to fabricate tissue engineering scaffolds, including fiber bonding, solvent casting [93] , electrospinning, and particulate leaching [94], membrane lamination, freeze-drying, gas foaming [95], self-assembly and 2-D printing [96]. The aim is to fabricate a three dimensional scaffold with specific geometry for various tissue engineering applications. High porosity with interconnected pore structure and desired mechanical strength are the essential properties. Main and common techniques for scaffold fabrication are briefly mentioned below.

a) Solvent casting

Solvent casting is the simplest method and appropriate for simple structure and initial experiments. It is low cost and easy to operate which is just based on the evaporation of the solvent. The process involves adding polymer solution into a mold and provide sufficient time for the solvent to evaporate or dipping the mold into polymer solution to create polymer membrane. Scaffolds with complex structure need other more complex techniques.

b) Electrospinning

Electrospinning is one of commonly used technique to produce fibers with diameter in nanoscale or microscale. The process involves a high voltage source, a syringe pump and a collector (Figure 2.9).

High intensity electric field is formed between two electrodes, one of which is placed in polymer solution while the other one is placed in collector. A drop of solution is formed by pumping syringe. When the electric field is increased, the forced produced will overcome the surface tension of the solution and to make polymer solution ejected and repel each other. Eventually, solvent starts to evaporate and results in the formation of fibers deposited to the collector. In tissue engineering field, electrospinning is applied to prepare fiber scaffolds. Over hundreds of polymer scaffolds have been designed through this technique such as CS [97],

collagen [98], gelatin [99]etc. Electrospinning can provide scaffolds with certain structure for cells to grow and subsequently generate tissue. However, to obtain more complex structures with a homogeneous distribution of pores remains a challenge to be addressed.

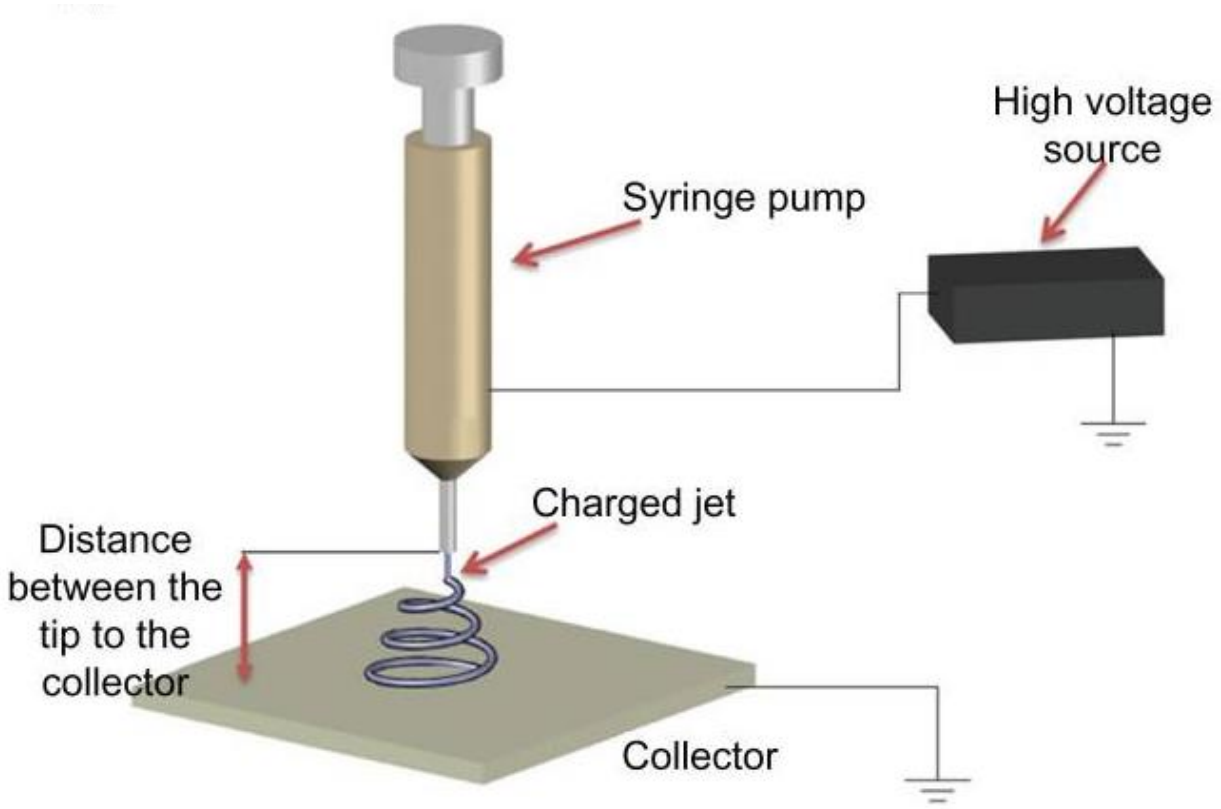


Figure 2.9. Electrospinning technique for three-dimensional biomimetic scaffold fabrication [100].

c) Freeze drying

Freeze drying is a dehydration process used to preserve a perishable material or make material more convenient for transport with a wide applications of food science and pharmaceuticals etc. In tissue engineering, the polymer solution is frozen at low temperature and placed under high vacuum chamber. In chamber, the ice can be removed directly by sublimation to fabricate porous structural scaffold. Size of pores is controlled by the freezing rate and pH: fast freezing rate produces smaller pores. Freeze drying technique have been applied to many homogenous porous scaffolds in last decades including PLLA, CS, PGA,

PLGA [101, 102]. This technique requires no high temperature and it uses water instead of organic solvent which can avoid cytotoxicity and poor biocompatibility. Nonetheless, this approach requires a long process period and have difficulty in being fabricated in hierarchical structures.

d) Self-assembly

The self-assembly process is a spontaneous organization process from a disordered system to well-ordered patterns or structures. Material based on self-assembly natural or synthetic molecules such as peptide-based bioactive hydrogel is formed through the molecular self-assembly induced by weak bonding or week interactions including electrostatic, van der Waals, hydrophobic interactions, ionic, hydrogen and coordination bonds [103]. Due to well biocompatibility and controlled degradation, functional materials constructed from the self-assembly of peptides present a great potential in many biomedical fields. In tissue engineering, peptides can be assembled into stiff, nanofibrous hydrogel network that can mimic essential features of the extracellular matrix. To be specific, the nanofibers can connect neighbor cells and provide them with mechanical support by wrapping around the surface of cells. Through self-assembly, various types of thin nanofiber can be easily achieved. Cytotoxicity is also reduced without the use of organic solvent in this approach. Nonetheless, it is still a challenge to fabricate complex 3-D structure due to its poor mechanical properties. Besides, the complicated process and high costs are limiting its applications.

## 2.4 Characterization of CS/ND Thin Films

### 2.4.1 Fourier Transform Infrared Spectroscopy

FTIR is a chemical analytical technique used to characterize the intermolecular interactions and chemical groups of materials by measuring the changes in the infrared intensity versus wavelength of light after passing through the specimen. In principle, chemical bonds stretch

when they are interacting with an infrared light, which results in absorbance of infrared radiation in a specific wavenumber range, the specific wavenumber peaks detected are correlated to chemical structure and used to identify different functional groups.

A common FTIR spectrometer (Figure 2.10) consists of a source used to generate radiation that passes the sample through an interferometer, a detector that used to receive signals, an amplifier which converts signal to digital signal and a computer for carrying out Fourier transform.

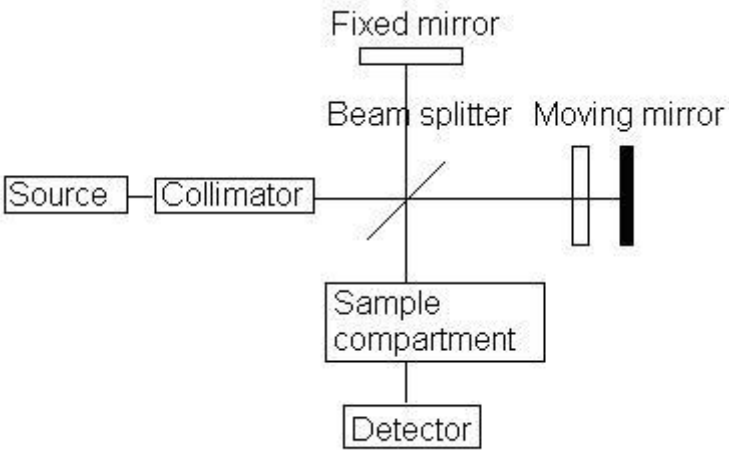


Figure 2.10. Block diagram of an FTIR spectrometer [104].

### 2.4.2 X-ray Diffraction

XRD technique is a non-destructive method to identify the arrangement of atoms or molecules structure in a crystal or semi-crystal material, which is one of the major characterization techniques widely applied in chemistry, materials science, engineering as well as biological and biomedical fields. XRD works based on Bragg's Law: $n\lambda=2d\sin\theta$ (Figure 2.11), named after English physicists Sir W.H. Bragg and his son. This equation explains why the cleavage faces of crystals appear to reflect X-ray beams at certain angles of incidence (theta, $\theta$). The variable d is the distance between atomic layers in a crystal, and the variable lambda $\lambda$ is the wavelength of the incident X-ray beam; n is an integer. In XRD characterization, the

crystalline atoms lead to X-ray beam to diffract into many specific directions from which the angles and intensities of the beams can be measured to draw a two dimensional images. The positions of atoms, molecular and chemical bonds can be determined and by a comparison to the fingerprint database, the structures and functional molecules of inorganic and biological materials can be revealed.

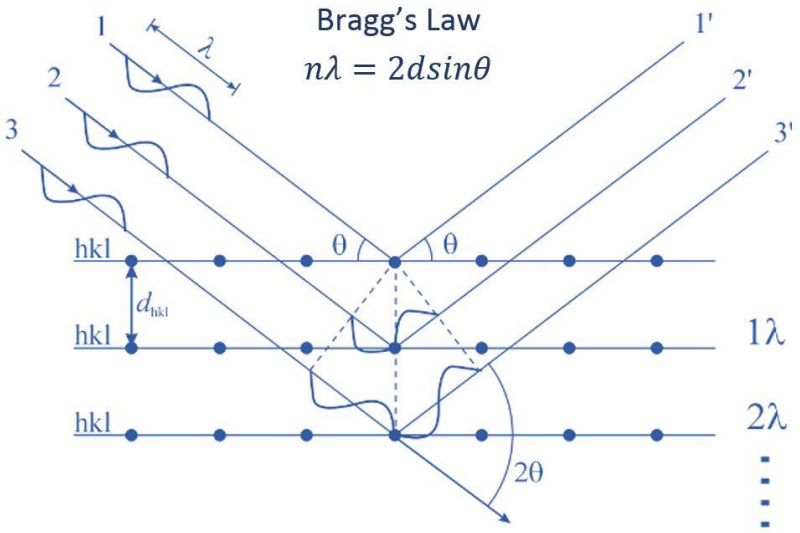


Figure 2.11. Bragg's Law [105].

### 2.4.3 Scanning Electron Microscopy

Scanning electron microscopy (SEM) is a common technique used to produce morphology images by scanning samples with a focused beam of electrons. In principle, electrons are accelerated in an SEM with high kinetic energy. The incident electrons when interact with the samples generate a variety of signals include secondary electrons, backscattered electrons, diffracted backscattered electrons and X-rays, among which, the secondary electrons and backscattered electrons are most commonly used for imaging sample topography. Thus, specimens must be electrically conductive. For nonconductive polymers or any other organic matters, surface gold coating is required to increase conductivity and prevent electrons accumulation.

### 2.4.4 Differential Scanning Calorimetry

Differential scanning calorimetry (DSC) is a common thermoanalytical technique for measuring thermal properties of materials which was developed by E.S. Watson and M.J. O'Neill in 1962 [106]. In DSC experiment, energy is introduced into a sample cell and reference cell to increase the temperature over time. The difference of heat required to match the temperature is measured as a function of temperature. Commonly, when the sample undergoes a phase transition, more or less heat flow is needed to reach temperature equilibrium which are known as the endothermic or exothermic process. Therefore, DSC is often applied for the measurement of glass transition, melting point, percent crystallinity, heat capacity, purities, completeness of cure, oxidative stabilities and thermal stabilities etc. [107] in a wide range of fields such as food science, nanoscience, bioengineering, medicine and chemistry [108].

### 2.4.5 Nanoindentation

Nano indentation technique was developed in the mid of 1970s that was designed in the attempt to provide surface mechanical characterization data in micro/nano scales. Unlike conventional indentation technique which measures the size of a residual plastic impression in the specimen and provides a function of a given load with the indentation area, Nano indentation allows a small continuous load and penetration depth measurement and for this unique property, it has been applied as one of the most common techniques for mechanical properties testing for various materials such as organic, inorganic coatings, thin films as well as metals, glasses, ceramics and their composites. This technique allows us to record the change of penetration depth under certain load so as to plot a load (P)-displacement (h) curves which can be used to analyze the mechanical properties including Young's modulus, hardness, creep

or fatigue. A brief schematic of Nano indentation tester is shown in Figure 2.12.

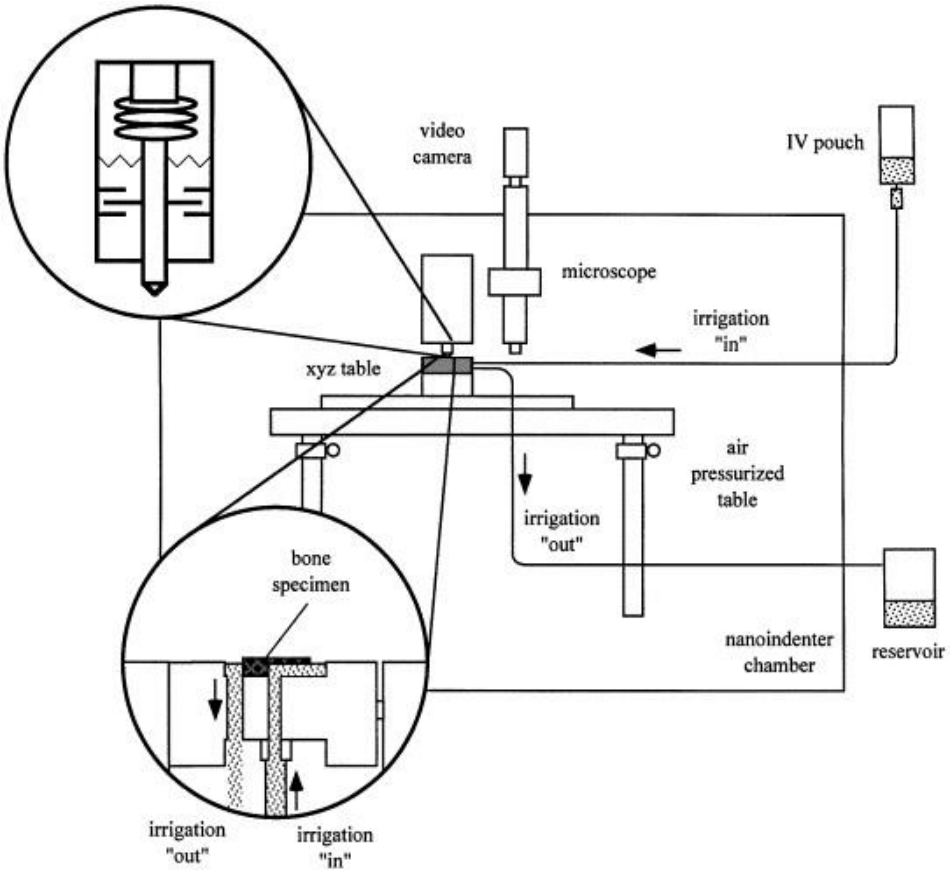


Figure 2.12. Schematic of Nano indentation tester CETR (Center for Tribology, Inc.)

The indenter geometry is usually a three-sided pyramid or sphere tip. For different applications, a proper selection of tips is essential. There are four main types of tips listed below with different geometries (Table2.3).

Vickers tip is a four-sided pyramid with opposing faces at a semi-angle of $\theta$ =68°, which makes the angle with the surface of specimen $\beta$=22°. As a method for mechanical properties measurement, Vickers indenter is suitable for bulk materials, films, scratch and wear testing in small scale.

Berkovich indenter is a three sided pyramid which is self-similar in geometry. The face angle of the indenter is commonly 65.35° which gives Berkovich the same projected area-to-depth ration as that of Vickers indenter. The superiority of Berkovich relies on its three

sided geometry rather than the four sided shape of Vickers indenter, which easily makes the edges ground to a single point. Besides, the 142.3° of the included angle can also minimize the friction. Berkovich indentation is more frequently used for bulk materials, thin films greater than 100 nanometers, scratching and wear properties, micro-electromechanical properties and polymers.

Another type of indenter is Cube-Corner, similar to Berkovich indenter, cube corner indenter is also a three sided pyramid but with a different centerline to face angle which is 34.3°. Due to the sharp angle, cube corner shape indenter produces smaller cracks and is more suitable for hard and brittle materials.

Conical indenter has axial symmetry and self-similar geometry, even though with conical indenter there is no stress concentrations at edges, the applications are limited due to the difficulty of manufacturing a conical shape diamond tip.

Spherical indenters are mostly used for micro-electromechanical system and soft materials such as polymers. Since spherical indenter provides elastic deformation initially, and a smooth transition from elastic to plastic deformation subsequently, stress-strain curve can be obtained in one single test by analyzing yielding and work hardening. However, sphere indenter is limited in comparable large scale rather than micro scale due to the difficulties in manufacturing perfect sphere of diamond or other hard tip, which also leads to deviations during test process.

Table 2.3. Geometries of various indenters.

| Features | Vickers | Berkovich | Cube-Corner | Conical | Sphere |
|---|---|---|---|---|---|
| Shape | 4-sided pyramid | 3-sided pyramid | 3-sided pyramid | Conical | Spherical |
| Applications | Bulk Materials, Films and Foils, Scratch Testing, Wear Testing | Bulk Materials, Thin Films, Polymers, Scratch Testing, | Thin Films, Scratch Testing, Fracture Toughness, | Modeling , Scratch Testing, | MEMS |

| | | | | | |
|---|---|---|---|---|---|
| | | Wear Testing, MEMS, Imaging | Wear Testing, MEMS, Imaging | Wear Testing, Imaging, MEMS | |
| Centerline-to-face angle, α | 68° | 65.3° | 35.2644° | | |
| Area(projected), A(d) | $24.504d^2$ | $24.56d^2$ | $2.5981d^2$ | $\pi a^2$ | $\pi a^2$ |
| Volume-depth relation, V(d) | $8.1681d^3$ | $8.1873d^3$ | $0.8657d^3$ | | |
| Projected area/face area A/Af | 0.927 | 0.908 | 0.5774 | | |
| Equivalent cone angle ,ψ | 70.2996° | 70.32° | 42.28° | ψ | |
| Contact radius | | | | d tan ψ | $(2Rd-d^2)^{1/2}$ |

A particularly meaningful quantity in indentation hardness is the mean contact pressure and is determined by dividing the indenter load by the projected area of the indentation. The mean contact pressure, when determined under conditions of a fully developed plastic zone, is usually defined as the "indentation hardness" of the specimen material. In nanoindentation testing, the displacement of the indenter is measured and the size of the contact area (at full load) is estimated from the depth of penetration with the known geometry of the indenter. For an extreme case of a rigid-plastic solid, where there is little elastic recovery of material, the mean contact pressure at a condition of a fully developed plastic zone is a true representation of the resistance of the material to permanent deformation. When there is substantial elastic recovery, such as in ceramics where the ratio of E/H is low, the mean contact pressure, at a condition of a fully developed plastic zone, is not a true measure of the resistance of the material to plastic deformation but rather measures the resistance of the material to combined elastic and plastic deformations. The distinction is perhaps illustrated by a specimen of rubber, which might deform elastically in an indentation test but undergo very little actual permanent deformation. In this case, the limiting value of mean contact pressure (the apparent indentation hardness) may be very low but the material is actually very resistant to permanent deformation

and so the true hardness is very high.

In depth-sensing indentation techniques used in nanoindentation, the elastic modulus of the specimen can be determined from the slope of the unloading of the load-displacement response. The modulus measured in this way is formally called the "indentation modulus". Ideally, the indentation modulus has the same meaning as the term "elastic modulus" or "Young's modulus" but this is not the case for some materials. The value of indentation modulus may be affected greatly by some material behaviors (e.g. piling-up) that is not accounted for in the analysis of load-displacement data. For this reason, care has to be taken when comparing the modulus for materials generated by different testing techniques and on different types of specimens.

**Berkovich Indenter**

The Berkovich indenter is used in this work for nanoindentation testing because it is more readily fashioned to a sharper point than the four-sided Vickers geometry, thus ensuring a more precise control over the indentation process. The mean contact pressure is usually determined from a measure of the contact depth of penetration, $h_p$, such that the projected area of the contact is given by:

$$A = 3\sqrt{3}h_p^2 \tan^2\theta \quad \cdots\cdots (2.1)$$

Where θ = 65.27°,

Thus the hardness is expressed as

$$H = \frac{P}{A} = \frac{\mathbf{P}}{\mathbf{24.5}h_p^2} \quad \cdots\cdots (2.2)$$

The original Berkovich indenter was designed to have the same ratio of actual surface area to indentation depth as a Vickers indenter and had a face angle of 65.03°. Since it is customary to use the mean contact pressure as a definition of hardness in nanoindentation, Berkovich indenters used in nanoindentation work are designed to have the same ratio of projected area to

indentation depth as the Vickers indenter in which case the face angle is 65.27°. The equivalent cone angle (which gives the same area to depth relationship) is 70.296°. From geometry, the ratio of the length of one side of the residual impression is related to the total depth of penetration by a factor of about 7.5.

**Load-Displacement Curves**

The principal goal of nanoindentation testing is to extract elastic modulus and hardness of the specimen material from the experimental readings of indenter load and depth of penetration. In a typical test, force and depth of penetration are recorded as load is applied from zero to some maximum and then from maximum force back to zero. If plastic deformation occurs, then there is a residual impression left in the surface of the specimen. Unlike conventional indentation hardness tests, the size (and hence the projected contact area) of the residual impression for nanoindentation testing is too small to be measured accurately with optical techniques. The depth of penetration together with the known geometry of the indenter provides an indirect measure of the area of contact at full load, from which the mean contact pressure, and thus hardness, can be estimated. When load is removed from the indenter, the material attempts to regain its original shape, but it prevented from doing so because of plastic deformation. However, there is some degree of recovery due to the relaxation of elastic strains within the material. An analysis of the initial portion of this elastic unloading response gives an estimate of the elastic modulus of the indented material.

The indentation modulus is usually determined from the slope of the unloading curve at maximum load. Equation shows that the indentation modulus (E) as a function of *dP/dh* and the area of the contact:

$$E = \frac{1}{2}\frac{\sqrt{\pi}}{\sqrt{A}}\frac{dP}{dh} \quad \text{.....(2.3)}$$

### 2.4.6 MTT Assay

MTT (3-(4,5-dimethylthiazol-2-yl)-2,5-diphenyltetrazolium bromide) assay is one of numerous basic assays for assessing cell viability and proliferation. MTT is a yellow tetrazole that could be reduced to dark purple insoluble formazan (Figure 2.13) in living cells by cellular oxidoreductase enzymes which reflect the number of viable cells. The purple insoluble formazan, during the MTT assay, is dissolved with dimethyl sulfoxide (DMSO) (or a solution of the detergent sodium dodecyl sulfate) into a purple solution. The absorbance of this purple solution can be measured by a spectrophotometer which is used as an index of cell viability, proliferation or cytotoxicity evaluation.

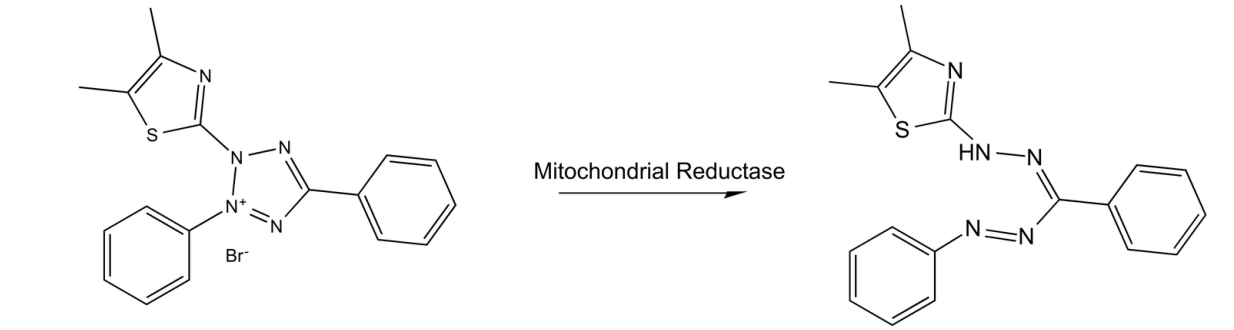


Figure 2.13. MTT reaction [109].

# CHAPTER 3 MATERIALS AND METHODS

## 3.1 Introduction

This chapter explains what materials were used in this work and their preparation and treatment process. An assortment of characterization methods for testing numerous essential factors of the hypothesis was also presented as well as a detailed introduction for each technique about how the procedure of testing was carried out.

## 3.2 Materials

CS holds a great potential as tissue engineered scaffold material due to its outstanding biological properties: biocompatibility, anti-microbial activity and biodegradability etc. as discussed in 2.3.3.3. CS is large-scale available and low-cost which has viability of being fabricated in various geometries with certain porosity. Under the function of catabolic enzymes (lysozyme, chitinase), CS could be converted into chitooligosaccharides. On this occasion, CS has a significant advantage over PLLA and PGA, of which in degradation process, produced carbon dioxide will result in local pH decrease and cause tissue necrosis [110]. However, CS films are highly brittle with no sufficient mechanical strength that is comparable to natural bone if used alone. To improve mechanical properties, blending fillers - NDs are introduced and investigated for their superior mechanical properties, extensive surface groups and functionalization potential. Possible factors introduced by NDs responsible for mechanical improvement and microstructure change were investigated by FTIR, XRD, DSC and nanoindentation.

### 3.2.1 CS

CS powder (β-1,4-linked N-acetyl-D-glucosamine (GlcNAc) with degree of deacetylation (DD) of approximately 80% were purchased from Sigma-Aldrich Canada and used as received.

The viscosity is less than 200 mPa.s and contains 1% in acetic acid (20°C). Low molecular weight and a comparable low DD were selected to eliminate cytotoxicity and possible inflammation. 2 wt. % CS polymer solution was prepared by dissolving 2 grams of CS powder in 100 mL 2 %( v/v) acetic acid. A good dispersion was achieved by continuous stirring for 12 hours on magnetic stirrer at temperature of 40℃.

### 3.2.2 NDs

#### 3.2.2.1 As-revived NDs

Explosion synthesized ND powders were purchased from Nanostructured and Amorphous Materials, Inc. with an average particle size of 5 nm and purity over 95% The surface groups of NDs contains -CH, -C=O, -COOH, -C-O-C, -CN and large amount of $sp^2$ carbon . The groups and chemical properties of ND vary greatly from suppliers. Possible surface groups can be achieved after appropriate purification or modification which are shown below in Figure 3.1.

Nanosized diamonds have high relative surface area thus high relative surface energy and more surface atoms. These atoms are unstable with vacant coordination sites. Therefore, ND particles tend to agglomerate to diminish this energy and unstability by forming bonds between the atoms from adjacent ND particles. sBesides, surface functional groups can also cause agglomeration via hydrogen bond formation or dipole-dipole and weak Van der Waals interactions between the functional groups on adjacent nanodiamond particles [111]. In order to get a better dispersion in polymer matrix and fully benefit from their surface chemical groups, sonication is commonly applied during the manufacturing process [112]. A better dispersion leads to improvement in interaction with polymer chains, which significantly affects the mechanical properties and stability of the composites.

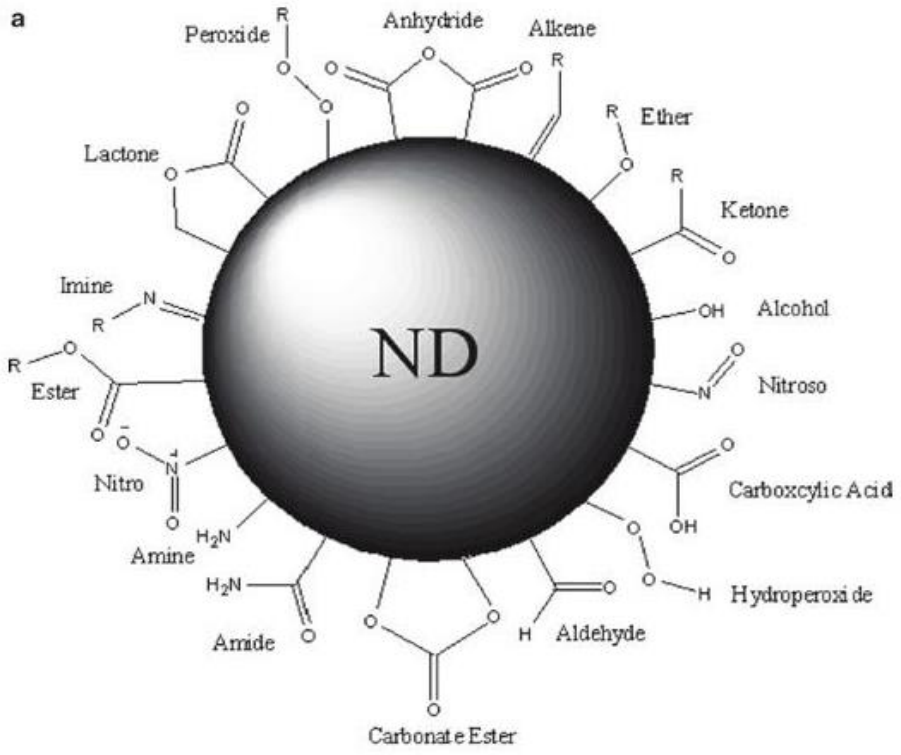


Figure 3.1. Schematics of surface groups reported for NDs after different types of purification/modicaication [113].

### 3.2.2.2 ND functionalization

As described, ND has large specific surface area and rich functional groups. In particular, the high density of carboxylic and hydroxyl groups on the surface of ND impart tenacious binding capacity in polymer matrix. Therefore, ND particles terminated with these groups followed by proper treatment is the most commonly used starting material for biological applications. Considering the major interaction occurs between the carboxylic groups on ND surface and CS polymer chains [114, 115], the as-received ND was treated by concentrated acid to increase the concentration of carboxylic group, as well as to remove the surface impurities introduced from manufacturing process such as oxides and carbides, including those of iron, chromium, silicon, calcium, copper, potassium, titanium, and sulfur, in addition to carbon soot [116], which may impact the properties of CS polymers. Detailed steps are described in the following paragraph. Such functionalized NDs was used as precursors for further

characterization and experiments.

5 gram as-received ND powder was treated with 150ml concentrated acid solution of $HNO_3$ (70%) and $H_2SO_4$ (98%) at a volume ratio of 1:3 [117], and sonicated (2510 BRANSON Sonicator) (Room 0C17, Engineering Building, University of Saskatchewan) for 1 h at room temperature for an adequate dispersion. Subsequently, the solution was heated at 60°C for 12h to remove impurities and oxidize surface groups. After the acid treatment, functionalized ND particles were applied to a centrifugation (Allegra X-22R Centrifuge, BECKMAN COULTER) (Room 0C17.1, Engineering Building, University of Saskatchewan) of 3000r/min for 15 minutes and rinsed with deionized water (DIW) three times. The cycles were repeated until the supernatant became pH neutral. The resultant product was dried in a freeze dryer overnight for 8 hours to yield purified carboxyl functionalized ND powders.

### 3.2.3 Other materials

Dulbecco's modified Eagle Medium (DMEM) and MTT (3-4, 5-dimethylthiazol-2yl {-2,5-diphenyl-2Htetrazolium bromide) were purchased from Sigma–Aldrich, USA. Foetal bovine serum (FBS) was purchased from Invitrogen Co, Carlsbad, California, CA, USA. NaOH (sodium hydroxide) and other reagents used were all of analytical grade.

Phosphate buffered saline (PBS) was prepared by dissolving pre-determined amount of reagent-grade NaCl (90 mg/ml), $NaH_2PO_4 \cdot H_2O$ (0.31725 mg/ml) and $Na_2HPO_4 \cdot 7H_2O$ (2.064 mg/ml) (Sigma-Aldrich, St. Louis, MO, USA) in DIW. To be specific, 1.269g $NaH_2PO_4 \cdot H_2O$, 8.256g $Na_2HPO_4 \cdot 7H_2O$ and 360g NaCl were weighed with an analytical balance respectively and dissolved in 4L DIW.

### 3.2.4 CS/ND composites

CS/ND composites were prepared through solvent casting method (Figure 3.2). A

predetermined amount of as-received NDs (1%w/w of CS) and functionalized NDs (1%; 2%; 3%; 4%; 5% w/w of CS) were weighed using an analytical balance and transferred into a 20 ml beaker with 10 ml 2% v/v acetic acid aqueous solution followed by ultra-sonication bath treatment for 30 min. The ND suspension was then added to the pre-prepared CS solution (2wt.%) (Section "3.1.1") and stirred on magnetic stirrer at room temperature until no visible chunks could be observed. Surface polished stainless steel discs were pre-placed on the bottom of each well of 6-well Petri dish for easy removal of the casted films. To completely eliminate the solvent, the blend liquid was dried in Petri dished at 35 ℃ for 48 hours and sonicated repeatedly every 8 hours during the evaporation. Films were obtained by peeling them off from the stainless steel discs and soaked in an aqueous solution of NaOH (0.4 wt %) at room temperature for 6 hours to remove the residual acetic acid. Followed by repeatedly rinsing with deionized water to remove Na+ ions, the samples were subsequently dried in vacuum and stored for further characterization.

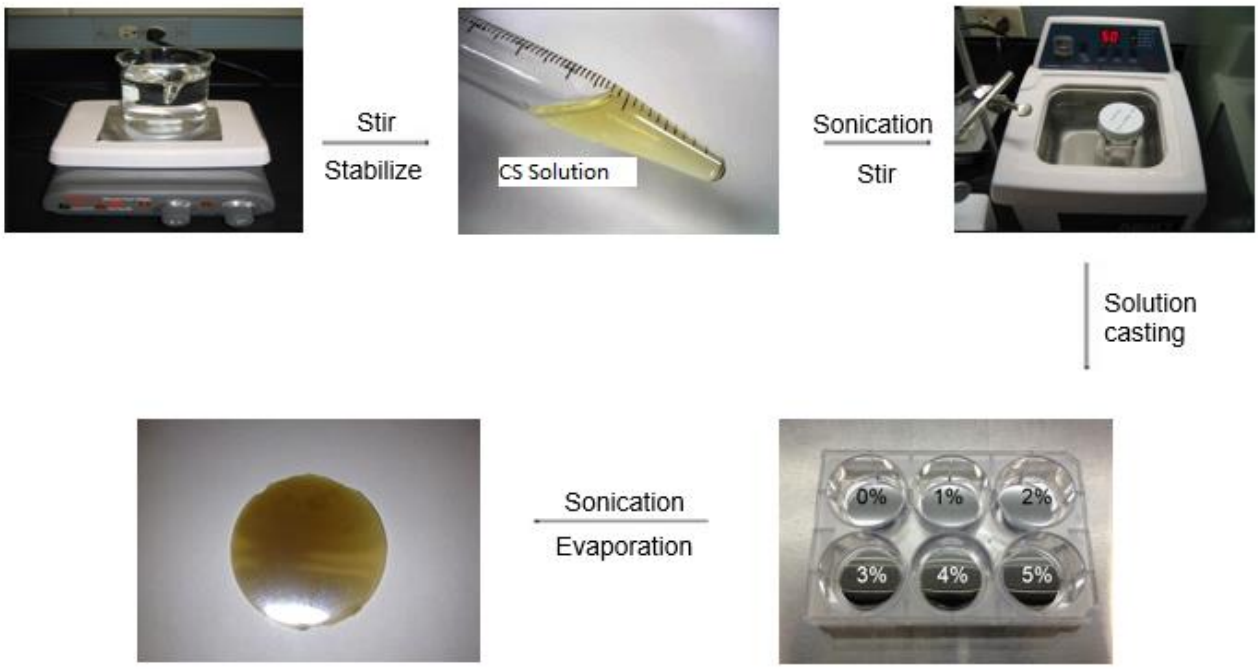


Figure 3.2. Schematic diagrams of the fabrication process of CS and CS/ND films with various amount of ND ranging from 1 wt. % up to 5 wt. %.

### 3.3 Characterization Methods

#### 3.3.1 Structural analysis of ND functionalization and CS/ND films

##### 3.3.1.1 FT-IR

In this research, FT-IR was used to confirm the carboxyl groups on ND surfaces. FT-IR spectra were recorded on a JASCO FT/IR-4100 spectrometer by KBr method (KBr: sample = 100:1, mass ratio). Samples were prepared by mixing 200 mg potassium bromide (KBr) with ~ 1.5 mg of ASND and FND, respectively. FT-IR spectra were recorded in the wavenumber range of 500-4000 $cm^{-1}$ at a resolution of 2 $cm^{-1}$.

##### 3.3.1.2 X-ray diffraction (XRD) analysis

To determine the crystalline structure of the CS/ND nanocomposites, a Rigaku (Rotaflex Ru-200) X-ray diffractometer with a Co Kα line (λ = 0.178897 nm) radiation resource was used (Figure 3.3). CS/ND nanocomposites were collected and mounted on the stage and analyzed in the scanning range from 5° to 50° in the increment of 0.05º steps at a scanning speed of 2 sec/step. The operation voltage and current of X-Ray source was 35 kV and 30 mA, respectively.

Figure 3.3. X-ray diffractometer. (Room 29, Physics Building, University of Saskatchewan).

Detailed crystallinity is determined under the assumption that the areas are proportional to the scattering intensities of crystalline and amorphous phases [118]. Thus, the diffraction profile is separated into 2 parts: peaks are related to diffraction of crystallites, broad alone is related to scattering of amorphous using OriginPro 8.5 (multiple peaks fitted with peak type of Gauss ), and the degree of crystallinity $X_c$ % is measured as the ratio of crystalline area to total area.

$$X_c = \frac{A_{cr}}{A_{cr} + KA_{am}} \quad \text{..... (3.1)}$$

Where

$X_c$ = Percentage of crystallinity

$A_{cr}$ = Area of crystalline phase

$A_{am}$ = Area of amorphous phase

$K$ = a constant related to the different scattering factors of crystalline and amorphous phases. For relative measures K = 1.

### 3.3.1.3 Scanning Electron Microscopy (SEM)

The morphology of the composite samples was examined using Scanning Electron Microscopy (A JEOL JSM-6010LV SEM. Jeol Ltd., Tokyo, Japan) (Room 2C27, Engineering Building, University of Saskatchewan) at 10kV acceleration voltage (Figure 3.4). Samples were cut into 1x1 cm films and immobilized to the top of specimen holders by carbon tapes.

All samples were coated with a thin layer of gold at a voltage of 1kV for 20 seconds under vacuum with Gold Sputter Coater (Edwards S150B) prior to SEM characterization.


Figure 3.4. Scanning electron microscopy JEOL JSM-6010LV (Room 2C27, Engineering Building, University of Saskatchewan).

#### 3.3.1.4 Differential Scanning Calorimetry (DSC)

The thermal properties including glass transition, degradation and interactions of CS/ND nanocomposites were studied using DSC (TA Instruments DSC Q100, NewCastle, DE) (Room 3C18, Engineering Building, University of Saskatchewan) over a temperature range from 20-300°C. Each type of specimen (~6 mg) was placed in sealed aluminum pans and heated under nitrogen atmosphere at a rate of 1°C/min. DSC was calibrated with an indium standard. All specimen were kept in a desiccator to protect them from humidity prior to measurement. The glass transition temperature ($T_g$) was obtained at the inflection point between the base lines where the heat capacity of the specimen changed.

### 3.3.2 Mechanical property characterization

The mechanical tests were performed from a micro-scale to nano-scale with the purpose of comparing the mechanical properties improvement of CS/ND (functionalized and non-functionalized) samples to those of pure CS samples. Nano-indentation was employed to evaluate the nano mechanical properties including compression strength and modulus.

Figure 3.5. Nano indentation tester CETR (Center for Tribology, Inc.) UNMT-1 Bruker Corporation (Room 1b70, Engineering Building, University of Saskatchewan).

In this work, nanoindentater manufactured by Center for Tribology, Inc. (Room 1b70, Engineering Building, University of Saskatchewan) (Figure 3.5) was carried out for the assessment of the micro/nano mechanical properties of CS/ND composites.

**Specimen Preparation and installation**

In spite of the fast development of nanoindentation testing instruments, the process of undertaking such a test requires considerable experimental skill and resources. Such tests are extremely sensitive to thermal expansion from temperature changes and mechanical vibration during testing. It is necessary to ensure that the specimen and the instrument are in thermal

equilibrium.

Composite films were cut into 5 mm×5 mm square shape, and stick onto the top of the metal mounts firmly with a very thin layer of superglue (as a thermal sensitive material, polymer is not suitable to be mounted with wax), then transferred into desiccator until the glue dries. In order to eliminate the thermal expansion and contraction during the experiment, all the specimen were placed on the stage inside the chamber of the nano-indentation instrument for thermal equilibrium for 3 hours. To reduce the variation from the noise in laboratory conditions, nanoindentation instrument was wrapped with soft cardboard with a 10 cm space in between, and all experiments were processed overnight. The indentation tests were performed with a strain rate of 0.03 $s^{-1}$, and a maximum load of 50 mN.

### 3.3.3 Biocompatibility characterization

Cell activity was determined by 3-[4, 5-dimethylthiazol-2-yl]-2, 5-diphenyl tetrazolum bromide (MTT) assay, which is used for in vitro measurement of the metabolic activity of cells in the solution containing CS/ND films after 12, 24, 48 hours.

#### 3.3.3.1 Cell culture

In recent years, considerable amount of studies have focused on parallel reconstruction of injured bone and nerves. An ideal engineered scaffold must enable the regeneration of both bones and nervous tissues such as orofacial reconstruction [119]. For this reason, Schwann cells were studied first as the initial biocompatibility experiments.

Schwann cells (RSC 96, CRL-2765, passage number from 14 to 22) purchased from ATCC (American Type Culture Collection ATCC, Manassas, VA) were collected from liquid nitrogen storage and thawed in 37 °C water bath. Growth medium used was prepared by standard Dulbecco's Modified Eagle Medium (DMEM), 10% fetal bovine serum (FBS) (Invitrogen Co,

Carlsbad, California, CA, USA), and 1% antibiotics (penicillin/streptomycin/amphotericin-B). When ready, the medium was carefully poured on the 10cm tissue culture dish (BD Falcon™, USA) and incubated at 37°C under a 5% $CO_2$ condition. Cells were immersed for 1 minute in 0.25% Trypsin/Ethylenediaminetetraacetic acid (EDTA, Invitrogen Co, Carlsbad, CA) when confluence was at 80-100% for detachment. Cell suspensions were transferred into a sterile falcon tube and centrifuged at a speed of 800 rpm for 5 minutes. Cells were counted using a haemocytometer. The achieved cells were re-suspended in fresh medium to a density of $1x10^4$/mL and seeded into three 24 well culture plates (10,000 cells per well). All culture plates were incubated at 37°C for 1 day for cell attachment and growth.

#### 3.3.3.2 Sample preparation

CS/ND films with an ND weight ratio of 0%, 1%, 2% and 3% were prepared as described in 3.1.4. After neutralization with NaOH, all samples were rinsed with deionized water for three times to remove the residual inorganic ions on surface. Then they were immersed in PBS for 24h. Subsequently, the samples were sterilized in 70% (v/v) ethanol overnight for 12h, and then rinsed with sterilized water and PBS solution for three times, respectively. Samples were dried in air at room temperature and cut into 0.5×0.5 cm square films.

#### 3.3.3.3 Cell seeding and MTT Assay

MTT assay was used to measure the in-vitro cytotoxicity of CS/ND samples. The oxidoreductase enzymes of cells were able to reduce tetrazolium dye MTT to its insoluble formazan. The absorbance of the purple solution reflected by spectrophotometer was used for assessing the cell viability.

For the experiment assessing the effect of CS/ND on Schwann cell viability, $1x10^4$ cells was placed in each well of three 24-well tissue culture plates with the cell density of $1x10^4$/ml

(Figure 3.6 a) ). All culture plates were incubated in the 5% $CO_2$, 95% air, 37°C, humidified incubator for 24 h for proliferation till the cells were over 90% confluent. Each type of sample films prepared were introduced into the cell suspension in the same order, respectively, in three 24-well culture plates. Then the three 24- well culture plates were transferred back into the incubator for 12 h, 24 h and 48 h, respectively, for further characterization.

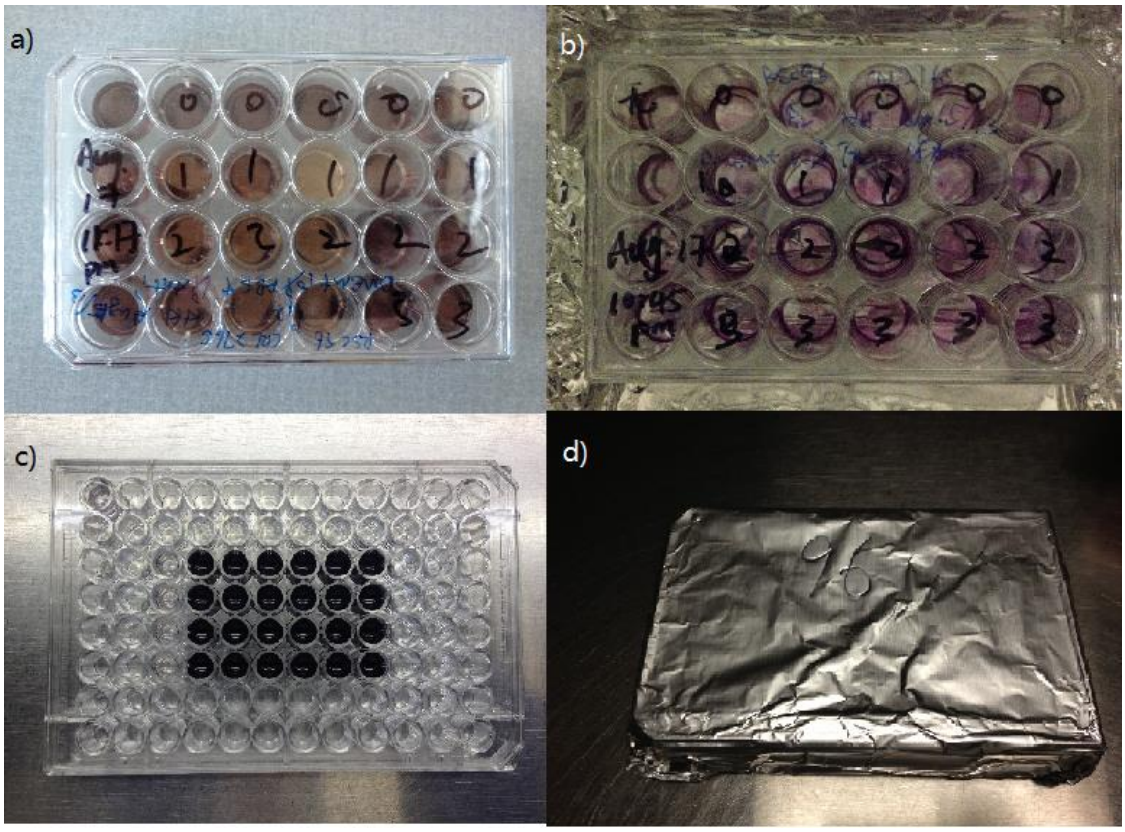


Figure 3.6. MTT assay schematic diagram a) 24-well tissue culture plate with cell density of $1\times10^4$/ml b) 24-well tissue culture plate with MTT solution c),d) 96-well tissue culture plate with formazan transferred from a 24-well tissue culture plate.

MTT assay was carried out in accordance with protocol. MTT stock solution at 5mg/ml was prepared with sterilized PBS. In particular, all medium including samples were aspirated without disturbing the cells. 120 μL MTT solution was added into each well of the culture plate followed by agitation for 5 minutes on an orbital shaker at 150 rpm. The culture plate with well mixed solution was incubated at 37°C for 4 hours to allow the MTT to be metabolized. After

incubation, all media was removed. Subsequently, 200uL dimethyl sulfoxide (DMSO) was added to each well, followed by another agitation for 5 minutes at 150rpm to thoroughly mix the formazan into the solvent. The received solution was carefully transferred to a 96-well culture plate shown in the Figure 3.6 c) and d), the absorbance of which was read by Spectra Max 340 plate reader (Figure 3.7 Molecular Device Inc., CA) at 560nm and subtract background at 670nm. Polystyrene (PS) surface of the 96-well culture plate was adopted as a negative control, while those with pure cells as positive control. The Cell Viability is evaluated as (Asample-Ablank)(negative control)/(Acontrol-Ablank)(positive control)*100%.

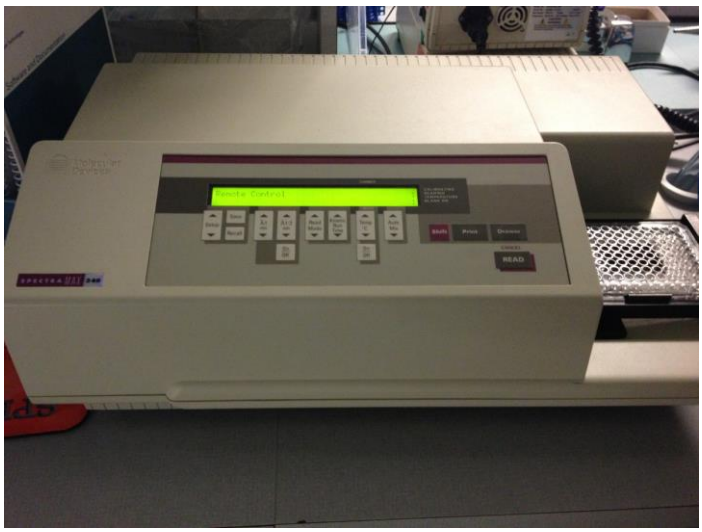

Figure 3.7. Spectra Max 340 plate reader (Molecular Device Inc., CA).

# CHAPTER 4 RESULTS AND DISSCUSSION

## 4.1 Introduction

This chapter presents the results of the experiments that were conducted based on the methods in Chapter 3. The data was obtained based on quantitative and qualitative measures from three aspects: spectroscopic analysis, mechanical properties and biocompatibility aiming to investigate the structural change resulting from the introduction of NDs as well as the reasons for the performance improvement of CS/ND composites. Experimental figures and related tables of data will be provided in this chapter.

## 4.2 Structural Analysis

### 4.2.1 Surface functionalization of ND particles assessed by FTIR spectroscopy

To provide evidence of functionalization of ND with acid, FTIR spectroscopy was performed on as-received ND powders (AR-ND) and after functionalized ND (F-ND). As it is shown in Figure 4.1, there are many peaks on both spectra including 3436 $cm^{-1}$; 2865 $cm^{-1}$; 2932 $cm^{-1}$; 1733 $cm^{-1}$ etc.. The peak at 3436 $cm^{-1}$ can be attributed to the stretching vibration of surface -OH groups. The peaks at 2865$cm^{-1}$ and 2932 $cm^{-1}$ are the characteristic peaks of ND, the stretching vibration of C-H bonding. The peaks around 1100-1400 $cm^{-1}$ are probably caused by C-N and N-H bonds due to nitrogen impurity distributed in diamond structure and –C-O-C- absorption [120]. Those peaks are similar in intensity for both the spectra. But the peak at 1733 $cm^{-1}$ due to the stretching of –C=O groups is much higher in the spectrum of F-ND than in the spectrum of AS-ND, indicating that the acid treatment process produces additional –C=O functional groups on diamond surfaces.

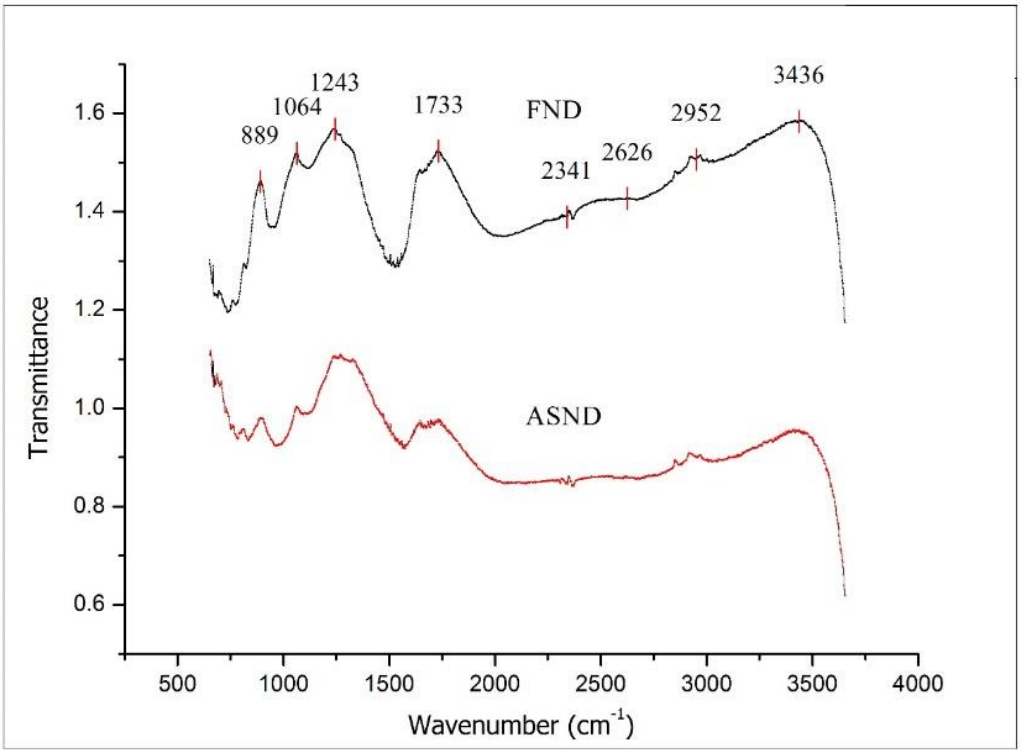


Figure 4.1. FTIR spectra of as-received ND (ASND) and functionalized ND (FND).

### 4.2.2 Morphology of CS/ND composites by SEM spectroscopy

SEM was used to observe diamond agglomeration, particle size and distribution in the composites. As we discussed in Chapter 2, ND particles have strong tendency to aggregate in order to reduce the surface energy, which is a big challenge for synthesis of strong ND reinforced composites. In addition to van der Waals force, groups introduced by surface functionalization may result in inter-particle hydrogen bonds. To prevent agglomeration, many ways including mechanical attrition, sonication and surfactant introduction are commonly used [121, 122]. In this research, sonication was used to facilitate the dispersion. The states of dispersion can be classified into 4 types: uniform dispersion, random dispersion, clustered random dispersion and agglomerated dispersion (Figure4.2).

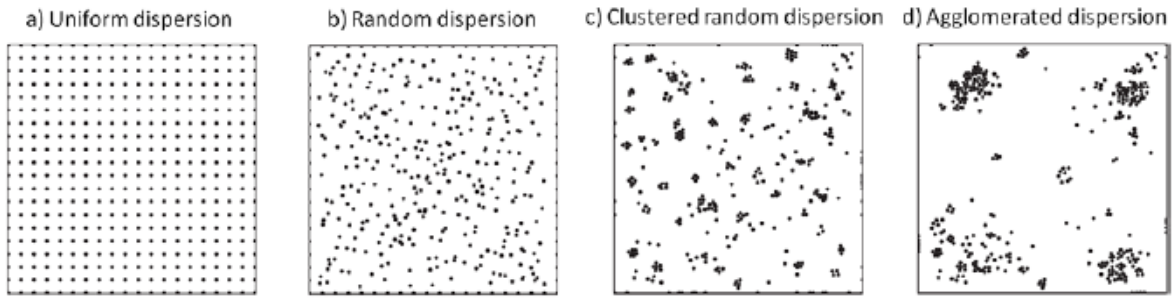


Figure 4.2. Dispersion and agglomeration states in particle reinforced polymer nanocomposites [123].

Figure 4.3 shows the surface morphology of CS, which is relatively flat and smooth comparing to the composite samples with ND fullers as shown in Fig.4.4. It can be seen from Figure 4.4, all composite samples with ND ranging from 1wt. % to 4wt. % illustrate a random distribution of NDs at low magnification. At higher magnification the sample with 4wt. % ND shows a typical clustered random dispersion pattern, which means local agglomeration of ND fillers exist. We can clearly see that when the amount of ND fillers increases, particle density increases, the interparticle distance of ND particles decreases, and the particle size shows no significant difference. These results illustrate that the CS/ND nanocomposites fabricated by continuous ultrasonication have a relatively low agglomeration, which is critical for the composites to take advantage of the large surface area of nanoparticles to form stronger interface for strengthening. From Figure 4.4 we can see that there are no crakes or microscale defects observed in the composites even the sample after nano-indentation (see Figure. 4.4 a), indicating a strong interfacial interaction and a strong strengthening potential.

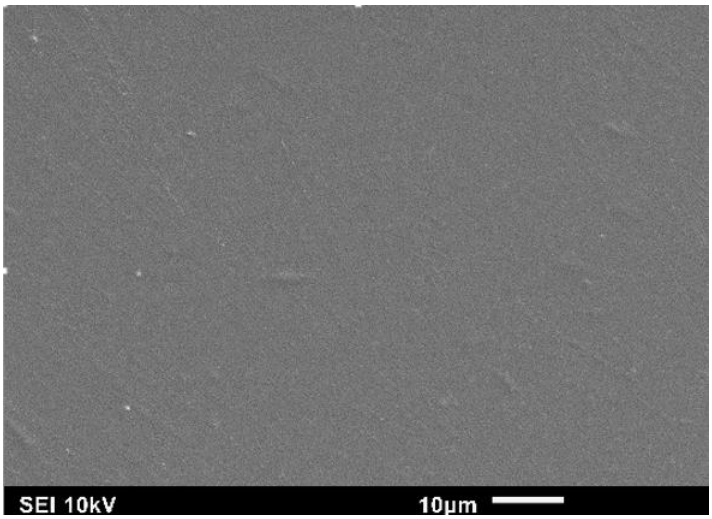


Figure 4.3. SEM image of pure CS.

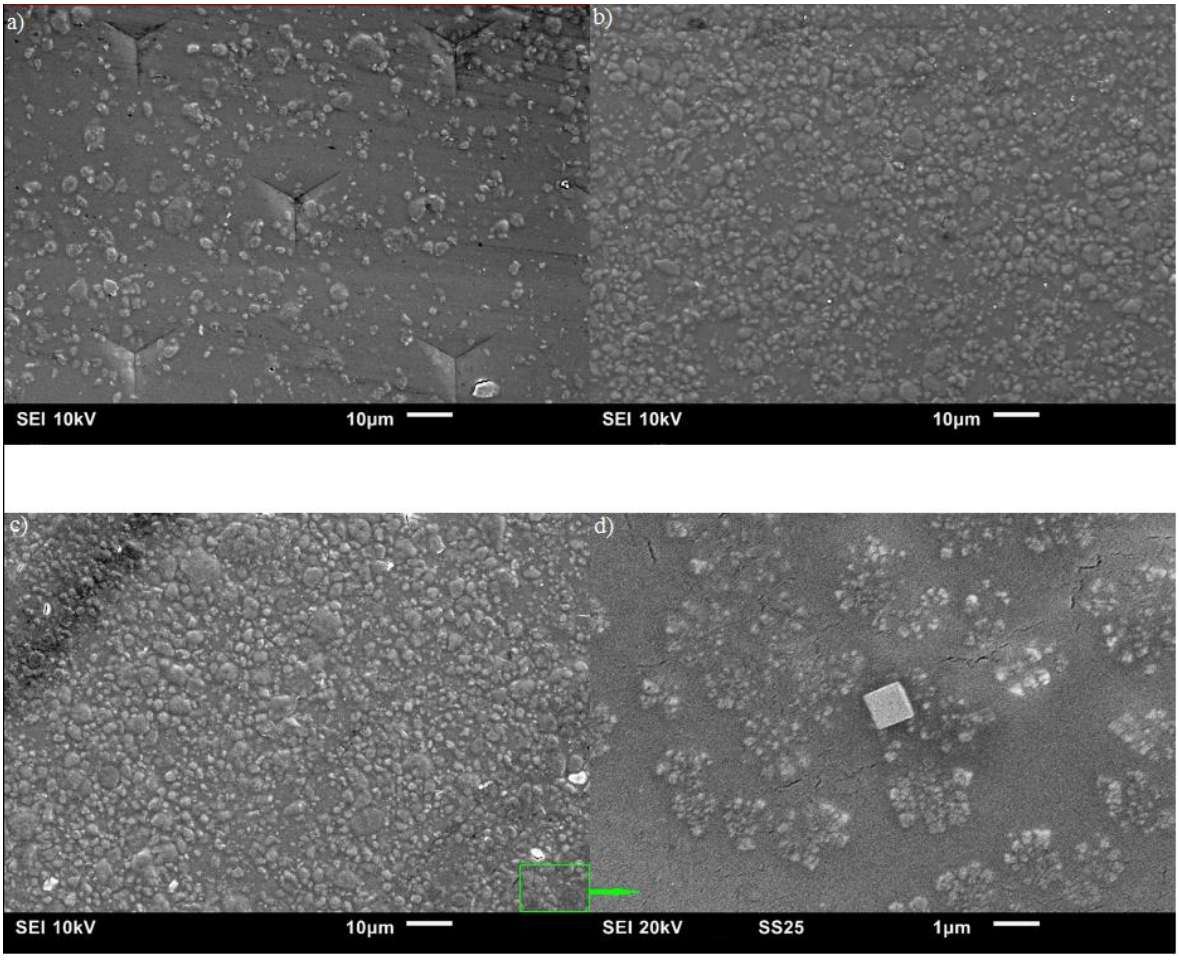


Figure 4.4. SEM images of CS with 1) 1wt. %ND (a); 2) 2wt. %ND (b); 3) 4wt. % (c) and CS with 4wt. % ND (d) with higher magnification.

### 4.2.3 Characterization of CS/ND composites by XRD

To identify the crystalline structure change of CS and how ND influences the crystallinity of CS composites, XRD was carried out on the samples. The XRD patterns of the all specimen are shown in Figure 4.5. All samples show the broad nature of the patterns which reveals that the CS and CS/ND composites are of a typical semi-crystalline structure. There is one broad peak appearing in all the patterns. This peak is at around 22° and can be am overlap of (0 2 0) planes of hydrated crystalline and amorphous structure of CS [124]. Upon the addition of ND to CS matrix, two new peaks at 13º and 26º appear which could be attributed to the new phases due to the interaction of CS and ND. Of these two peaks, the intense of the peak at 26º increases as ND content increases compared to the typical peak of CS at 22º, which also reveals that the new formed phase is a result of the interaction between ND and CS matrix.

The degree of crystallinity *Xc* for each sample was calculated and listed in Table 4.1 using the method mentioned in 3.3.1.2. It has been also noticed that, by introducing ND into CS matrix, the crystalline part of the peak at 22 º and the peak at 26º increases, indicating the increased crystallinity of CS/ND composites comparing to neat CS. This can be explained by the enhanced nucleation of ND particles on CS matrix, which helps the transformation of CS chains from amorphous state to crystalline state. Moreover, the functional groups and bonded polymer chains on ND surfaces can also partially regularize the order of matrix molecules and so as to enhance crystallization.

By a continuous increase of the amount of ND fillers from 1wt. % up to 4 wt. %, the degree of crystallinity of CS/ND drops from 0.286 to 0.241. It can be interpreted as the interactions between ND fillers and CS matrix which are restricting the mobility of the polymer chains to form crystal plates and thus result in a reduction of the crystallinity of CS in the composites. Higher amount of ND provides more surface area for the interaction with polymer chains, thereby, result in lower crystallinity.

Table 4.1. Degree of crystallinity of CS/ND composites measured by XRD

| Sample component | CS | CS/1 wt. % ND | CS/2 wt. %ND | CS/3 wt. %ND | CS/ 4 wt. % ND |
|---|---|---|---|---|---|
| Degree of crystallinity ($X_c$) | 21.1/100 | 28.6/100 | 25.6/100 | 24.2/100 | 21.4/100 |

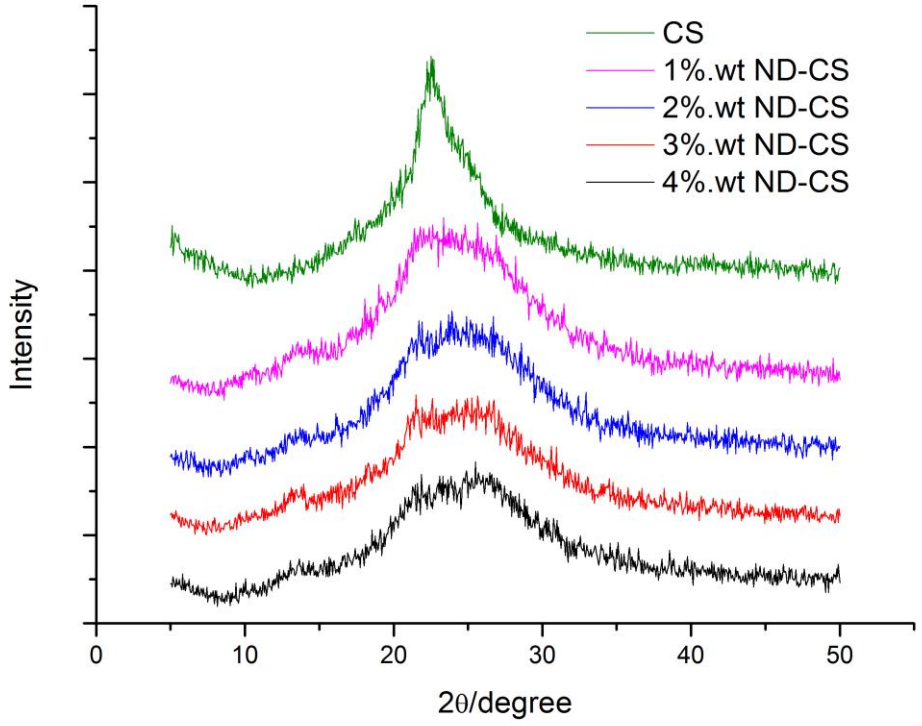


Figure 4.5. XRD patterns of pure CS and CS/ND composites with various ND concentrations.

### 4.2.4 Characterization of CS/ND nanocomposites by DSC

DSC analysis was conducted to understand the interaction between CS and ND. The DSC thermogram of CS (Figure 4.6) indicated exothermic transitions at 262.91°C and 271.86 °C along with two endothermic transitions at 94.61°C and 141.25°C. The exothermic transition is an indication of CS degradation at 261.71°C [125]. The occurrence of an endothermic transition at 94.61°C could be attributed to the moisture present in the specimens or the loss of

water associated with the hydrophilic groups of polymers. The presence of peak at 141.25°C could be attributed to the interchain hydrogen bonding dissociation process of CS [125, 126]. The glass transition temperature $T_g$ was found at 174.93°C for pristine CS, which is close to the reported value in the literature [126].

Figure 4.7 shows the DSC Thermogram of CS/ND with 1wt%ND. The curve illustrates the moisture endothermic peak at 95.37°C, hydrogen bonding dissociation at 142.38°C, glass transition temperature at 180.36°C and degradation temperature at 257.88°C/273.22°C, respectively. The hydrogen bonding dissociation temperature is consistent with a previous literature in which the peak is around 180°C [127-129].

DSC curves of CS/ND with 2 wt. %ND and 4 wt. % were obtained as well and are shown in Figure 4.8 and 4.9, respectively. The moisture endothermic peak, hydrogen bonding dissociation, glass transition temperature and degradation temperature of those two samples along with other samples are summarized in Table 4.2.

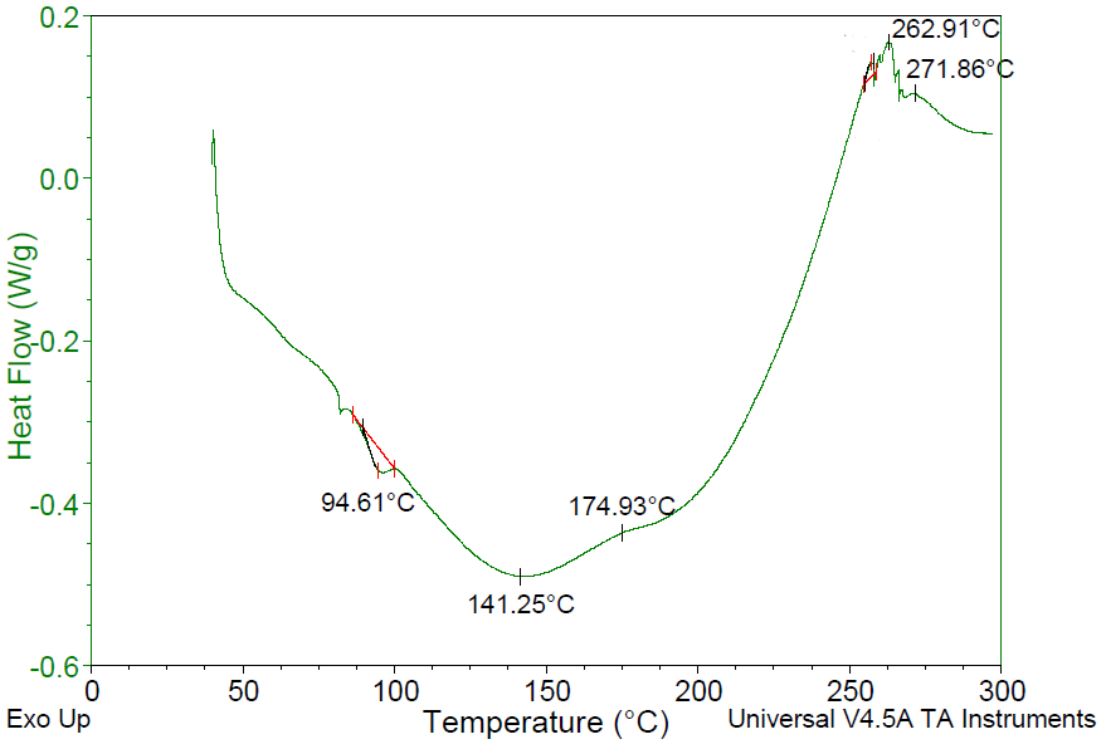


Figure 4.6. DSC Thermogram of pure CS at a heating rate of 10°C/min in nitrogen.

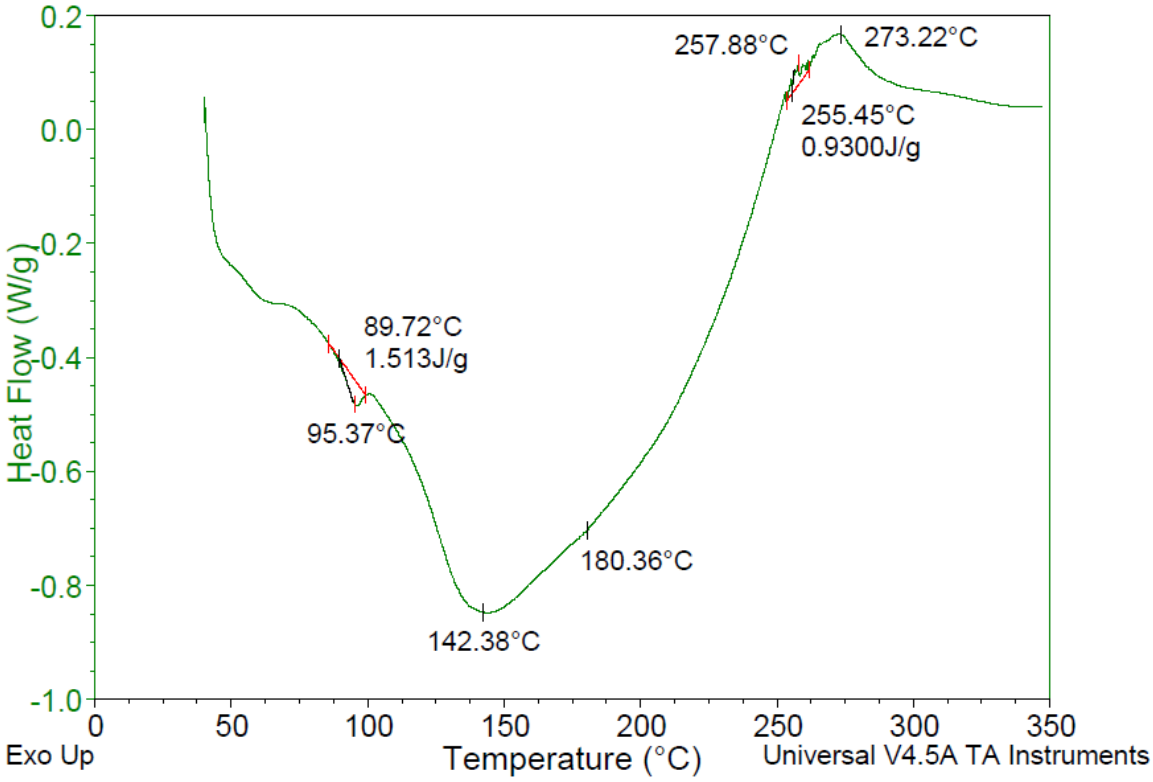


Figure 4.7. DSC Thermogram of CS/ND composite with 1 wt. %ND at a heating rate of 10°C/min in nitrogen.

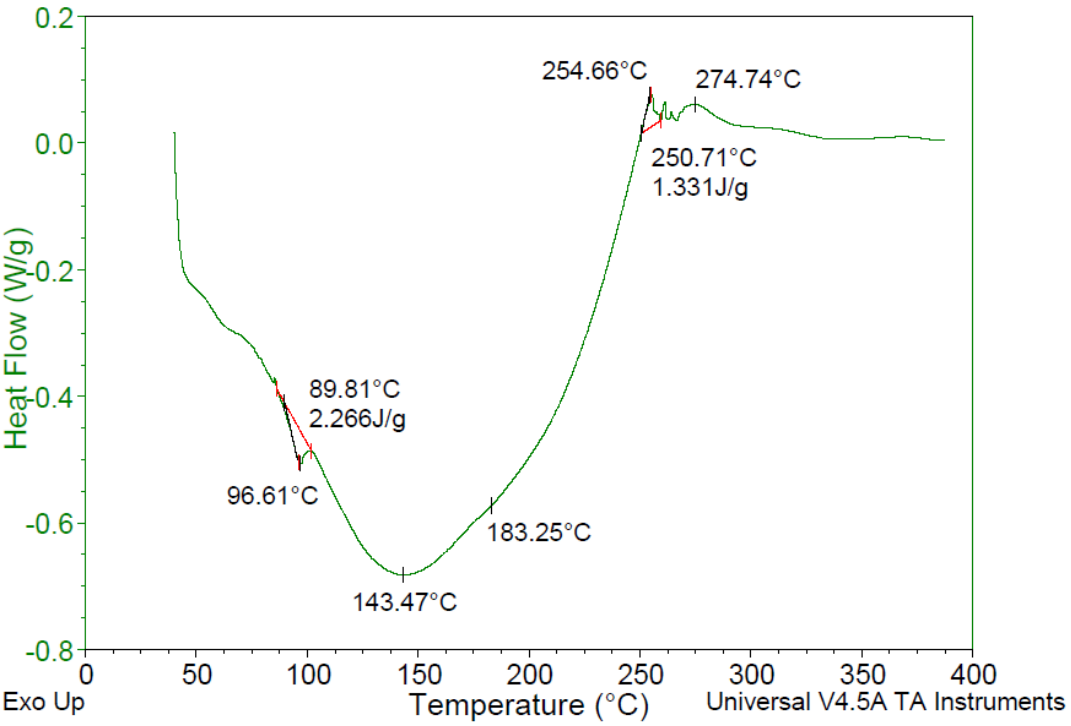


Figure 4.8. DSC Thermogram of pure CS/2 wt. %ND at a heating rage of 10°C/min in atmosphere of nitrogen.

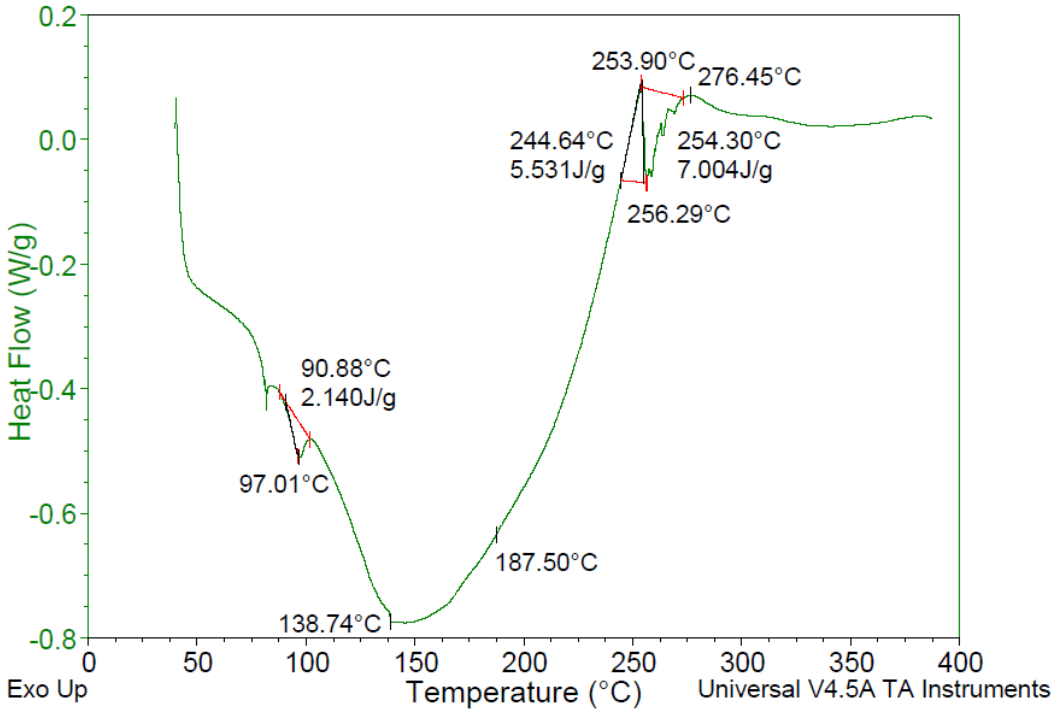


Figure 4.9. DSC Thermogram of pure CS/4wt. %ND at a heating rage of 10°C/min in atmosphere of nitrogen.

The endothermic peaks at around 95 °C associated with loss of water from the hydrophilic groups of polymers varies from 95.37°C to 97.01°C for composite samples with ND, a little bit higher than 94.61°C obtained for CS, indicating that the structure change of CS/ND results in an energy increase for water to thermally evaporate.

$T_g$ is an important parameter for the miscibility of polymer and fillers. Any physical property change in polymers due to filler incorporation can be reflected in $T_g$. The raised glass transition temperature with increasing ND content could be explained that with the incorporation of ND, the mobility of polymer chains was decreased and restricted due to the interaction of ND and CS chains which also limited the formation of polymer crystal. The result is consistence with the result of XRD in which the crystallinity was found decreased.

By comparing the degradation temperature of various specimen, it is clearly noticed that the thermal stability of second stage degradation increased with the addition of ND which can also

be explained by the strong interaction between ND surface groups and polymer chains. For the first degradation process, a decreasing degradation temperature $T_d$ could be explained as reason that in crystallized molecules of pure CS, they are arranged in a way where the interaction are the most strongest, when ND is introduced and interact with polymer chains, the molecules are moved away from their original position which may break the molecular symmetry, thus the formation of weaker interaction appears, and less energy is required to break them.

Table 4.2. DSC endothermic and exothermic peaks for CS and CS/ND composites.

| Components/Peaks | Endothermic (°C) | | | Exothermic (°C) |
|---|---|---|---|---|
| CS | 94.61 | 141.25 | 174.93 | 262.91/271.86 |
| CS/1wt%ND | 95.37 | 142.38 | 180.36 | 257.88/273.22 |
| CS/2wt%ND | 96.61 | 143.47 | 183.25 | 254.66/274.74 |
| CS/4wt%ND | 97.01 | 149.92 | 187.50 | 253.90/276.45 |

DSC curves of CS and CS/ND at 1 and 2 wt. % content were put together in Figure 4.12 for enthalpy observation and comparison. Detailed parameters were listed in Table 4.3. Enthalpy of loss of water increased from 1.158 J/g to 2.140 J/g when ND content increases to 4 wt. %, illustrating that CS/ND composites have a higher water retention capability which is consistent with the results of moisture endothermic peaks. The endothermic peak at approximately 145º increases significantly with the increase of ND content. This might be attributed to hydrogen bonding resulting from the massive carboxyl, amino and hydroxyl groups introduced by ND as well as local partial melting of CS. As the hydrogen bonding occurs when a hydrogen atom bound to highly electronegative atom such as nitrogen and oxygen experiences attraction to other highly electronegative atoms. In this work, among hydroxyl groups and amino groups existing in both polymer and ND particles, more energy was required to break this electrostatic

attraction.

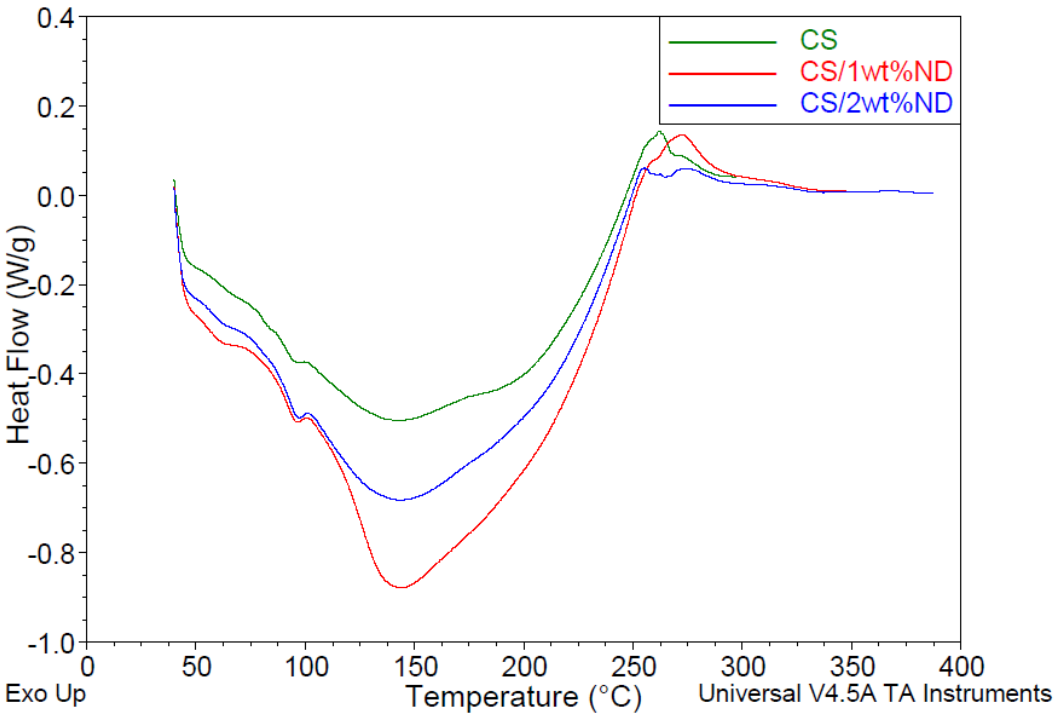


Figure 4.10. DSC Thermogram of CS, CS/ND composites with 1 and 2 wt. %ND at a heating rate of 10°C/min in nitrogen.

Multiple peaks show in the curves ranging from 250°C to 275°C. The overlap peaks of CS can be roughly described as two exothermic degradation peaks. A new endothermic peak appears at around 256°C for the CS/ND composites, as shown in Figure 4.10 and Figure 4.11. As the enthalpy of the new phase is positively associated with the amount of ND, it could be speculated that this new phase or structure with an endothermic thermal property might result from the interaction between ND and CS matrix. Further investigation using high resolution transmission electron microscope is required in order to identify if the new phase exists as an interphase surrounding NDs or not.

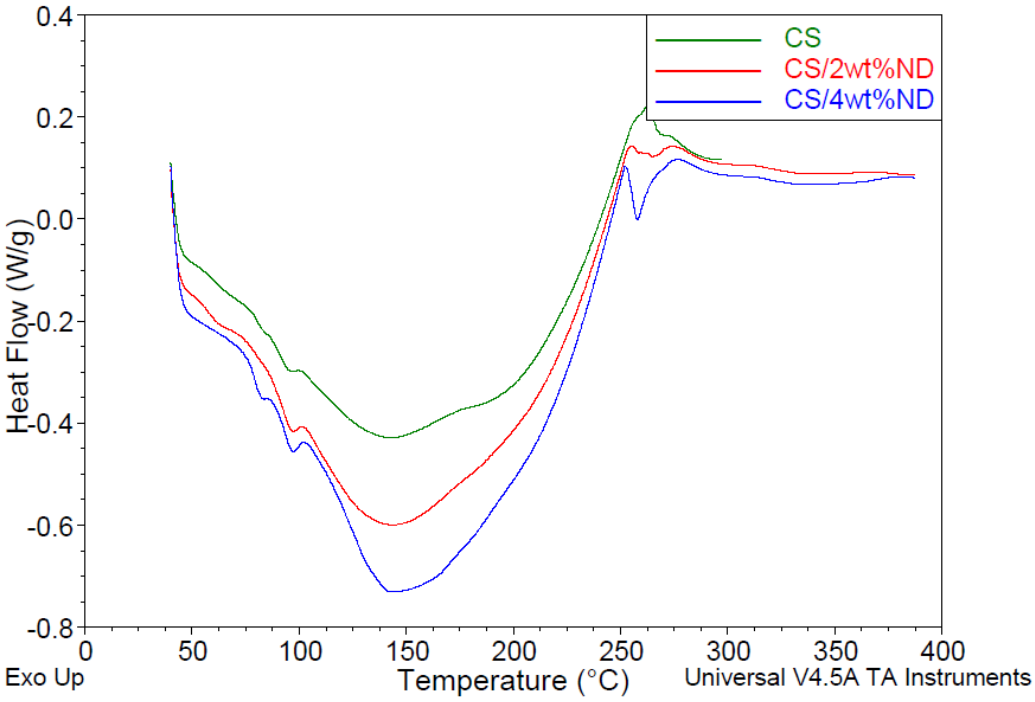


Figure 4.11. DSC Themogram of CS and CS/ND composites with 2wt% and 4 wt. %ND at a heating rate of 10°C/min in nitrogen.

Table 4.3. DSC Endothermic Enthalpy results for CS and CS/ND composites.

| Component/Enthalpy | Endothermic Enthalpy (J/g) | Exothermic Enthalpy (J/g) | |
|---|---|---|---|
| | | New Phase | Degradation |
| CS | 1.158 | / | 0.213 |
| CS/1wt%ND | 1.513 | / | 0.930 |
| CS/2wt%ND | 2.266 | / | 1.831 | 1.331 |
| CS/4wt%ND | 2.140 | / | 7.004 | 5.531 |

### 4.3 Mechanical properties of CS/ND composites

Scaffolds should provide a sufficient mechanical strength for their clinical applications. Therefore, the mechanical properties of the composites, Young's modulus and hardness were characterized by nano-indentation technique. 25 indents were applied for each type of samples and are shown as a pattern in Figure 4.12. Load-displacement curves were plotted and

manually corrected through UMT software as shown in Figure 4.13. Young's modulus and hardness of each specimen were subsequently calculated and plotted as described in Figure 4.14. Young's modulus is calculated from the slope of Figure 4.13. The hardness is given as the ratio of maximum load to the indentation area. All the results were expressed as the mean value with a standard deviation.

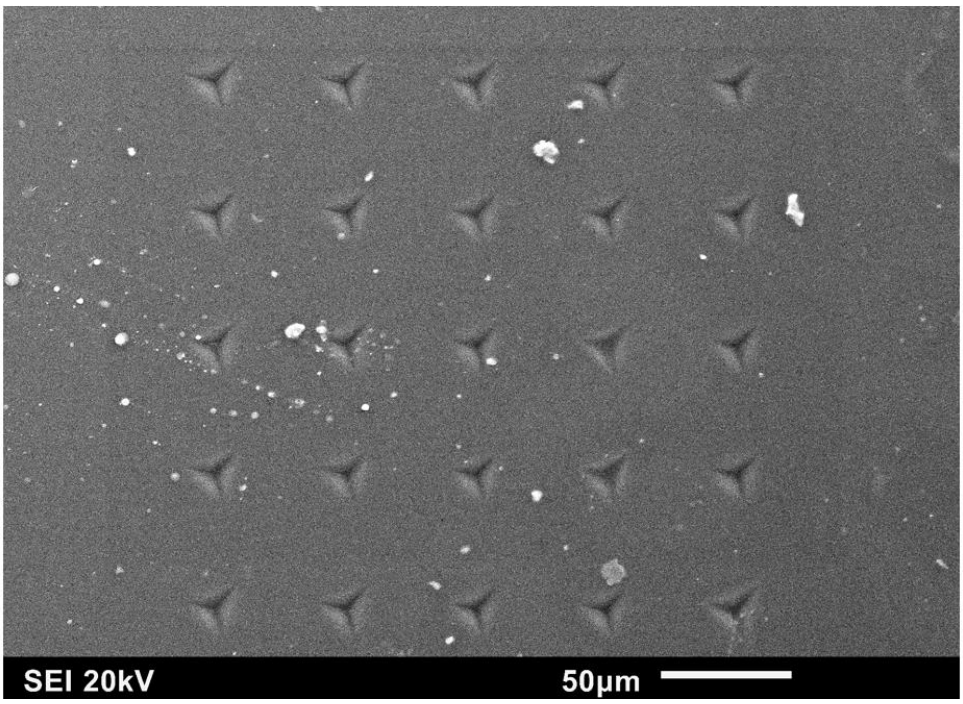


Figure 4.12. SEM image of 5×5 25 residual indents on CS film.

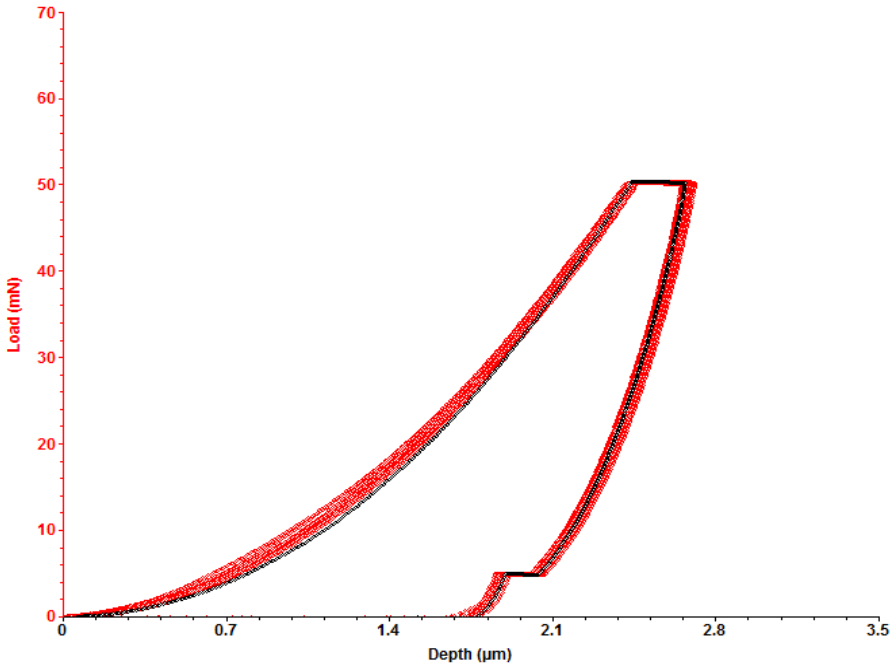


Figure 4.13. Typical load-displacement curves obtained from the nanoindentation tests for CS/ND composite. The specimens were submitted loading-unloading cycle with 50mN. 25 curves were plotted and corrected.

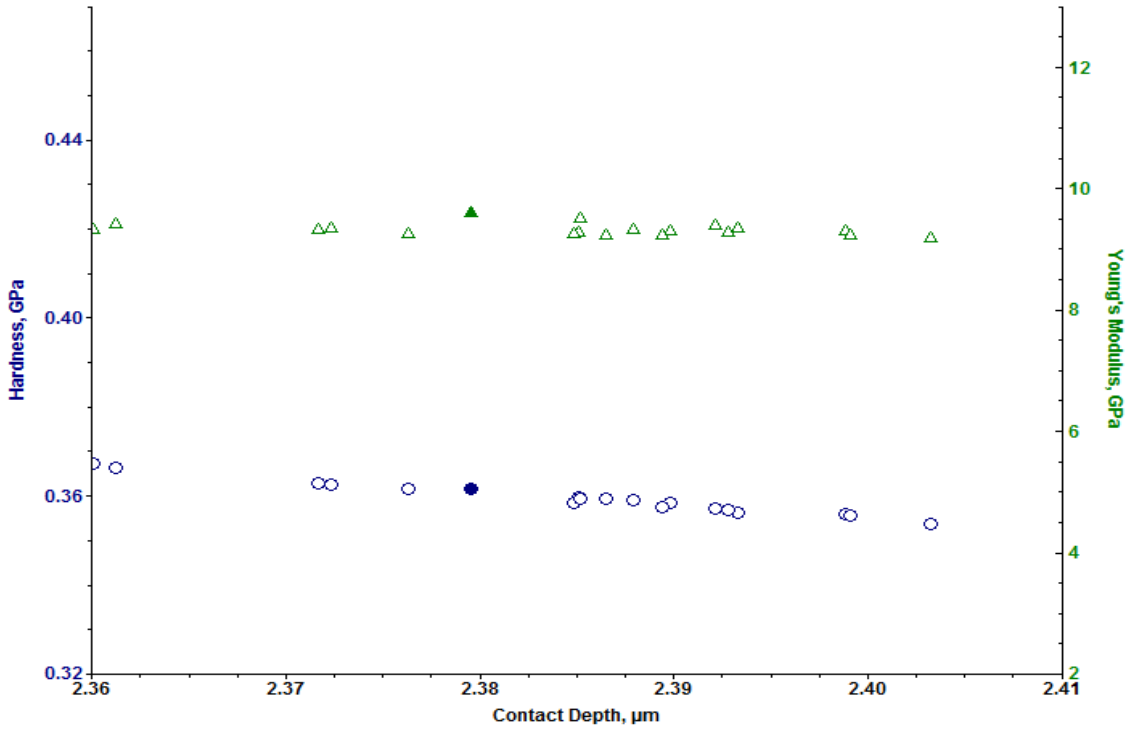


Figure 4.14. Mechanical properties of CS/ND (3wt. %). The apparent hardness (o) and Young's modulus (Δ) were determined by nanoindentation with UMT nanoindentation

program through a series of 25 load-displacement measurements

### 4.3.1 Young's Modulus

Figure 4.15 shows the Young's modulus of pure CS and CS/ND (functionalized) composites with a ND content ranging from 1% to 5%. The experimentally determined Young's modulus of CS is 2.22±0.06 GPa, which is very close to the values reported in a previous literature [130]. The modulus values of the composites are much higher than pure CS and increase with the increase of ND content in the samples. The value for the CS/ND sample with 1 wt % ND is 7.55±0.09 GPa, 2.4 times of that of pure CS. The value for CS/ND with 5 wt% ND is 9.83GPa ±0.20 GPa, 3.4 times more than that of the pure CS.

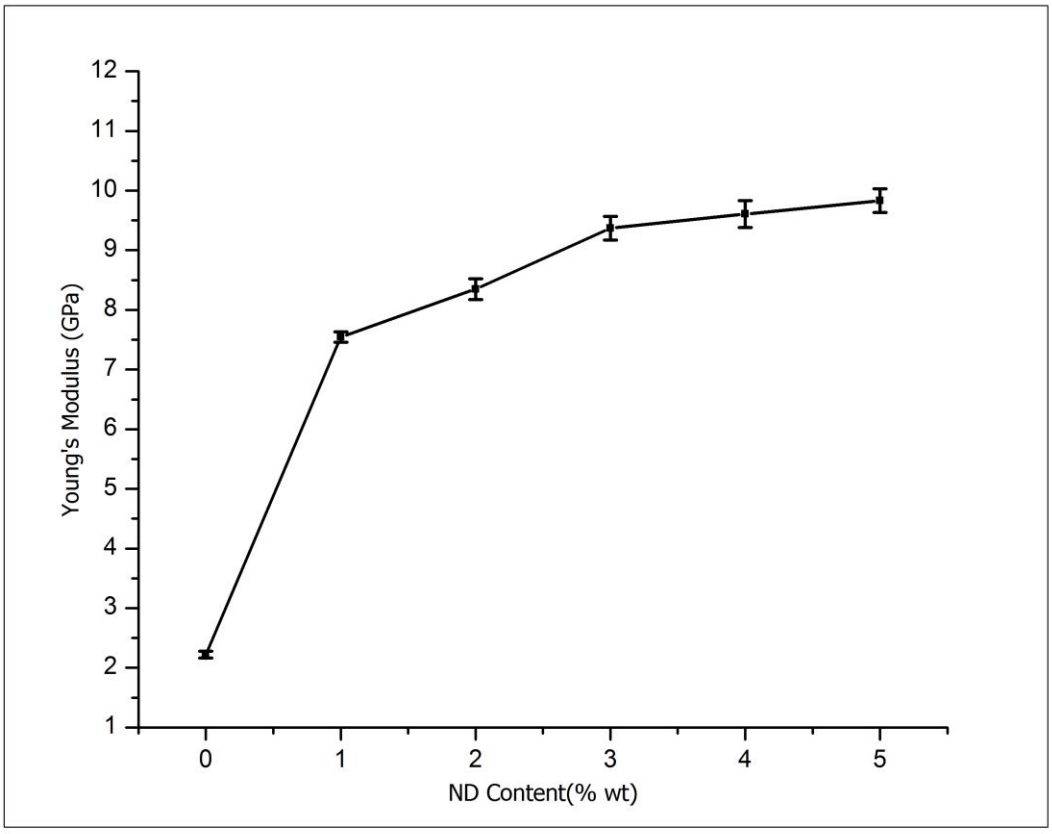


Figure 4.15. Young's modulus of CS/ND plotted as a function of ND content.

Some analogous composites of polymer and nano-filler system from previous literature have also been claimed to have increased Young's modulus. It has been reported that ND-ODA/PLLA with a 5 wt % ND has a Young's modulus of 5.9±0.3 GPa, 2.27 times of that for the pure polymer matrix, measured by nano-indentation [131], whereas for PVA-ND with 0.6 wt.% ND, the improvement of Young's modulus was 98 % to the PVA reference samples[132], and for epoxy/ND, the highest value of modulus is reported to be 6.12±0.03 GPa at 4.0 wt% ND, 57 % higher than that of the epoxy matrix [92]. Modulus loss was also found in some polymer/nano-fillers systems such as CS/Alg/n$SiO_2$, modulus measured was decreased by 9% with the addition of 1wt% n$SiO_2$ from 8.99±0.02MPa to 8.16±0.57MPa [133].

Overall, the addition of ND into CS results in a great increment in Young's Modulus. We attribute the results to two major factors: good dispersion and strong interaction between ND surface groups and CS matrix. A homogenous dispersion of ND provides large contact area to interact with the matrix. Functionalized surface groups on ND participate in the reaction with CS chains and cross link the particles and polymer matrix with hydrogen bonding to form a network structure, as suggested by DSC patterns, which could greatly hinder the chain's movement and enhance the load transfer ability. This effect is illustrated by the significant Young's modulus incresement in CS/ND composites with 1wt%ND. However, the increase of the modulus with ND content is not linear. This might be attributed to the increased ND agglomeration at higher ND content. Agglomeration would decrease effective area of ND to interact with polymer matrix. Besides, ND agglomeration form a network of ND particles with weak secondary bonding. These agglomerations are infiltrated by CS matrix, which is also the reason causing structure instability. Young's modulus improvement shown in Table 4.4 suggests that the Young's modulus of the composites is strongly related to the degree of interaction between ND surface groups and polymer matrix, ND content, dispersion, and surface functional groups.

Table 4.4. Mechanical properties of CS/ND composites measured by nano-indentation (Note: the errors are the standard deviation based on 20 measurements)

| Sample composites | Young's Modulus(GPa) | Improvement (%) | Hardness (GPa) | Improvement (%) |
|---|---|---|---|---|
| **CS/ 0%wt ND** | 2.22±0.06 | 0 | 0.17±0.01 | 0 |
| **CS/ 1%wt ND** | 7.55±0.09 | 239 | 0.28±0.01 | 68 |
| **CS/ 2%wt ND** | 8.35±0.17 | 276 | 0.33±0.01 | 96 |
| **CS/ 3%wt ND** | 9.37±0.20 | 321 | 0.36±0.01 | 114 |
| **CS/ 4%wt ND** | 9.61±0.23 | 333 | 0.37±0.02 | 118 |
| **CS/ 5%wt ND** | 9.83±0.20 | 343 | 0.38±0.01 | 127 |
| **CS/ 1%wt ASND** | 7.14±0.20 | 221 | 0.21±0.01 | 26 |

### 4.3.2 Hardness

Hardness of CS/ND composites with ND content ranging from 0 % to 5 wt. % measure by nanoindentation is shown in Figure 4.16. The hardness of the composites are much higher than CS and increases with the increase of ND content. Compared with the pure CS, the addition of 1%, 2%, 3%, 4%, 5% wt. ND increases the hardness by 68%, 96%, 114%, and 118%, and 127%, respectively.

To understand the effect of functionalization, CS/1%wt as-received ND (AS-ND) composite was tested as reference. As shown in Table 4.4, the addition of as-received ND can also lead an increase in both Young’s modulus and Hardness, however, the improvement is less than the ones with functionalized ND, suggesting that surface modification of ND is effective in enhancing interaction between ND and CS matrix and thus enhance the strength and stiffness of the composites.

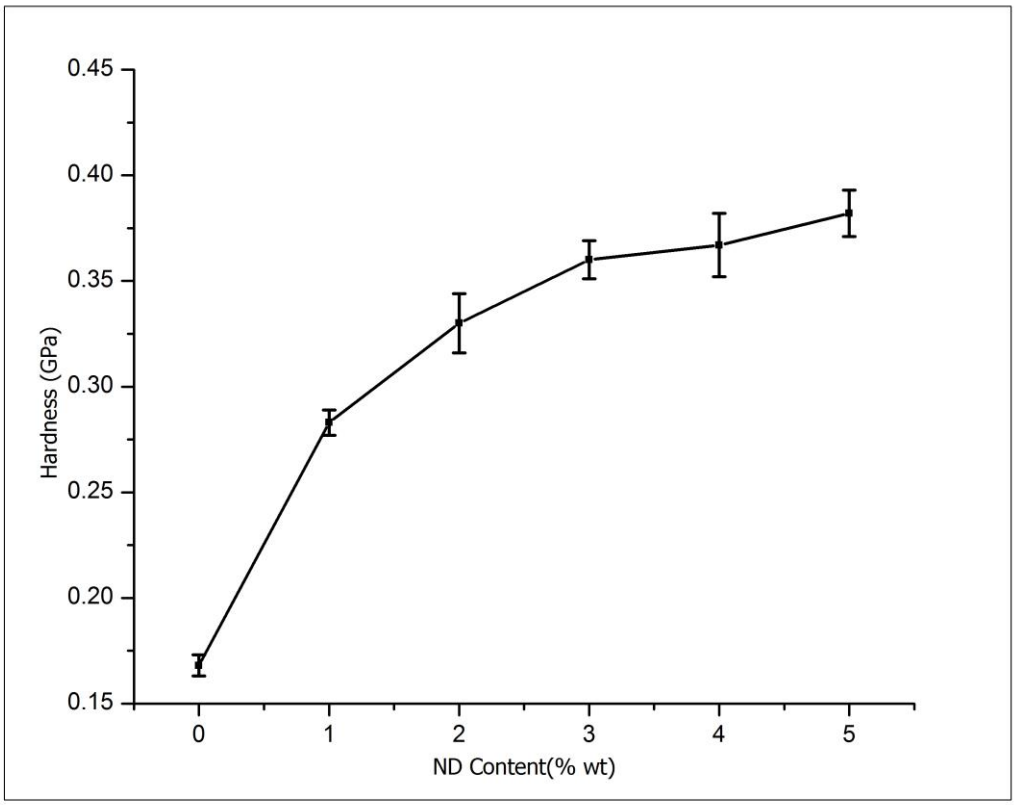


Figure 4.16. Hardness of CS/ND plotted as a function of ND content.

Figure 4.17 shows a hypothetical structure change because of the addition of ND, in which the surface groups of ND particles are surrounded and hydrogen bonded to CS chains. This network structure is the key factor in enhancing mechanical strength by transferring load from ND particles to the CS matrix.

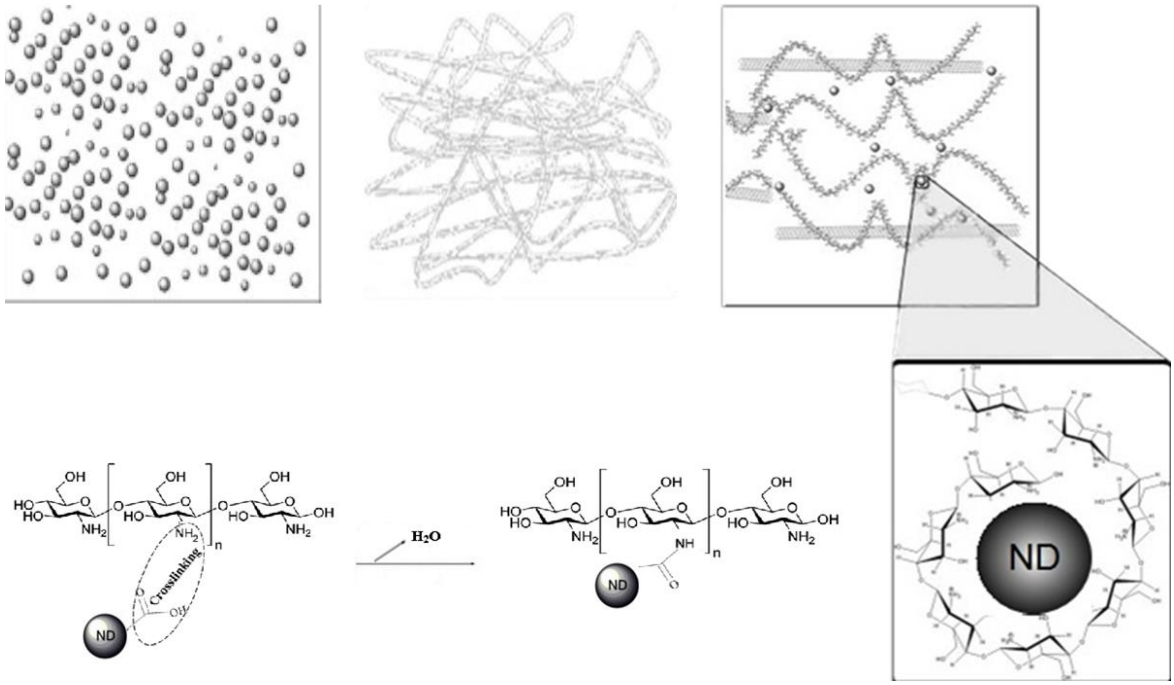


Figure 4.17. Hypothetical microstructure changes of ND/CS composites.

### 4.4 Biocompatibility of CS/ND composites

A well bio-friendly material should exhibit no toxicity or no negative impact on cell growth and proliferation. MTT assay was used to evaluate the biocompatibility of CS/ND composites to see its potential for biomedical applications. The MTT assay was carried out using the methods described in Chapter 3. CS/ND composites with different ND content as well as CS were used as samples for testing. The concentration range of ND was set from 1% to 3% considering the microstructure structure and mechanical properties are close since the concentration ranges from 3% up to 5%. Measured values are expressed as means ± standard deviation. Levels of significance for comparing mean values of absorbance in the MTT assay were calculated using one-way ANOVA with Turkey posttest. All calculations were made using GraphPad Prism 6.0.

The results from MTT assay are showed in Figure.4.18. Cell number for samples from 12h incubation to 48h incubation is reflected by absorption strength. There was a slight difference between control group and all CS contained samples (Cell viability of control group is slightly

higher than that of CS contained groups), which is consistent with previous research [134]. Subsequent studies using CS of lower molecular weight were found not to be toxic against L132 human embryonic lung cells or CCRF-CEM human lymphoblastic leukemia cells up to a concentrations of 500 ug/ml [135]. In general, CS exhibits a slightly lower cell proliferation rate, but no cytotoxic effect.

In the first 12 hours incubation, compared with pure CS, the addition of ND did not show any obvious effect on the cell proliferation. All CS contained specimen exhibited close proliferation rate on Schwann cells.

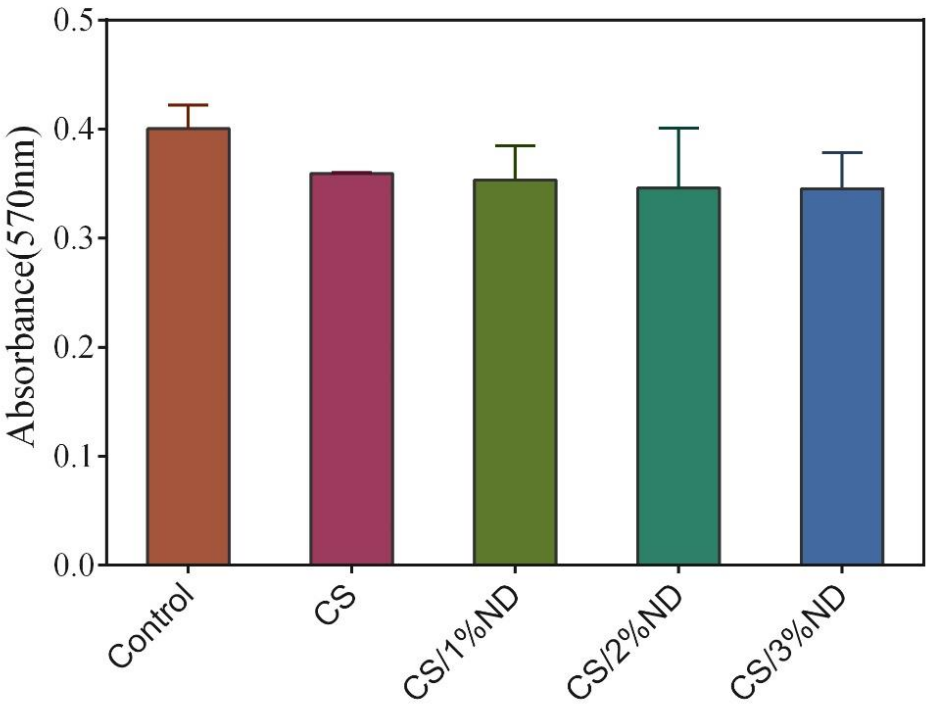


Figure 4.18. MTT analysis of control, CS, CS/1wt. %ND, CS/2wt. % ND, CS/3wt. %ND at 12 h.

With a longer incubation for 24 hours (see Figure 4.19), the cell proliferation increases with the addition of ND, and for the one with 2% ND content, the cell concentration is very close to that of the control group. The results show that in 24 hours, the addition of ND does not

negatively affect the biocompatibility of CS itself but increase the cell viability when ND content ranging from 1wt%, to 3wt%. This proliferation increase might also result from the cell recovery due to the addition of ND. In order to identify the in-depth mechanism, further detailed investigation is needed.

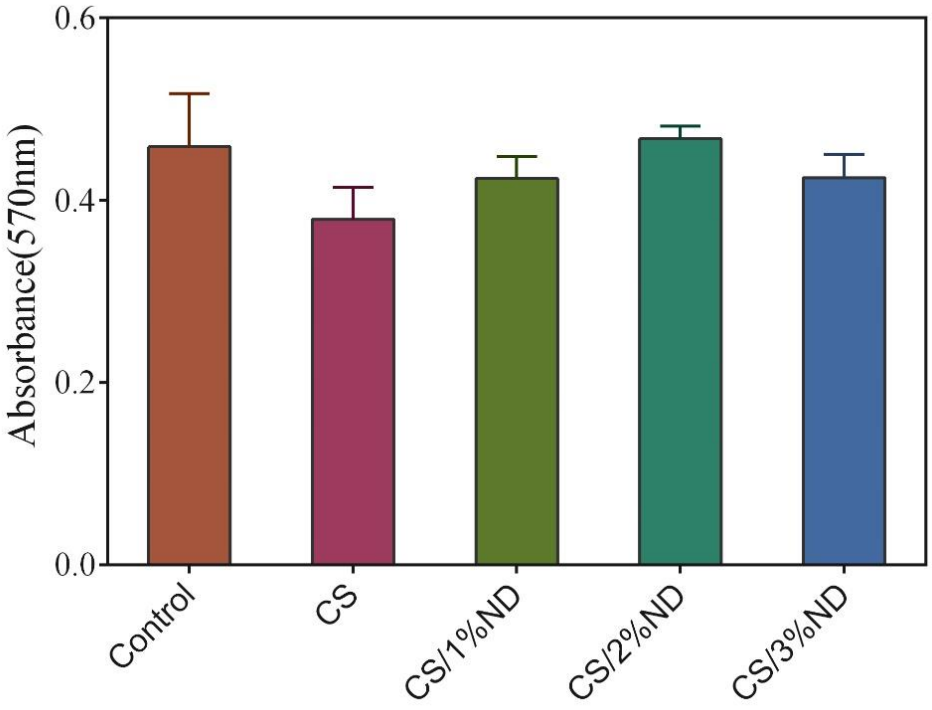


Figure 4.19. MTT analysis of control, CS, CS/1wt. %ND, CS/2wt. %ND, CS/3wt. %ND at 24 h.

A longer term of incubation for 48 hours was also performed and the results are shown in Figure 4.20. The results indicates that there are no significant difference in cell viability among all samples. Cell viability of control groups is the highest comparing with other samples, consistent with the results for 12 hours and 24 hours incubation. It is observed that after 48 hours incubation, an increase in cell viability from addition of ND still exists when ND content is 1wt% and 3 wt%. A comparison of various samples in different periods is also shown in Figure 21. It should be noted that it is possible that the MTT results could be partially affected

by cell recovery and MTT as a mutagen may also affect the resultant cells.

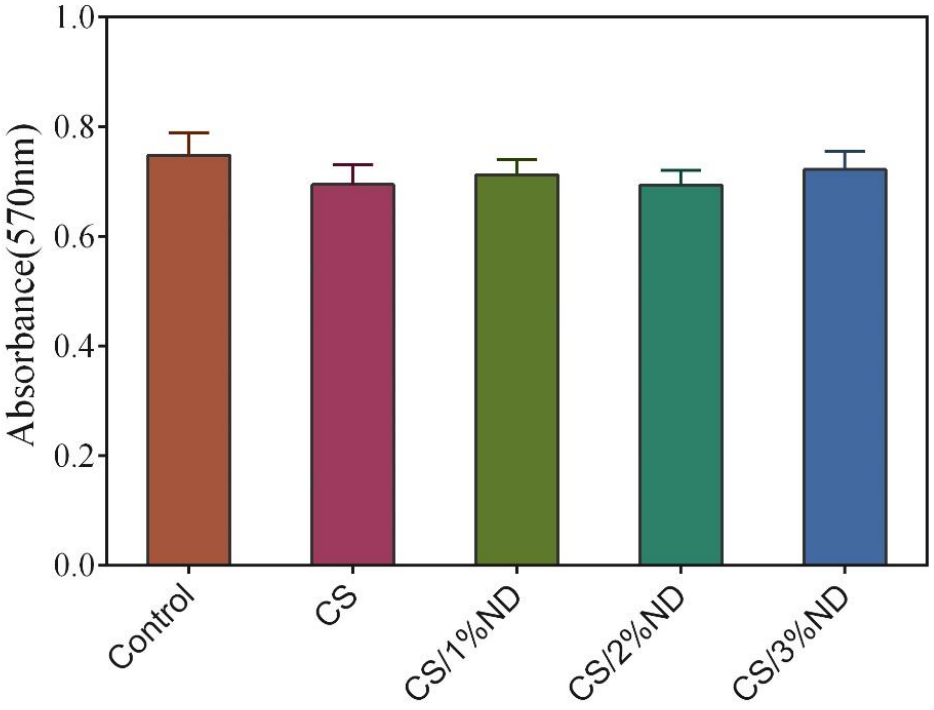


Figure. 4.20 MTT analysis of control, CS, CS/1wt. %ND, CS/2wt. %ND, CS/3wt. %ND at 48 h.

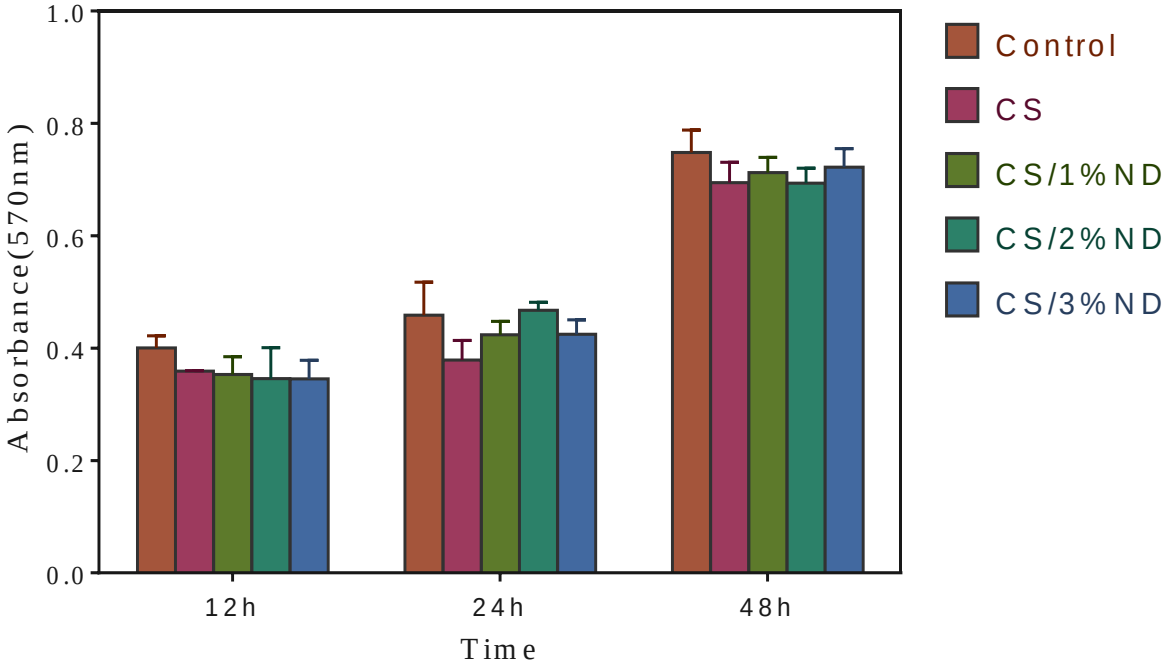

Figure 4.21. MTT analysis of control, CS, CS/1wt. %ND, CS/2wt. %ND, CS/3wt. %ND, at 12, 24, 48 hours' time interval. Values are reported as mean ± standard deviation (n=3), significant differences for *p<=0.05 and **p<=0.01 were found.

# CHAPTER 5 SUMMARY, CONCLUSIONS, AND RECCOMENDATIONS

## 5.1 Summary and Conclusions

Synthetic biodegradable CS and ND composites were investigated for bone tissue scaffold application. The composite films were synthesized using a simple conventional method, solvent casting. The composites were then characterized by various advanced techniques to evaluate the structural, mechanical, and biomedical properties. The results and conclusions are summarized as follows:

1) SEM observation shows that ND particles in the composites disperse uniformly into the CS matrix n and have good affinity with the CS matrix.
2) XRD results suggests that the addition of ND to CS decreases the crystallinity of CS, which gives evidence to support that ND with functional groups could interact with CS chains and form a more complex network.
3) The mechanical properties of CS/ND composites measured by nanoindentation have been significantly improved with the addition of ND: 1wt% ND had 239% improvement in Young's modulus and 68% improvement in hardness. And the mechanical properties are positively correlated with ND content. With 5%ND, the Young's modulus is increased by 3.4 times and the hardness is increased by 1.2 times. AS-ND is less effective in enhancing the mechanical properties of CS/ND composites than F-ND, indicating that surface groups on ND play important roles in enhancement of mechanical properties.
4) DSC results show that the addition of ND can increase the glass transition temperature and the glass transition temperature increases with the increase of ND content, which further confirms the structure change of CS induced by the addition of ND.
5) Biocompatibility and cytotoxicity evaluation results indicate that CS and CS/ND are not toxic to Schwann cells, and in terms of cell numbers incubated for various periods,

the addition of ND, in some ways could support the cell proliferation instead of a negative effect on cell viability.

6) CS/ND composites exhibit combined advantageous properties of the CS and ND. The composites “inherits” the biocompatibility, tunable biodegradability of CS and the high hardness and stiffness of ND and are very promising to be used as bone tissue scaffolds in tissue engineering.

### 5.2 Recommendations for Future Work

CS/ND nanocomposite films were fabricated by solvent casting and characterized by various techniques in this work and the results demonstrate the great potential to be used as bone tissue scaffold material. Further work Fshould focus on fabrication of CS/ND scaffolds with a more complex 3D structure and controlled porosity and the evaluation of their properties including strength, stiffness, hardness, corrosion, fatigue, and property degradation. Agglomeration is one of the critical limitations impeding the extensive use of ND, more desirable strategies are required to eliminate agglomeration in order to take full advantage of ND’s high specific area to allow a high degree of interaction between nanofiller (ND) and polymer matrix.

According to clinical requirements, more specific functionalization methods for ND might be needed. A pharmaceutical compound or chemical formulation carried by ND would be transported to the site of injury for a better treatment.

Biocompatibility test was carried out on Schwann cells initially. Osteoblast cells in vitro culture and the combination of Schwann and Osteoblasts cells are taken into consideration in order to further confirm the feasibility of this material for the application in bone tissue engineering.

In vitro and in vivo degradation of the composite materials and the effect of ND on the

biodegradation are important for their application and need to be taken into consideration in the future work. An adjustable degradation rate for scaffold is essentially required to meet various demands in practice.

In summary, incorporation of ND particles with rich and diverse functionalized groups into CS shows great potential for tissue regeneration and recovery. More research is needed in order to integrate them with other biomaterials and bioactivator to meet the requirements for tissue scaffolds in clinical applications.

## REFERENCES


1. Fractures/Broken Bones Data. [cited 2015 05.01]; Available from: http://www.schwebel.com/userfiles/files/Fractures(1024).pdf.
2. Burge, R., B. Dawson-Hughes, D.H. Solomon, J.B. Wong, A. King, and A. Tosteson, Incidence and Economic Burden of Osteoporosis-Related Fractures in the United States, 2005–2025. Journal of Bone and Mineral Research, 2007. **22**(3): p. 465-475.
3. Baroli, B., From natural bone grafts to tissue engineering therapeutics: Brainstorming on pharmaceutical formulative requirements and challenges. J Pharm Sci, 2009. **98**(4): p. 1317-75.
4. Langer, R., Biomaterials in Drug Delivery and Tissue Engineering: One Laboratory's Experience. Accounts of Chemical Research, 2000. **33**(2): p. 94-101.
5. O'Brien, F.J., Biomaterials & scaffolds for tissue engineering. Materials Today, 2011. **14**(3): p. 88-95.
6. Wolter, J.R. and R.F. Meyer, Sessile Macrophages Forming Clear Endotheliumlike Membrane on the inside of Successful Keratoprosthesis. Graefes Archive for Clinical and Experimental Ophthalmology, 1985. **222**(3): p. 109-117.
7. A Proposal to the National Science Foundation for An Engineering Research Center at UCSD, CENTER FOR THE ENGINEERING OF LIVING TISSUES. in 1985 ERC proposal from UCSD. August 23, 2001. An Engineering Research Center at UCSD: Y.C. Fung.
8. Franco, B., V. Vincenzo, D.V. Alessandro, C. Tonello, G. Abatangelo, and F. Mazzoleni, Tissue engineering approaches for the construction of a completely autologous tendon substitute. Indian J Plast Surg, 2008. **41**(1): p. 38-46.
9. Green, W.T., Jr., Articular cartilage repair. Behavior of rabbit chondrocytes during tissue culture and subsequent allografting. Clin Orthop Relat Res, 1977(124): p. 237-50.
10. Langer, R. and J.P. Vacanti, Tissue engineering. Science, 1993. **260**(5110): p. 920-6.
11. Dvir, T. Laboratory for Tissue Engineering and Regenerative Medicine. Available from: http://www.lifesciences.tau.ac.il/departments/biotech/members/dvir/dvir.html.
12. Long Bone. [cited 2015 07.20]; Available from: http://w3.shorecrest.org/~Lisa_Peck/anatomy_phys/ch_5skeletal/ch5_Images/images/05.02_LongBone_1.jpg.
13. Harversian system. [cited 2015 07-20]; Available from: http://webs.ashlandctc.org/mflath/KEY%20SKELETAL%20I%20OBJECTIVES.htm.
14. Ruppel, M.E., L.M. Miller, and D.B. Burr, The effect of the microscopic and nanoscale structure on bone fragility. Osteoporos Int, 2008. **19**(9): p. 1251-65.
15. Bone Development and Growth. [cited 2015 07.21]; Available from: http://classes.midlandstech.edu/carterp/Courses/bio110/chap06/chap06.html.
16. Goulet, J.A., L.E. Senunas, G.L. DeSilva, and M.L. Greenfield, Autogenous iliac crest bone graft. Complications and functional assessment. Clin Orthop Relat Res, 1997(339): p. 76-81.
17. Greenwald, A.S., S.D. Boden, V.M. Goldberg, Y. Khan, C.T. Laurencin, R.N. Rosier, and I. American Academy of Orthopaedic Surgeons. The Committee on Biological, Bone-graft substitutes: facts, fictions, and applications. J Bone Joint Surg Am, 2001. **83-A Suppl 2 Pt 2**: p. 98-103.
18. Ruediger, T., A. Berg, A. Guellmar, C. Rode, M. Schnabelrauch, A. Urbanek, K. Wagner, R. Wyrwa, R.W. Kinne, and B.W. Sigusch, Cytocompatibility of

polymer-based periodontal bone substitutes in gingival fibroblast and MC3T3 osteoblast cell cultures. Dent Mater, 2012. **28**(10): p. e239-49.
19. Mauck, J.A.B.l.R.L., Biomaterials for Tissue Engineering Applications. 2011, NewYork: SpringerWien.
20. Amini, A.R., C.T. Laurencin, and S.P. Nukavarapu, Bone tissue engineering: recent advances and challenges. Crit Rev Biomed Eng, 2012. **40**(5): p. 363-408.
21. Petite, H., V. Viateau, W. Bensaid, A. Meunier, C. de Pollak, M. Bourguignon, K. Oudina, L. Sedel, and G. Guillemin, Tissue-engineered bone regeneration. Nat Biotechnol, 2000. **18**(9): p. 959-63.
22. Rose, F.R. and R.O. Oreffo, Bone tissue engineering: hope vs hype. Biochem Biophys Res Commun, 2002. **292**(1): p. 1-7.
23. Lu, L., S.J. Peter, M. D. Lyman, H.-L. Lai, S.M. Leite, J.A. Tamada, S. Uyama, J.P. Vacanti, L. Robert, and A.G. Mikos, In vitro and in vivo degradation of porous poly(dl-lactic-co-glycolic acid) foams. Biomaterials, 2000. **21**(18): p. 1837-1845.
24. Gaspar, A., L. Moldovan, D. Constantin, A.M. Stanciuc, P.M. Sarbu Boeti, and I.C. Efrimescu, Collagen-based scaffolds for skin tissue engineering. J Med Life, 2011. **4**(2): p. 172-7.
25. Sakai, S. and K. Kawakami, Development of Porous Alginate-Based Scaffolds Covalently Cross-Linked through a Peroxidase-Catalyzed Reaction. J Biomater Sci Polym Ed, 2010.
26. Zakhem, E., S. Raghavan, R.R. Gilmont, and K.N. Bitar, Chitosan-based scaffolds for the support of smooth muscle constructs in intestinal tissue engineering. Biomaterials, 2012. **33**(19): p. 4810-7.
27. Polymeric Scaffolds in Tissue Engineering Application: A Review. International Journal of Polymer Science, 2011. **2011**.
28. Furlong, R.J. and J.F. Osborn, Fixation of hip prostheses by hydroxyapatite ceramic coatings. J Bone Joint Surg Br, 1991. **73**(5): p. 741-5.
29. Liao, S.S., F.Z. Cui, W. Zhang, and Q.L. Feng, Hierarchically biomimetic bone scaffold materials: nano-HA/collagen/PLA composite. J Biomed Mater Res B Appl Biomater, 2004. **69**(2): p. 158-65.
30. Neitzel, I.M., V.; Gogotsi, Y., In Nanocrystalline Diamond. 2012: CRC Taylor and Francis Group.
31. Liang, Y., T. Meinhardt, G. Jarre, M. Ozawa, P. Vrdoljak, A. Scholl, F. Reinert, and A. Krueger, Deagglomeration and surface modification of thermally annealed nanoscale diamond. J Colloid Interface Sci, 2011. **354**(1): p. 23-30.
32. Rajesh Davé, R.G., Robert Pfeffer, Deagglomeration and Mixing of Nanoparticles, in NSF Nanoscale Science and Engineering Grantees Conference. 2006, New Jersey Institute of Technology: Newark, New Jersey.
33. Suh, J.K. and H.W. Matthew, Application of chitosan-based polysaccharide biomaterials in cartilage tissue engineering: a review. Biomaterials, 2000. **21**(24): p. 2589-98.
34. Lahiji, A., A. Sohrabi, D.S. Hungerford, and C.G. Frondoza, Chitosan supports the expression of extracellular matrix proteins in human osteoblasts and chondrocytes. J Biomed Mater Res, 2000. **51**(4): p. 586-95.
35. Chitosan Market - Global Industry Analysis, Size, Share, Growth, Trends and Forecast 2014 - 2020. 2014.
36. Juneja, V.K., H. Thippareddi, and M. Friedman, Control of Clostridium perfringens in cooked ground beef by carvacrol, cinnamaldehyde, thymol, or oregano oil during chilling. J Food Prot, 2006. **69**(7): p. 1546-51.
37. Rouget, M.C., Des substances amylacées dans les tissus des animaux, spécialement des

Articulés (chitine). Comp. Rend, 1895. **48**: p. 792-795.
38. F. Hoppe-Seyler, B.D., Chem. Ges, 1984: p. 27, 3329.
39. Madihally, S.V. and H.W. Matthew, Porous chitosan scaffolds for tissue engineering. Biomaterials, 1999. **20**(12): p. 1133-42.
40. Chenite, A., C. Chaput, D. Wang, C. Combes, M.D. Buschmann, C.D. Hoemann, J.C. Leroux, B.L. Atkinson, F. Binette, and A. Selmani, Novel injectable neutral solutions of chitosan form biodegradable gels in situ. Biomaterials, 2000. **21**(21): p. 2155-61.
41. Nilsen-Nygaard, J., S. Strand, K. Vårum, K. Draget, and C. Nordgård, Chitosan: Gels and Interfacial Properties. Polymers, 2015. **7**(3): p. 552.
42. Kang, Y.M., B.N. Lee, J.H. Ko, G.H. Kim, K.N. Kang, Y. Kim da, J.H. Kim, Y.H. Park, H.J. Chun, C.H. Kim, and M.S. Kim, In vivo biocompatibility study of electrospun chitosan microfiber for tissue engineering. Int J Mol Sci, 2010. **11**(10): p. 4140-8.
43. Chellat, F., M. Tabrizian, S. Dumitriu, E. Chornet, P. Magny, C.H. Rivard, and L. Yahia, In vitro and in vivo biocompatibility of chitosan-xanthan polyionic complex. J Biomed Mater Res, 2000. **51**(1): p. 107-16.
44. Liu, B.J., L.N. Ma, J. Su, W.W. Jing, M.J. Wei, and X.Z. Sha, Biocompatibility assessment of porous chitosan-Nafion and chitosan-PTFE composites in vivo. J Biomed Mater Res A, 2014. **102**(6): p. 2055-60.
45. Mori, T., M. Okumura, M. Matsuura, K. Ueno, S. Tokura, Y. Okamoto, S. Minami, and T. Fujinaga, Effects of chitin and its derivatives on the proliferation and cytokine production of fibroblasts in vitro. Biomaterials, 1997. **18**(13): p. 947-51.
46. Nishimura, K., S. Nishimura, N. Nishi, I. Saiki, S. Tokura, and I. Azuma, Immunological activity of chitin and its derivatives. Vaccine, 1984. **2**(1): p. 93-9.
47. Liu, Y., L. Ma, and C. Gao, Facile fabrication of the glutaraldehyde cross-linked collagen/chitosan porous scaffold for skin tissue engineering. Materials Science and Engineering: C, 2012. **32**(8): p. 2361-2366.
48. Li, L.H., K.P. Kommareddy, C. Pilz, C.R. Zhou, P. Fratzl, and I. Manjubala, In vitro bioactivity of bioresorbable porous polymeric scaffolds incorporating hydroxyapatite microspheres. Acta Biomater, 2010. **6**(7): p. 2525-31.
49. Li, Z., H.R. Ramay, K.D. Hauch, D. Xiao, and M. Zhang, Chitosan-alginate hybrid scaffolds for bone tissue engineering. Biomaterials, 2005. **26**(18): p. 3919-28.
50. Liu, Y.-L., W.-H. Chen, and Y.-H. Chang, Preparation and properties of chitosan/carbon nanotube nanocomposites using poly(styrene sulfonic acid)-modified CNTs. Carbohydrate Polymers, 2009. **76**(2): p. 232-238.
51. Ma, L., C. Gao, Z. Mao, J. Zhou, J. Shen, X. Hu, and C. Han, Collagen/chitosan porous scaffolds with improved biostability for skin tissue engineering. Biomaterials, 2003. **24**(26): p. 4833-41.
52. Ballantyne, B., R.C. Myers, and D.L. Blaszcak, Influence of alkalinization of glutaraldehyde biocidal solutions on acute toxicity, primary irritancy, and skin sensitization. Vet Hum Toxicol, 1997. **39**(6): p. 340-6.
53. Park, E.J., J. Roh, S.N. Kim, M.S. Kang, B.S. Lee, Y. Kim, and S. Choi, Biological toxicity and inflammatory response of semi-single-walled carbon nanotubes. PLoS One, 2011. **6**(10): p. e25892.
54. Tong, L., W. Zhang, H. Hang, Z. Yu, P.K. Chu, and A. Xu, Toxicity of carbon nanotubes to p21 and hus1 gene deficient mammalian cells. J Nanosci Nanotechnol, 2011. **11**(12): p. 11001-5.
55. Wang, J., Y. Xu, Z. Yang, R. Huang, J. Chen, R. Wang, and Y. Lin, Toxicity of carbon nanotubes. Curr Drug Metab, 2013. **14**(8): p. 891-9.
56. Zebarjad, S.M., S.A. Sajjadi, A. Yaghmaei, and T. Ebrahimi Sadrabadi, A Study on Mechanical Properties of PMMA/Hydroxyapatite Nanocomposite. Engineering, 2011.

57. Grigor'ian, A.S., A. Emtsev, V.I. Lizunkov, and A.I. Dobridenev, [The fate of hydroxyapatite ceramic granulate when implanted in a secondary bone defect of the mandible]. Stomatologiia (Mosk), 1996. **75**(5): p. 51-4.
58. Mendelson, B.C., S.R. Jacobson, A.M. Lavoipierre, and R.J. Huggins, The fate of porous hydroxyapatite granules used in facial skeletal augmentation. Aesthetic Plast Surg, 2010. **34**(4): p. 455-61.
59. Morejon, L., A.E. Mendizabal, J.A. Garcia-Menocal, M.P. Ginebra, C. Aparicio, F.J. Mur, M. Marsal, N. Davidenko, M.E. Ballesteros, and J.A. Planell, Static mechanical properties of hydroxyapatite (HA) powder-filled acrylic bone cements: effect of type of HA powder. J Biomed Mater Res B Appl Biomater, 2005. **72**(2): p. 345-52.
60. Marquis, D.M.G., É.; Chivas-Joly, Properties of nanofillers in polymer. In Nanocomposites and Polymers with Analytical Methods, 2011: p. 261–284.
61. (ISO), I.O.f.S., Nanotechnologies—Terminology and Definitions for Nano-Objects—Nanoparticle, Nanofibre and Nanoplate. 2008: Geneva, Switzerland.
62. Iijima, S., Nature, 1991. **354**: p. 56-58.
63. Salvetat, J.-P.B., G. A. D.; Bonard, J.-M.; Bacsa, R. R.; Kulik, A. J.; Stöckli, T.; Burnham, N. A.; Forró, L., Physical Review Letters. Physical Review Letters. **82**: p. 944-947.
64. Hu, B., N. Hu, Y. Li, K. Akagi, W. Yuan, T. Watanabe, and Y. Cai, Multi-scale numerical simulations on piezoresistivity of CNT/polymer nanocomposites. Nanoscale Res Lett, 2012. **7**(1): p. 402.
65. Rangari, V.K., G.M. Mohammad, S. Jeelani, A. Hundley, K. Vig, S.R. Singh, and S. Pillai, Synthesis of Ag/CNT hybrid nanoparticles and fabrication of their nylon-6 polymer nanocomposite fibers for antimicrobial applications. Nanotechnology, 2010. **21**(9): p. 095102.
66. Robert, C., J.F. Feller, and M. Castro, Sensing skin for strain monitoring made of PC-CNT conductive polymer nanocomposite sprayed layer by layer. ACS Appl Mater Interfaces, 2012. **4**(7): p. 3508-16.
67. Seidel, G.D.L., D. C., Mechanics of Materials. Vol. 38. 2006.
68. Liu, Y., Y. Zhao, B. Sun, and C. Chen, Understanding the toxicity of carbon nanotubes. Acc Chem Res, 2013. **46**(3): p. 702-13.
69. J.A. Sowjanyaa, J.S., T. Mohitaa, S., Biocomposite scaffolds containing chitosan/alginate/nano-silica for bone tissue engineering. Colloids and Surfaces B: Biointerfaces, 2013. **109**: p. 294–300.
70. M. Q. Zhang, M.Z.R., W. H. Ruan, Nano and MicroMechanics of Polymer Blends and Composites. Cincinnati: Hanser Publishers.
71. Amal Nassar, E.N., Study on Mechanical Properties of Epoxy Polymer Reinforced with NanoSiC particles. Nanoscience and Nanoengineering, 2013. **1**(2): p. 89-93.
72. H., A., Science and Medical Applications of Hydroxyapatite. Japanese Association of Apatite Science, 1991.
73. LL, H., Bioceramics: from concept to clinic. J Am Ceram Soc, 1991. **74**: p. 1487-1510.
74. Suchanek W, Y.M., Processing and properties of hydroxyapatite-based biomaterials for use as hard tissue replacement implants. J Mater Res, 1998. **13**: p. 94-117.
75. With G de, V.D.H., Hattu N, Prijs K., Preparation, micro- structure and mechanical properties of dense polycrystalline hydroxy apatite. J Mater Sci, 1981. **16**: p. 1592-1598.
76. Danilenko, V.V., On the history of the discovery of nanodiamond synthesis. Physics of the Solid State, 2004. **46**(4): p. 595-599.
77. Olga A. Shenderova, D.M.G., Ultrananocrystalline Diamond: Synthesis, Properties and Applications. 2012.

78. Bergonzo, P., R.B. Jackman, K.P. Loh, G.M. Swain, and O.A. Williams, Diamond Electronics and Biotechnology - Fundamentals to Applications V. 2012: Materials Research Society.
79. Yu, B.O., H.C. Tai, W. Xue, L.J. Lee, and R.J. Lee, Receptor-targeted nanocarriers for therapeutic delivery to cancer. Molecular membrane biology, 2010. **27**(7): p. 286-298.
80. Heidrich, N.F.I.f.A.S.S.P.I., Freiburg, Germany ; Hees, J. ; Zuerbig, V. ; Iankov, D., Nano-diamond vacuum MEMS for RF applications. 2013, IEEE: Barcelona. p. 218 - 221.
81. Yury Gogotsi, V.P., Carbon Nanomaterials. 2006.
82. William A. Goddard III, D.B., Sergey Edward Lyshevski, Gerald J Iafrate, Handbook of Nanoscience, Engineering, and Technology. 2012.
83. Fang, J. and Y.C. Chen, Nanomaterials for photohyperthermia: a review. Curr Pharm Des, 2013. **19**(37): p. 6622-34.
84. Schrand, A.M., S.A.C. Hens, and O.A. Shenderova, Nanodiamond Particles: Properties and Perspectives for Bioapplications. Critical Reviews in Solid State and Materials Sciences, 2009. **34**(1-2): p. 18-74.
85. Mochalin, V.N., O. Shenderova, D. Ho, and Y. Gogotsi, The properties and applications of nanodiamonds. Nat Nanotechnol, 2012. **7**(1): p. 11-23.
86. Hristova, K., E. Pecheva, L. Pramatarova, and G. Altankov, Improved interaction of osteoblast-like cells with apatite-nanodiamond coatings depends on fibronectin. J Mater Sci Mater Med, 2011. **22**(8): p. 1891-900.
87. S. Morimune, M.K.a.T.N., POLY (VINYL ALCOHOL) COMPOSITE WITH NANODIAMOND.
88. Zhang, Q., V.N. Mochalin, I. Neitzel, I.Y. Knoke, J. Han, C.A. Klug, J.G. Zhou, P.I. Lelkes, and Y. Gogotsi, Fluorescent PLLA-nanodiamond composites for bone tissue engineering. Biomaterials, 2011. **32**(1): p. 87-94.
89. Attia, N.F., J.P. Rao, and K.E. Geckeler, Nanodiamond–polymer nanoparticle composites and their thin films. Journal of Nanoparticle Research, 2014. **16**(4): p. 1-12.
90. Hengsberger, S., A. Kulik, and P. Zysset, A combined atomic force microscopy and nanoindentation technique to investigate the elastic properties of bone structural units. Eur Cell Mater, 2001. **1**: p. 12-7.
91. Rho, J.Y., M.E. Roy, 2nd, T.Y. Tsui, and G.M. Pharr, Elastic properties of microstructural components of human bone tissue as measured by nanoindentation. J Biomed Mater Res, 1999. **45**(1): p. 48-54.
92. Neitzel, I., V. Mochalin, I. Knoke, G.R. Palmese, and Y. Gogotsi, Mechanical properties of epoxy composites with high contents of nanodiamond. Composites Science and Technology, 2011. **71**(5): p. 710-716.
93. Horch, R.A., N. Shahid, A.S. Mistry, M.D. Timmer, A.G. Mikos, and A.R. Barron, Nanoreinforcement of poly(propylene fumarate)-based networks with surface modified alumoxane nanoparticles for bone tissue engineering. Biomacromolecules, 2004. **5**(5): p. 1990-8.
94. Laurencin, C.T., M.A. Attawia, H.E. Elgendy, and K.M. Herbert, Tissue engineered bone-regeneration using degradable polymers: the formation of mineralized matrices. Bone, 1996. **19**(1 Suppl): p. 93S-99S.
95. Poursamar, S.A., J. Hatami, A.N. Lehner, C.L. da Silva, F.C. Ferreira, and A.P.M. Antunes, Gelatin porous scaffolds fabricated using a modified gas foaming technique: Characterisation and cytotoxicity assessment. Materials Science and Engineering: C, 2015. **48**: p. 63-70.
96. Cui, X., T. Boland, D.D. D'Lima, and M.K. Lotz, Thermal Inkjet Printing in Tissue Engineering and Regenerative Medicine. Recent patents on drug delivery &

formulation, 2012. **6**(2): p. 149-155.
97. Geng, X., O.-H. Kwon, and J. Jang, Electrospinning of chitosan dissolved in concentrated acetic acid solution. Biomaterials, 2005. **26**(27): p. 5427-5432.
98. Mathews, D.P., The pediculated connective tissue graft: a technique for improving unaesthetic implant restorations. Pract Proced Aesthet Dent, 2002. **14**(9): p. 719-24; quiz 726.
99. An, K., H. Liu, S. Guo, D.N.T. Kumar, and Q. Wang, Preparation of fish gelatin and fish gelatin/poly(l-lactide) nanofibers by electrospinning. International Journal of Biological Macromolecules, 2010. **47**(3): p. 380-388.
100. Lu, T., Y. Li, and T. Chen, Techniques for fabrication and construction of three-dimensional scaffolds for tissue engineering. International Journal of Nanomedicine, 2013. **8**: p. 337-350.
101. Niu, X., X. Li, H. Liu, G. Zhou, Q. Feng, F. Cui, and Y. Fan, Homogeneous chitosan/poly(L-lactide) composite scaffolds prepared by emulsion freeze-drying. J Biomater Sci Polym Ed, 2012. **23**(1-4): p. 391-404.
102. Sultana, N. and M. Wang, PHBV/PLLA-based composite scaffolds fabricated using an emulsion freezing/freeze-drying technique for bone tissue engineering: surface modification and in vitro biological evaluation. Biofabrication, 2012. **4**(1): p. 015003.
103. Joshi, K.B., S. Prabhpreet, and V. Sandeep, Fabrication of platinum nanopillars on peptide-based soft structures using a focused ion beam. Biofabrication, 2009. **1**(2): p. 025002.
104. How an FTIR Spectrometer Operates. [cited 2015 08.02]; Available from: http://chemwiki.ucdavis.edu/Physical_Chemistry/Spectroscopy/Vibrational_Spectroscopy/Infrared_Spectroscopy/How_an_FTIR_Spectrometer_Operates.
105. Development of X-ray crystallography. [cited 2015 08.02]; Available from: https://publish.illinois.edu/x-raycrystallography/2014/12/18/introduction/.
106. J, O.M. and W.E. S, Differential microcalorimeter. 1966, Google Patents.
107. Differential Scanning Calorimetry DSC. [cited 2015 08.02]; Available from: http://instrument-specialists.com/applications/differential-scanning-calorimetry-dsc/.
108. Gill, P., T.T. Moghadam, and B. Ranjbar, Differential Scanning Calorimetry Techniques: Applications in Biology and Nanoscience. Journal of Biomolecular Techniques : JBT, 2010. **21**(4): p. 167-193.
109. MTT reaction. [cited 2015 08.02]; Available from: https://en.wikipedia.org/wiki/File:MTT_reaction.png.
110. Liu, H.L., S.J. Liu, Z.L. Xiao, Q.Y. Chen, and D.W. Yang, Excess molar enthalpies of binary mixtures for (tributyl phosphate+methanol/ethanol) at 298.15 K. Journal of Thermal Analysis and Calorimetry, 2006. **85**(3): p. 541-544.
111. Krueger, A., New carbon materials: biological applications of functionalized nanodiamond materials. Chemistry, 2008. **14**(5): p. 1382-90.
112. Pichot, V. and R. Institut Franco-Allemand de, Dispersion of detonation nanodiamonds in a liquid medium The American Carbon Society International Conference on Carbon, Seattle/WA, US, July 15 - 20, 2007. 2007, Saint-Louis, France; Weil am Rhein: ISL.
113. Ho, D., Nanodiamonds: Applications in Biology and Nanoscale Medicine. 2009: Springer Science & Business Media. 286.
114. Behler, K.D., A. Stravato, V. Mochalin, G. Korneva, G. Yushin, and Y. Gogotsi, Nanodiamond-polymer composite fibers and coatings. ACS Nano, 2009. **3**(2): p. 363-9.
115. Neitzel, I., Nanodiamond–Polymer Composites. 2012, Drexel University.
116. VY, D., Detonation synthesis ultradispersed diamonds: properties and applications. Russian Chemical Reviews, 2001. **70**(7): p. 607–626.

117. Shenderova OA, H.S., Detonation nanodiamond particles processing, modification and bioapplications. 2010, New York, NY: Springer: Nanodiamonds: Applications in Biology and Nanoscale Medicine.
118. Lee, T.H., F.Y.C. Boey, and K.A. Khor, X-ray diffraction analysis technique for determining the polymer crystallinity in a polyphenylene sulfide composite. Polymer Composites, 1995. **16**(6): p. 481-488.
119. Haastert, K., N. Semmler, M. Wesemann, M. Rücker, N.-C. Gellrich, and C. Grothe, Establishment of Cocultures of Osteoblasts, Schwann Cells, and Neurons Towards a Tissue-Engineered Approach for Orofacial Reconstruction. Cell Transplantation, 2006. **15**(8-1): p. 733-744.
120. Table of Characteristic IR Absorptions. [cited 2015 07.20]; Available from: http://orgchem.colorado.edu/Spectroscopy/specttutor/irchart.pdf; http://www.chem.ucla.edu/~webspectra/irtable.html.
121. Liang Y1, O.M., Krueger A., A general procedure to functionalize agglomerating nanoparticles demonstrated on nanodiamond. ACS Nano, 2009. **3**(8): p. 2288-96.
122. Sun, Y., P. Olsén, T. Waag, A. Krueger, D. Steinmüller-Nethl, A.-C. Albertsson, and A. Finne-Wistrand, Disaggregation and Anionic Activation of Nanodiamonds Mediated by Sodium Hydride—A New Route to Functional Aliphatic Polyester-Based Nanodiamond Materials. Particle & Particle Systems Characterization, 2015. **32**(1): p. 35-42.
123. Khare, H.S.B., D. L., Polymer. Vol. 51. 2010.
124. Yamaguchi, I., K. Tokuchi, H. Fukuzaki, Y. Koyama, K. Takakuda, H. Monma, and J. Tanaka, Preparation and microstructure analysis of chitosan/hydroxyapatite nanocomposites. J Biomed Mater Res, 2001. **55**(1): p. 20-7.
125. Zeng, M., Z. Fang, and C. Xu, Effect of compatibility on the structure of the microporous membrane prepared by selective dissolution of chitosan/synthetic polymer blend membrane. Journal of Membrane Science, 2004. **230**(1–2): p. 175-181.
126. Chuang, W.Y., T.H. Young, C.H. Yao, and W.Y. Chiu, Properties of the poly(vinyl alcohol)/chitosan blend and its effect on the culture of fibroblast in vitro. Biomaterials, 1999. **20**(16): p. 1479-87.
127. Esam A. EL-HEFIAN , E.S.E., Azizah MAINAL,, Characterization of chitosan in acetic acid: Rheological and thermal studies. Turkish Journal of Chemistry, 2009.
128. Chuang, W.Y.Y., T.H.; Yao, C.H. Chui W.Y., Biomaterials. 1999. p. 1479-1487.
129. Liao, S.-K., C.-C. Hung, and M.-F. Lin, A kinetic study of thermal degradations of chitosan/polycaprolactam blends. Macromolecular Research, 2004. **12**(5): p. 466-473.
130. Kim, S.-K., Chitin, Chitosan, Oligosaccharides and Their Derivatives: Biological Activities and Applications. 2010.
131. Zhang, Q., V.N. Mochalin, I. Neitzel, K. Hazeli, J. Niu, A. Kontsos, J.G. Zhou, P.I. Lelkes, and Y. Gogotsi, Mechanical properties and biomineralization of multifunctional nanodiamond-PLLA composites for bone tissue engineering. Biomaterials, 2012. **33**(20): p. 5067-75.
132. Maitra, U., K.E. Prasad, U. Ramamurty, and C.N.R. Rao, Mechanical properties of nanodiamond-reinforced polymer-matrix composites. Solid State Communications, 2009. **149**(39–40): p. 1693-1697.
133. Sowjanya, J.A., J. Singh, T. Mohita, S. Sarvanan, A. Moorthi, N. Srinivasan, and N. Selvamurugan, Biocomposite scaffolds containing chitosan/alginate/nano-silica for bone tissue engineering. Colloids and Surfaces B: Biointerfaces, 2013. **109**(0): p. 294-300.
134. Rodrigues, S., M. Dionísio, C.R. López, and A. Grenha, Biocompatibility of Chitosan Carriers with Application in Drug Delivery. Journal of Functional Biomaterials, 2012.

**3**(3): p. 615.
135. Bruno Sarmento, J.d.N., Chitosan-Based Systems for Biopharmaceuticals: Delivery, Targeting and Polymer Therapeutics. 2012.